

STUDIES ON NEURITE OUTGROWTH AND RECEPTOR PHOSPHORYLATION  
FOLLOWING KAPPA OPIOID RECEPTOR ACTIVATION

---

A Dissertation  
Submitted to  
the Temple University Graduate Board

---

In Partial Fulfillment  
of the Requirements for the Degree  
DOCTOR OF PHILOSOPHY

---

by  
Yi-Ting Chiu  
May 2016

Examining Committee Members:

Lee-Yuan Liu-Chen, PhD (Advisor)  
Barrie Ashby, PhD (Examining Committee Chair)  
Ellen Unterwald, PhD  
Mary Abood, PhD  
Douglas Tilley, PhD  
Jeffrey Benovic, PhD (External Examiner)

©  
Copyright  
2016

by

Yi - Ting Chiu  
All Rights Reserved

## ABSTRACT

### STUDIES ON NEURITE OUTGROWTH AND RECEPTOR PHOSPHORYLATION FOLLOWING KAPPA OPIOID RECEPTOR ACTIVATION

Yi-Ting Chiu

Doctor of Philosophy

Temple University, 2016

PhD's Advisory Committee Chair: Lee-Yuan Liu-Chen, PhD

Kappa opioid receptor (KOPR) is involved in many physiological functions and pharmacological responses such as analgesia, anti-pruritic effect, sedation, motor incoordination and aversion (Simonin et al., 1998; Liu-Chen, 2004). The cellular mechanisms following activation of KOPR involve in part Gi/o protein-dependent pathways (Law et al., 2000). Following KOPR activation, the receptor is phosphorylated and arrestins are recruited. Arrestins mediate agonist-dependent KOPR desensitization, internalization and down-regulation (Liu-Chen, 2004). In recent years, arrestins were found to initiate arrestin-dependent downstream signaling. Thus, agonist-promoted KOPR phosphorylation plays a pivotal role in KOPR regulation and signaling.

Previous studies from our lab showed that in Chinese hamster ovary (CHO) cells stably transfected with the human KOPR (hKOPR), U50,488H induced phosphorylation (Li et al., 2002a); however, sites of phosphorylation were not determined. Using LC-MS/MS, our lab recently identified four residues (S356, T357, T363 and S369) to be the sites of U50,488H-promoted phosphorylation in the mouse KOPR (mKOPR) stably expressed in N2A cells (Chen et al., 2016). Antibodies were generated against phosphopeptides and purified and three antibodies were found to have high specificity for the mKOPR phosphorylated at S356/T357, T363 and S369, respectively (Chen et al., 2016). Our lab previously showed that while U50,488H promoted robust hKOPR

phosphorylation and internalization, etorphine induced little phosphorylation and internalization, although both were potent full agonists in enhancing [<sup>35</sup>S]GTPγS (Li et al., 2002a; Zhang et al., 2002; Li et al., 2003). Etorphine caused lower levels of KOPR phosphorylation at all the four residues than U50,488H by immunoblotting with the phospho-specific antibodies (Chen et al., 2016). Using the SILAC (stable isotope labeling by amino acids in cell culture) approach, we have found that compared to etorphine, U50,488H promoted higher levels of single phosphorylation at T363 and S369 and double phosphorylation at T363+S369 and T357+S369 as well as triple phosphorylation at S356+T357+S369 (Chen et al., 2016). These results indicate that an above-threshold phosphorylation is required for KOPR internalization.

It has been reported that KOPR is involved in neuronal differentiation and neurogenesis. In the first chapter, I focused on whether there are differences in the mechanisms underlying neurite outgrowth induced by U50,488H and etorphine. In the chapter 2, mechanisms of KOPR phosphorylation were characterized in detail using phospho-specific KOPR antibodies. Protein kinase C was found, for the first time, to be involved in agonist-promoted KOPR phosphorylation. The roles of PKC in behavioral effects induced by KOPR agonists in mice were examined.

For the chapter 1, in Neuro2a mouse neuroblastoma cells stably transfected with the hKOPR (N2A-3HA-hKOPR), U50,488H robustly induced neurite outgrowth, but etorphine caused outgrowth to a much lower extent. G protein-dependent pathway was found to be involved in the actions of both agonists, but β-arrestin-dependent pathway was not. Inhibition of ERK1/2 phosphorylation decreased neurite outgrowth promoted by both agonists, indicating the roles of MAP kinase cascades in KOPR agonist-induced

neuritogenesis. In contrast,  $\beta$ -arrestin2, 14-3-3 $\zeta$ , GEC1 and Rap1 are not involved in U50,488H- or etorphine-promoted neurite outgrowth. Thus, the two agonists appear to share the same signaling pathways and the difference between two agonists is likely due to the lower efficacy of etorphine.

For the chapter 2, U50,488H caused phosphorylation of the mKOPR at S356, T357, T363 and S369 in N2A cells stably transfected with FmK6H (FmK6H-N2A cells). NorBNI abolished U50,488H-induced KOPR phosphorylation at all four residues. GRKs (GRKs2, 3, 5 and 6) and PKCs were involved in U50,488H-mediated KOPR phosphorylation. In addition, PKC also participated in agonist-independent KOPR phosphorylation. This is the first time that PKC was shown to be involved in agonist-induced KOPR phosphorylation. We found that U50,488H caused KOPR phosphorylation at T363 and S369 in the mouse brain and PKC participated in phosphorylation of S369, but not T363, by using the PKC inhibitor chelerythrine (CHL). Thus, we further characterized effects of PKC inhibition on KOPR-mediated behaviors in CD1 mice. PKC was involved in KOPR-mediated sedation, motor incoordination and conditioned place aversion, but not analgesia and anti-scratching effect in mice.

Studies in this thesis revealed the mechanisms of KOPR-mediated neurite outgrowth and KOPR-mediated phosphorylation and the involvement of PKC in KOPR-mediated pharmacological effects *in vivo*. These studies push the frontier of molecular pharmacology of the KOPR, which may be useful for development of KOPR agonists for therapeutic use.

## **DEDICATION**

This dissertation is dedicated to **my parents** for their love and support  
throughout my life and my educational endeavor .

## ACKNOWLEDGMENTS

I would like specially to thank Department of Pharmacology, Temple University School of Medicine which gave me the opportunity to pursue higher education in the USA and everyone who gave me support, help and suggestions throughout my graduate studies.

First of all, I would like to thank my advisor Dr. Lee-Yuan Liu-Chen who gave me the opportunity to come to Temple University from Taiwan. She is very passionate and knowledgeable about research. She has taught me how to think and solve problems in a scientific way for my Ph.D. training. She is also very nice, warm-hearted and helpful to me living in a foreign country with different customs and culture. I hereby give my highest appreciations and respect to her.

I would like to thank my committee members. Dr. Barrie Ashby gave me suggestions for course selection and instructions for every step of my graduate training. I would like to thank Dr. Ellen Unterwald, who gave me a chance to do my rotation in her laboratory, taught me how to do brain dissections and gave her advice on my thesis studies. I would like to thank Dr. Mary Abood, who gave me her expert suggestions on GPCRs and encouraged me. I thank Dr. Douglas Tilley, who gave me insightful suggestions and advice on experimental designs. I appreciate Dr. Jeffrey Benovic for his willingness to take time to serve as an external examiner of my thesis and his insightful comments.

I also want to thank people in my laboratory. I especially thank Chongguang Chen, who helped me and taught me a great deal about experimental design and technical details. I express my appreciation to other lab members (Peng Huang, Yujun Wong, Kelly DiMattio, Susan Rasakham and Wei Xu), for their support, suggestions, and guidance on

my experiments and their friendship through my graduate study.

I am grateful to Dr. Alan Cowan, who taught me how to do the anti-scratching test and rotarod test and guided me on related experimental designs. I also thank Dr. Ronald Tallarida for his expert advice on statistical analyses and the honor of receiving Tallarida Pharmacology Fellowship. I appreciate our collaborator Dr. Stefan Schulz of Jena University Hospital, Jena, Germany, who shared with us the pS356/pT357 phospho-KOPR specific antibodies and helpful comments on my project.

I would like to express my gratitude to all the professors and staff in the Department of Pharmacology and Center for Substance Abuse Research (CSAR), especially for the leadership of Dr. Ellen Unterwald as the CSAR director, Dr. Nae J. Dun, the former Pharmacology chair and Dr. Walter Koch, the current Pharmacology chair.

I am grateful to fellow graduate students (Pu Fang, Ying Yin, Xinyuan Li, Jen-Kuan Chang and Nicole Enman) and friends in CSAR (Xiangdang Shi, Mary Mccafferty, Chen Li, and Hongbo Li) for their friendship and experimental discussions with me. I wish to express my best gratitude to my host family parents (Arthur and Bonnie Drescher) to give me an opportunity to stay with them to experience American culture and take care of me.

I would love to thank Dr. Barrie Ashby, the former Associate Dean for Graduate Studies, Dr. Scott Shore, the Associate Dean for Graduate Studies and Dr. Dianne R. Soprano, Associate Dean for MD/PhD and Graduate Studies for their great efforts for the graduate programs.

Lastly, I would thank the funding and the scholarship support I have received throughout my graduate study from the NIH, Temple University, Department of

Pharmacology and CSAR.

# TABLE OF CONTENTS

	Page
ABSTRACT.....	iii
DEDICATION.....	vi
ACKNOWLEDGMENTS.....	vii
LIST OF TABLES.....	xvi
LIST OF FIGURES.....	xvii
LIST OF ABBREVIATIONS.....	xx
GENERAL INTRODUCTION	
Opioid receptors.....	xxii
biased agonism at opioid receptors.....	xxv
Scientific rationale.....	xxviii
CHAPTER	
1. STUDIES ON NEURITE OUTGROWTH FOLLOWING KAPPA OPIOID	
RECEPTOR ACTIVATION.....	1
Introduction.....	1
Kappa opioid receptor-induced signaling.....	1
Neurite outgrowth.....	1
Experimental hypothesis.....	2
Materials and Methods.....	3
Materials.....	3

Cell culture.....	4
Neurite outgrowth assay .....	5
Western blotting.....	6
Data Analysis and Statistics.....	7
<b>Results</b>	
U50,488H- and etorphine-induced neurite outgrowth .....	8
U50,488H- and etorphine-induced neurite outgrowth is mediated by the KOPR.....	8
Gi/o <sub>α</sub> proteins are involved in U50,488H- and etorphine-induced neurite outgrowth, but not G <sub>βγ</sub> proteins .....	13
β-arrestins were not involved in U50,488H- and etorphine-induced neurite outgrowth .....	15
ERK1/2 play roles in the KOPR-mediated neurite outgrowth.....	17
Lack of involvement of PKC or PI3K signal pathways in KOPR- induced neuronal differentiation .....	22
The roles of the KOPR interacting proteins 14-3-3ζ or GEC1 in U50,488H- and etorphine-induced neurite outgrowth .....	25
The role of G protein regulated inducer of neurite outgrowth 1 or 2 (GRIN1 or 2) in U50,488H- and etorphine-induced neurite outgrowth .....	29
To examine if Rap1-STAT3 pathway is involved in KOPR agonist-induced neurite outgrowth .....	31
<b>Discussion</b>	

Summary .....	34
KOPR-mediated neurite outgrowth is G protein- but not $\beta$ -arrestin- dependent .....	36
Roles of KOPR- and $G_{o\alpha}$ -interacting proteins in neurite outgrowth .....	37
The role of MAPK in KOPR-mediated cellular functions.....	38
$G_i/o\alpha$ -coupled GPCR-mediated neurite outgrowth .....	39
Similarities and differences between U50,488H and etorphine.....	39
2. STUDIES ON RECEPTOR PHOSPHORYLATION FOLLOWING KAPPA OPIOID RECEPTOR ACTIVATION .....	41
Introduction.....	41
Phosphorylation of GPCR.....	41
G protein receptor kinase (GRK) .....	44
Protein kinase C (PKC).....	47
KOPR-mediated pharmacological effects.....	50
Materials and Methods.....	52
Materials .....	52
Cell culture.....	54
Drug treatment .....	54
Receptor purification and Western blot .....	56
Detection of endogenous GRKs and the specificity of GRK siRNAs in N2A cells.....	57
Reverse transcription-polymerase chain reaction (RT-PCR) .....	58
On cell western for receptor internalization.....	59

Animals .....	60
Effect of PKC inhibition on U50,488H-induced KOPR phosphorylation in mouse brain.....	61
Formalin test .....	63
Anti-scratching test .....	63
Novelty-induced locomotor activity .....	64
Rotarod performance assay.....	65
Conditioned place aversion (CPA) .....	65
Data Analysis and Statistics.....	67
Results.....	68
U50,488H-induced KOPR phosphorylation is mediated by KOPR .....	68
Time course and dose-response relationship of U50,488H-induced KOPR phosphorylation.....	70
Roles of GRKs in U50,488H-induced KOPR phosphorylation.....	73
Roles of PKCs on KOPR phosphorylation <i>in vitro</i> .....	82
PKC-mediated KOPR phosphorylation on KOPR internalization .....	92
Investigation on suitability of phospho-KOPR antibodies in immunocytochemistry: test on internalized KOPR following U50,488H treatment.....	94
Studies on roles of PKC in KOPR-related pharmacological effects.....	96
Effect of PKC inhibitor CHL on KOPR phosphorylation in mouse brain .....	97
Effect of PKC inhibition on KOPR-mediated analgesia.....	100

Effect of PKC inhibition on KOPR-mediated antipruritic effect.....	102
Effect of PKC inhibition on KOPR-mediated sedation and motor incoordination .....	106
Effect of PKC inhibition on KOPR-mediated aversion in the conditioned place aversion (CPA) test.....	111
Discussion .....	114
Study on KOPR phosphorylation following U50,488H stimulation <i>in vitro</i> .....	114
Time course of KOPR phosphorylation.....	114
GRK-induced KOPR phosphorylation .....	115
Bar code hypothesis .....	116
Other studies related to GRK-mediated KOPR phosphorylation .....	117
Phosphorylation sites in GPCRs .....	118
PKC-mediated KOPR phosphorylation .....	119
PKC-mediated agonist-independent KOPR phosphorylation.....	119
Involvement of PKC in agonist-dependent KOPR phosphorylation .....	120
U50,488H-induced KOPR internalization .....	123
Multiple protein kinases are involved in GPCR phosphorylation .....	124
Generation and specificity of KOPR phosphoantibodies .....	126
Pros and cons of combined SILAC and LC-MS/MS and immunoblotting with phosphospecific antibodies .....	129
Effects of KOPR expression level and 6XHis tag on agonist- promoted KOPR phosphorylation.....	130

The role of PKC on U50,488H-induced pharmacological effects <i>in vivo</i> .....	130
Limitation of using a PKC inhibitor in behavior studies .....	131
PKC-mediated KOPR phosphorylation following U50,488H treatment <i>in vivo</i> .....	132
Effect of PKC inhibition on KOPR-induced analgesic effect and anti-pruritic effect .....	133
Effect of PKC inhibition on KOPR-mediated sedation and motor incoordination .....	134
Effect of PKC inhibition on KOPR-induced CPA.....	135
Doses of U50,488H chosen for behavior tests.....	136
Future studies .....	138
β-arrestin recruitment following GRK- or PKC-mediated KOPR phosphorylation in cells .....	138
Effects of PKC inhibition, GRK knockdown and β-arrestin knockdown on U50,488H-induced KOPR internalization in mouse brains.....	138
Phosphorylation-deficient mice .....	138
CONCLUSIONS.....	140
REFERENCES .....	142

## LIST OF TABLES

Table	Page
1. Sequences of phosphopeptides used as the antigens for antiserum generation .....	128

## LIST OF FIGURES

Figure	Page
1. Opioid receptor-mediated signal pathways .....	xxiv
2. Effects of U50,488H and etorphine on neurite outgrowth: dose-response relationship .....	10
3. Effect of KOPR agonists on untransfected N2A cells .....	11
4. U50,488H- and etorphine-induced neurite outgrowth is KOPR-mediated.....	12
5. The role of G protein in U50,488H- and etorphine-induced neurite outgrowth .....	14
6. Role of $\beta$ -arrestin1 and $\beta$ -arrestin2 in U50,488H- and etorphine-induced neurite outgrowth.....	16
7. (A) U50,488H and etorphine enhanced ERK1/2 phosphorylation in PTX-sensitive manner.....	19
(B) ERK1/2 played a role in U50,488H- or etorphine-induced neurite outgrowth Cells .....	20
8. Effect of p38 MAPK inhibition on U50,488H- and etorphine-induced neurite outgrowth.....	21
9. Effect of PKC inhibition on U50,488H- and etorphine-induced neurite outgrowth.....	23
10. The role of PI3K in U50,488H- and etorphine-induced neurite outgrowth.....	24
11. Role of the KOPR interacting protein 14-3-3 $\zeta$ in KOPR-mediated neurite outgrowth.....	27
12. Role of the KOPR interacting protein GEC1 in KOPR-mediated neurite outgrowth.....	28
13. Role of the G $\alpha$ -binding proteins GRIN1 and GRIN2 in KOPR-mediated neurite outgrowth.....	30
14. Effect of Rap1 on U50,488H- or etorphine-induced neurite outgrowth.....	32

15. Effect of STAT3 on U50,488H- or etorphine-induced neurite outgrowth.....	33
16. Summary of KOPR-dependent and KOPR-independent neurite outgrowth.....	35
17. The barcode hypothesis.....	43
18. GRKs subfamily.....	46
19. PKC isoforms.....	49
20. U50,488H-promoted KOPR phosphorylation was blocked by norBNI.....	69
21. Time course of U50,488H-induced KOPR phosphorylation.....	71
22. Dose-response relationship of U50,488H-induced KOPR phosphorylation.....	72
23. Detection of endogenous GRKs 2, 3 and 6 in Neuro2a cells.....	74
24. Specificity of siRNAs against GRK2, GRK3, and GRK6 in N2A cells.....	76
25. Effects of knockdown of GRK2 and GRK3 on U50,488H-induced KOPR phosphorylation at S356/T357, T363 and S369.....	78
26. Effect of GRK6 knockdown on U50,488H-induced KOPR phosphorylation at S356/T357, T363 and S369.....	79
27. Effects of GRK5 expression and expression + knockdown on U50,488H-induced KOPR phosphorylation at S356/T357, T363 and S369.....	81
28. Endogenous PKC isoforms in N2A cells, detected with RT-PCR.....	83
29. Effect of PKC activation on KOPR phosphorylation.....	85
30. Effects of two nonselective PKC inhibitors on U50,488H-induced KOPR phosphorylation at S356/T357, T363 and S369.....	88
31. Effect of the selective PKC $\alpha$ and $\beta$ 1 inhibitor Go6976 on U50,488H-induced KOPR phosphorylation at S356/T357, T363 and S369.....	90
32. Effects of knockdown of PKC $\alpha$ and PKC $\epsilon$ on U50,488H-induced KOPR phosphorylation at S356/T357, T363 and S369 phosphoresidues.....	91

33. Effect of PKC inhibitors on U50,488H-induced internalization.....	93
34. Internalized KOPR following U50,488H treatment is phosphorylated at T363.....	95
35. Effect of the PKC inhibitor CHL on U50,488H-induced KOPR phosphorylation in mouse brains.....	99
36. Effect of the PKC inhibitor CHL on U50,488H-induced analgesia in the formalin test.....	101
37. Effect of the PKC inhibitor CHL on U50,488H-induced anti-scratching behavior .....	103
38. Repeated U50,488H injection did not cause tolerance development in anti-scratching test.....	105
39. Effect of the PKC inhibitor CHL on U50,488H-induced sedation in the novelty-induced locomotor activity model.....	107
40. Effect of the PKC inhibitor CHL on U50,488H-induced motor incoordination in the rotarod performance assay.....	110
41. Effect of the PKC inhibitor CHL on U50-induced CPA.....	112

## LIST OF ABBREVIATIONS

AUC	area under curve
βARK	β-adrenergic receptor kinase
β2AR	β2-adrenergic receptor
BCA	bicinchoninic acid assay
CHL	chelerythrine chloride
CHO	Chinese hamster ovary
CPA	conditioned place aversion
DAG	diacylglycerol
DDM	dodecyl-β-Dmaltoside
DN	dominant negative
DOPR	delta opioid receptor
DTT	dithiothreitol
ECL	enhanced chemiluminescence
EDTA	ethylenediaminetetraacetic acid
ESC	embryonic stem cells
FmK6H	FLAG tag at the N-terminus and 6×His at the C-terminus of KOPR
GPCR	G protein-coupled receptor
GRIN	G protein regulated inducer of neurite outgrowth
GRK	G protein receptor kinase
hKOPR	human kappa opioid receptor
HPLC	high performance liquid chromatography
HRP	horseradish peroxidase
KLH	keyhole limpet hemocyanin
KO	Knockout
KOPR	kappa opioid receptor
LC-MS/MS	liquid chromatography-tandem mass spectrometry
MAPK	mitogen-activated protein kinase
MEM	minimal essential medium
mKOPR	mouse kappa opioid receptor
MOPR	Mu opioid receptor
NES	nuclear export signal
nor-BNI	norbinaltorphimine
NLS	nucleat localization signal
NTF	Nontransfection
ni-NTA	nickel-nitrilotriacetate
N2A	neuro2A
OR	opioid receptor
PI3K	Phosphatidylinositol-4,5-bisphosphate 3-kinase
PKC	protein kinase C

PMA	phorbol-12-myristate-13-acetate
PTX	pertussis toxin
rKOPR	rat kappa opioid receptor
RT-PCR	reverse transcription– polymerase chain reaction
SILAC	stable isotope labeling by amino acids in cell culture
7TMR	seven-transmembrane receptor

## GENERAL INTRODUCTION

### Opioid receptors (ORs)

Opioid receptors (ORs) belong to the class A (rhodopsin) subfamily of seven-transmembrane receptors (7TMRs) or G protein-coupled receptors (GPCRs). There are three major types of ORs, the mu opioid receptors (MOPR, mu for morphine), the delta opioid receptors (DOPR, delta for *deferens* because it was first found in the mouse *vas deferens*) and the kappa opioid receptor (KOPR, kappa for the drug ketocyclazocine which is active at this receptor) according to pharmacological and radioligand binding approaches and molecular cloning (Lord et al., 1977; Knapp et al., 1995).

In the 1990's, three ORs were cloned, leading to many studies on receptor-ligand interactions and structure-function relationship, regulation and signaling of these receptors (Knapp et al., 1995). ORs are Gi/o protein-coupled receptors with an extracellular N-terminal domain, an intracellular C-terminal domain and seven transmembrane domains with three extracellular loops and three intracellular loops. Three ORs share ~60% overall sequence identity with ~90% identity in the transmembrane helices, with major differences in the extracellular loops and N- and C-terminal domains (Chen et al., 1993). Like other GPCRs, ORs have two conserved cysteine residues in the 1st and 2nd extracellular loops that form a disulfide bond and highly conserved Asp-Arg-Tyr (DRY) motif at the intracellular end of the TM3. In addition, the N-terminal domains of three ORs are modified by Asn-linked glycosylation (Schwartz, 1994). In 2012, crystal structures of the MOPR, DOPR and KOPR were revealed, providing a new avenue for structure-guided opioid drug discovery (Granier et al., 2012; Manglik et al., 2012; Wu et al., 2012).

ORs are the major targets of endogenous neuropeptides (endorphins for MOPR,

enkephalins for DOPR and dynorphins for KOPR), naturally occurring plant opiates and synthetic opioids. Signal transduction after activation of opioid receptors by agonists is depicted in the figure 1. In inactive states, the heterotrimer G protein is composed of GDP bound  $G_i/o_\alpha$  and  $G_{\beta\gamma}$ . After receptor activation, GDP on  $G_i/o_\alpha$  is replaced with GTP and GTP- $G_i/o_\alpha$  and  $G_{\beta\gamma}$  are dissociated, which trigger downstream signaling.  $G_i/o_\alpha$  protein inhibits adenylyl cyclases and activates  $K^+$  channels and MAP kinases (early phase).  $G_{\beta\gamma}$  inhibit  $Ca^{2+}$  inward current. ORs are phosphorylated by G protein receptor kinases (GRKs) and  $\beta$ -arrestin binds to phosphorylated receptors, causing receptors to dissociate from  $G_i/o_\alpha$  protein, leading to receptor desensitization, as well as  $\beta$ -arrestin-dependent signal transduction including activation of p44/42 MAP kinases (late phase) and p38 MAP kinase. In addition,  $\beta$ -arrestin also binds to clathrin, resulting in internalization and down-regulation. Opioid agonists act through  $G_i/Go$  proteins and arrestins to regulate downstream signaling pathways, leading to different cellular functions, physiological and pharmacological functions (Law et al., 2000; Liu-Chen, 2004; Al Hasani and Bruchas, 2011).

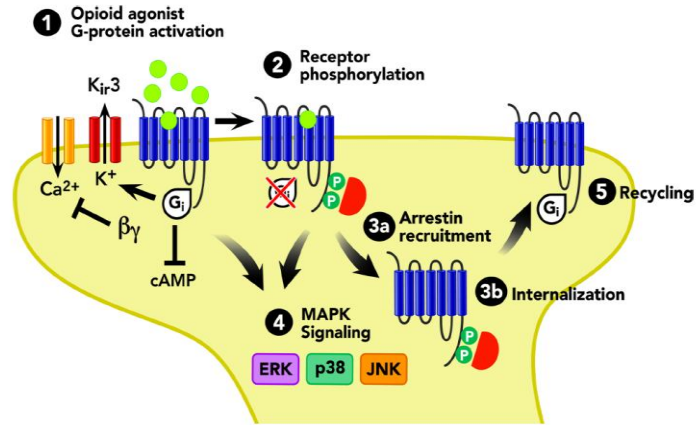


**Figure1. Opioid receptor-mediated signal pathways (Al Hasani and Bruchas, 2011)**

ORs are present in the peripheral and central nervous systems. All the three ORs are distributed in the striatum and dorsal horn of the spinal cord, but some regions are abundant in one receptor, for example, the thalamic nuclei for MOPR and the claustrum for KOPR (Mansour et al., 1995). This system responds to environmental stimuli (stress, pain and pleasurable stimuli) to regulate sensory inputs, reward and autonomic functions, such as respiration, thermoregulation and gastrointestinal motility (Olson et al., 1991). Studies with selective agonists and antagonists and knockout mice have shown that ORs have many physiological and pharmacological effects. The most well-studied ORs is the MOPR. MOPR agonists are highly efficacious analgesics, but also produce constipation, respiratory depression, tolerance and addiction (Koob and Bloom, 1988; Kong et al., 1994). DOPR agonists have antidepressant activities and are also analgesics, but with low efficacy. KOPR agonists are analgesics and anti-pruritic agents, but induce sedation and dysphoria (Dosaka-Akita et al., 1993). In MOPR knockout (KO) mice, morphine does not produce analgesia, reward, withdrawal, respiratory depression, constipation and immunosuppression. DPDPE does not induce spinal analgesia in DOPR KO mice. U50,488H-induced antinociception, aversion and hypolocomotion are abolished in KOPR KO mice [reviewed in (Kieffer, 1999)].

### **Biased agonism at opioid receptors**

Recent studies have supported the concept of biased agonism for GPCRs (Pradhan et al., 2012; Marti-Solano et al., 2013). Early studies on  $\beta$ -arrestin2<sup>-/-</sup> mice by Bohn et al. have demonstrated that the analgesic effects of morphine is enhanced by  $\beta$ -arrestin2 deletion, whereas respiratory depression and inhibition of GI transit induced by

morphine were decreased, suggesting that while the analgesic effect of MOPR activation is mediated by the G protein pathway, the GI transit inhibition and respiratory depression may be mediated at least in part by the  $\beta$ -arrestin pathway (Bohn et al., 1999). Subsequent studies have revealed that different ligands can preferentially activate G protein- or  $\beta$ -arrestin-mediated pathways, resulting in ligand-dependent responses. This notion is useful for drug development in that drugs can be developed which act preferentially on the pathways resulting in beneficial effects, while producing lower degrees of the unwanted side effects. Many studies have since shown functional selectivity of agonists for the MOPR, DOPR and KOPR (Pradhan et al., 2012).

For the MOPR, morphine and fentanyl drive different pathways to affect dendritic spine stability in hippocampus neurons. Morphine enhanced ERK1/2 phosphorylation via PKC and activated ERK1/2 stayed in the cytosol, leading to instability of dendritic spines. In contrast, fentanyl stimulated ERK1/2 through  $\beta$ -arrestin2 pathway and activate ERK1/2 were translocated into nucleus, leading to a cascade of events that increased the stability of dendritic spines (Zheng et al., 2010a; Zheng et al., 2010b; Zheng et al., 2013). TRV130 was recently reported to be a G protein-biased MOPR agonist, which was more potent and efficacious than morphine in producing analgesia, while causing less GI transit inhibition and respiratory depression than morphine (DeWire et al., 2013).

For the DOPR, chronic SNC80 treatment induced receptor internalization and degradation, leading to tolerance to anxiolysis, locomotion and analgesia, while ARM390 did not induce internalization and caused only analgesic tolerance (Pradhan et al., 2009; Pradhan et al., 2010). In addition, etorphine treatment resulted in  $\beta$ -arrestin1-mediated hDOPR endocytosis, whereas DPDPE and deltorphin I caused  $\beta$ -arrestin1-mediated

hDOPR desensitization and this agonist-dependent DOPR regulations may be due to different DOPR conformations induced by agonists (Aguila et al., 2012).

For the KOPR, 6'-GNTI was found to activate G protein, but did not recruit  $\beta$ -arrestin2 in HEK293T cells and primary striatal neurons. Moreover, 6'-GNTI antagonized KOPR agonists-induced  $\beta$ -arrestin2 recruitment, demonstrating that 6'-GNTI is a G protein-biased ligand (Rives et al., 2012; Schmid et al., 2013). RB64 was reported to be a G protein-biased KOPR agonist. RB64 was tested in WT type and  $\beta$ -arrestin2 KO mice. This study showed analgesia and aversion caused by RB64 was G protein-mediated, while motor incoordination, sedation and anhedonia was due to  $\beta$ -arrestin signaling (White et al., 2015).

## Scientific rationale

Our lab has long been interested in regulation, trafficking and signaling of the KOPR. The major theme of this dissertation is to focus on two events following KOPR activation: neurite outgrowth and KOPR phosphorylation. Studies for Chapter 1 on KOPR agonist-induced neurite outgrowth provide evidence for the regulatory role of KOPR in neuronal development and mechanistic insights for the process. Studies for Chapter 2 enhance our understanding of molecular mechanisms of agonist-promoted KOPR phosphorylation *in vitro* and the role of PKC in the pharmacological effects of the KOPR agonist U50,488H *in vivo*.

Previous studies have suggested that the KOPR plays a role in the neurite outgrowth and neurogenesis (Bi et al., 2006; Kim et al., 2006; Hahn et al., 2010; Tsai et al., 2010; Wei, 2011). Our lab showed that U50,488H induced internalization, but etorphine did not in Chinese hamster ovary (CHO) cells stably transfected with the human KOPR (hKOPR), although both were potent full agonists in enhancing [<sup>35</sup>S]GTPγS (Li et al., 2003). My results showed that U50,488H induced neurite outgrowth to a greater extent than etorphine in N2A-3HA-hKOPR cells. Subsequently, I tested the hypothesis that U50,488 and etorphine activate different signal pathways to cause different levels of neurite outgrowth. We examined several molecules known to be involved in neurite outgrowth or interact with the KOPR for their involvement in the effects of the two agonists (the specific aim 1).

Many studies have shown phosphorylation of agonist-activated GPCR causes receptor desensitization, receptor internalization and arrestin-dependent signaling (Lefkowitz and Shenoy, 2005). Thus, phosphorylation states of GPCRs can regulate

signaling and trafficking of the receptors. Agonist-induced KOPR phosphorylation has not been fully characterized yet. Our lab showed previously that U50,488H induced phosphorylation of the hKOPR stably expressed in CHO cells using metabolic labeling with  $^{32}\text{P}$ -orthophosphate (Li et al., 2002). U50,488H enhances hKOPR phosphorylation to much greater extents than etorphine and etorphine reduces U50,488H-promoted KOPR phosphorylation (Li et al., 2003). Rat KOPR(S369A)-GFP mutant did not undergo U50,488H-induced phosphorylation as detected with phosphospecific antibody against the KOPR peptide 359-372 containing pS369 in HEK cells (McLaughlin et al., 2003). Recently, our lab demonstrated that U50,488H caused mKOPR phosphorylation at S356, T357, T363 and S369 (Chen et al., 2016). Phosphospecific antibodies were generated at each site and purified antibodies were found to be highly specific in immunoblotting for phosphorylated mKOPR (Chen et al., 2016). For the chapter 2, molecular mechanisms of agonist-induced KOPR phosphorylation *in vitro* and PKC-related KOPR-mediated pharmacological effect *in vivo* were examined in the specific aim 2.

Specific aims were as follows:

**Specific Aim 1. Examine the mechanisms underlying KOPR agonist-induced neurite outgrowth. I investigated:**

Study 1: the role of KOPR in KOPR agonist-promoted neurite outgrowth by using the selective KOPR antagonist norBNI and untransfected neuro2a cells

Study 2: the role of G proteins in KOPR-induced neurite outgrowth by use of pertussis toxin (PTX) to inactivate  $\text{Gi}/\text{o}_\alpha$  protein and gallein and  $\beta\text{ARKct}$  to inhibit  $\text{G}_{\beta\gamma}$  subunits

Study 3: the role of  $\beta$ -arrestins in KOPR-promoted neuronal differentiation by using siRNAs targeting  $\beta$ -arrestin1 and  $\beta$ -arrestin2

Study 4: the roles of protein kinases in KOPR-mediated neurite outgrowth by using inhibitors of MAPK kinase (ERK1/2, and p38), PKC and PI3K

Study 5: the roles of interacting proteins in KOPR-induced neuronal extension by employing siRNAs targeting KOPR-interacting proteins (14-3-3 $\zeta$  and GEC1) and G $\alpha$ -interacting proteins (GRIN1/2)

Study 6: the role of Rap1-STAT3 pathway by use of siRNA and dominant negative mutant.

**Specific Aim 2. Characterize agonist-induced KOPR phosphorylation *in vitro* and the role of PKC in KOPR-mediated effects *in vivo***

Study 1: examine time-course and dose-response relationship of U50,488H-promoted KOPR phosphorylation *in vitro*

Study 2: characterize the involvement of GRKs in U50,488H-promoted KOPR phosphorylation *in vitro*

Study 3: examine PKC-mediated KOPR phosphorylation *in vitro*

Study 4: investigate if PKC participated in U50,488H-promoted KOPR phosphorylation in mouse brains.

Study 5: determine the role of PKC in pharmacological effects of KOPR in mice (analgesia, antipruritic effect, sedation, motor incoordination and aversion)

**CHAPTER 1**  
**STUDIES ON NEURITE OUTGROWTH**  
**FOLLOWING KAPPA OPIOID RECEPTOR ACTIVATION**

**Introduction**

Activation of the KOPR, one of the three opioid receptors, produces many effects such as analgesia, water diuresis, hypothermia, sedation, dysphoria and antipruritic effects [reviewed in (Liu-Chen, 2004)]. The cellular mechanisms following activation of KOPR include Gi/o protein-dependent pathways such as inhibition of adenylyl cyclases and Ca<sup>2+</sup> inward current, and activation of K<sup>+</sup> channels and p44/42 MAP kinases (early phase) (Law et al., 2000; Al Hasani and Bruchas, 2011). In addition, activated KOPR is phosphorylated by G protein-coupled receptor kinases (GRKs), leading to arrestin recruitment, which results in agonist-dependent KOPR desensitization, internalization and down-regulation (Liu-Chen, 2004).  $\beta$ -arrestin-dependent signaling pathways are also activated, including phosphorylation of p44/42 MAP kinases (late phase) and p38 MAP kinase (Law et al., 2000; Al Hasani and Bruchas, 2011).

Neuronal development involves morphological changes of soma and neurite outgrowth to become functional axons and dendrites (Mortimer et al., 2008). Neurite outgrowth is an essential early process for differentiation of precursor cells into mature neurons bearing neurites (axons and dendrites). Neurite outgrowth is composed of morphological (the neurite extension) and biochemical changes. Many neurotransmitters and receptors have been shown to be involved in neuronal development (such as glutamate, dopamine and cannabinoid receptors) (Knapp et al., 1995; van Kesteren and Spencer, 2003; Mattson, 2008; Gaffuri et al., 2012). Receptor-mediated G protein-dependent signaling is one mechanism to regulate cytoskeletal dynamics (Flavell and

Greenberg, 2008). Particularly,  $G_{i/o}$  proteins are rich in the brain and are abundant in neuronal growth cones where cytoskeletons have high remodeling activity (He et al., 2006). Opioid receptors have been reported to be involved in neuronal differentiation. Axonal trafficking of KOPR mRNA is involved in neurite outgrowth (Bi et al., 2006; Wei, 2011). During embryonic spinal cord development, increasing KOPR protein level and KOPR signaling contributed to EGF-induced neurite outgrowth (Tsai et al., 2010). Mu- and kappa-opioids induced differentiation of embryonic stem cells (ESC) and neural progenitors (NPs) via ERK1/2 signaling (Kim et al., 2006; Hahn et al., 2010). These studies have indicated that the KOPR plays a role in neuronal differentiation and neurogenesis.

Our previous study showed that the KOPR agonist U50,488H induced KOPR internalization, which was mediated by GRKs and arrestins (Li et al., 1999; Li et al., 2003). In contrast, etorphine did not promote KOPR internalization, although like U50,488H, etorphine showed high efficacy in enhancing [ $^{35}$ S]GTP $\gamma$ S binding in CHO cells stably transfected with the KOPR (Li et al., 2003) and in N2A-3HA-hKOPR cells (DiMattio et al., 2015). Here we found that U50,488H induced neurite outgrowth to greater extents than etorphine in N2A-3HA-hKOPR cells. Subsequently, we determined if the differences between the two agonists are due to actions through different signaling pathways and/or differences in efficacy.

## Materials and Methods

### Materials

(-)-U50,488H, etorphine and NorBNI were obtained from the Drug Supply Program of the National Institute on Drug Abuse (Bethesda, MD). Pertussis toxin (PTX) was purchased from List Biological Laboratories, Inc. (Campbell, CA). PD98059, SB203580, GF109203X, wortmannin, G418 and anti- $\beta$ III-tubulin antibody were purchased from Sigma-Aldrich (St. Louis, MO). Antibodies against ERK1/2 phosphorylated at Thr202 and Tyr204 and total ERK1/2 were from Cell Signaling Technology (Danvers, MA). Fetal bovine serum (FBS), minimum essential medium (MEM) and Hoechst 33258 were from Life Technologies (Carlsbad, CA). Goat anti-mouse IgG conjugated with infrared dye 680 and goat anti-rabbit IgG conjugated with infrared dye 800CW were purchased from LI-COR Biosciences (Lincoln, NE). HA-14-3-3 $\zeta$  in pcDNA3 was obtained from Addgene Inc. (Cambridge, MA). Rabbit polyclonal anti-GAPDH antibody conjugated with horseradish peroxidase (ab9385) was obtained from Abcam (Cambridge, MA). Rabbit anti-14-3-3 $\zeta$  antibody and GRK2 antibody (sc562) were purchased from Santa Cruz Biotechnology (Santa Cruz, CA). Antibodies against  $\beta$ -arrestin1 and  $\beta$ -arrestin2 were generous gifts from Dr. Jeffrey Benovic of Thomas Jefferson University (Philadelphia, PA). A cDNA clone of the C-terminal 194aa of the beta-adrenergic receptor kinase ( $\beta$ ARKct) (GRK2 amino acids 495-689) in the vector pRK5 was kindly given by Dr. Walter Koch of Temple University (Philadelphia PA). Gallein was kindly provided by Dr. Jay McLaughlin of Torrey Pines Institute (St. Lucie, FL). cDNA constructs of Rap1 and Rap1-dominant negative form were given generously by Dr. Xin-Yun Huang of Weill Cornell Medical College (New York, NY).

siRNAs against mouse  $\beta$ -arrestin1,  $\beta$ -arrestin2, 14-3-3 $\zeta$  (sc-29585), GEC1, GRIN1 and GRIN2 were purchased from Santa Cruz Biotechnology (Santa Cruz, CA) and each is a mixture of three or four siRNAs. The sequences of mouse  $\beta$ -arrestin1 siRNAs are as follows: GCAUCAUCGUUCCUACAAtt, CUAGUCAGCUUAUCUGAUAtt, CAUGCCCAGUGUUUGUUGUtt, and UGAACC UCCUACAUUUCAUtt. The sequences of mouse  $\beta$ -arrestin2 siRNAs are as follows: ACUGCAAGCUCACCGUGUA tt, CCAAGACCGUCAAGAAGAAtt, and CCAACCUCAUCGAAUUCGAtt. The sequences of mouse 14-3-3 $\zeta$  siRNAs are as follows: CUGCUGGUGAUGACAAGAATT, CCAUGUCUAAGCAAAGAAATT, and CCUCAGUACUUUACAGAAATT. The sequences of mouse GRIN1 siRNAs are as follows: GAAAGGGAAUCCUGUUAACtt, GUGUGC CAGGAUUGAUGUAAtt and CUACUAACUGUCACAGUAUtt. The sequences of mouse GRIN2 siRNAs are as follows: CACUCAGACUUGGUACAUAAtt, CCAACCGU AGAACUAGAAGtt and GGAUGAAAUCCACUGUAAtt. Mouse STAT3 siRNA was bought from Qiagen (Hilden, Germany) and the sequences are GAGGGUCUCGGAAA UUUAATT, UAAAAUUUCCGAGACCCUCTG.

### **Cell Culture**

3xHA-tagged human KOPR (3HA-hKOPR) was cloned into the vector pcDNA3. Clonal Neuro2a cells stably transfected with 3HA-hKOPR were generated (N2A-3HA-hKOPR). Cells were grown in 10% FBS, 2.2 g/L NaHCO<sub>3</sub>, 110 mg/L pyruvic acid, 2 mg/mL G418, MEM and 100 units/ml penicillin/ streptomycin in a humidified atmosphere with 5% CO<sub>2</sub>, 95% air at 37°C. Saturation binding of [<sup>3</sup>H]diprenorphine to membranes was performed and K<sub>d</sub> and B<sub>max</sub> values were determined to be 0.12 ± 0.001

nM and  $0.76 \pm 0.07$  pmole/mg (mean  $\pm$  s.e.m., n=3), respectively.  $K_i$  values of U50,488H and etorphine were determined to be  $3.09 \pm 1.12$  and  $0.73 \pm 1.12$ nM (mean  $\pm$  s.e.m., n=3), respectively, by competitive inhibition of [ $^3$ H]diprenorphine binding assay. Both U50,488H and etorphine enhanced [ $^{35}$ S]GTP $_{\gamma}$ S binding with EC $_{50}$  values of  $28.2 \pm 1.2$  and  $2.95 \pm 1.27$ nM (mean  $\pm$  s.e.m., n=3), respectively. Emax value of etorphine was  $72.2 \pm 1.9\%$  of that of U50,488H.

### **Neurite outgrowth assay**

Cells were seeded at  $5 \times 10^4$  cells/well in 6-well plates and grown for 2 days. For dose-response experiments, cells were treated with U50,488H or etorphine at indicated concentration and examined for neurite outgrowth as described below. For treatment with various inhibitors, cells were treated with vehicle or one of the following compounds, including norBNI (1  $\mu$ M), PTX (50 ng/ml, 1 h), gallein (50  $\mu$ M) and inhibitors of various kinases (PD98059, SB203580, GF109203X and wortmannin) and vehicle, 10  $\mu$ M U50,488H or 1  $\mu$ M etorphine was added for another 10 min. For experiments requiring transfection, cells were transfected with siRNAs (40 pmole) against  $\beta$ -arrestin1,  $\beta$ -arrestin2, 14-3-3 $\zeta$ , GEC1, GRIN1, GRIN2 or STAT3 or cDNAs (1.6  $\mu$ g) of  $\beta$ ARKct, 14-3-3 $\zeta$  or GEC1, Rap1 or Rap1-DN with Lipofectamine 2000 in 6-well plates. Forty-eight hours later, cells were treated with vehicle, 10  $\mu$ M U50,488H or 1  $\mu$ M etorphine. Incubation with an agonist lasted 10 min unless indicated otherwise.

Following treatment with vehicle or an agonist, cells were grown in 0.1% FBS-containing medium for neuronal differentiation for 24 hr. Cells were fixed with 4% paraformaldehyde and then stained with anti- $\beta$ III-tubulin antibodies (1:1000) followed by

Alexa Fluor 488-conjugated goat anti-mouse IgG secondary antibody (1:1000) and Hoechst 33258 (1:10,000).  $\beta$ III-tubulin (a neuronal marker) staining allowed software to trace neurite lengths. Hoechst 33258 (a nucleus marker) was used for cell number counting. Cells were examined with a fluorescence microscope (Nikon Eclipse TE3000) and images randomly captured. Neurite lengths were analyzed with Neurite-Tracer ImageJ plug-in software. The software provided the total neurite length of neurons and the number of neurons in one image. The average neurite length was obtained by dividing the total neurite length by the cell number. For all neurite outgrowth experiments, 700-1000 cells/ each group in each experiment were analyzed. Average neurite lengths of treated groups were normalized against the control untreated group. Each experiment was performed at least 3 times.

### **Western blotting**

Forty-eight hours after cells were transfected with siRNA against  $\beta$ -arrestin1,  $\beta$ -arrestin2 or 14-3-3 $\zeta$ , or the cDNA construct of  $\beta$ ARKct or 14-3-3 $\zeta$ , cells were lysed with 2x Laemmli sample buffer (4% SDS, 100 mM DTT, 10% glycerol, 62.5 mM Tris, 0.01% bromophenol blue, pH6.8) for immunoblotting. For ERK1/2 activation experiments, cells were left untreated or treated with PTX (200  $\mu$ g/ml, 2 hr, 37 °C) and subsequently 100 nM U50,488H, 10 nM etorphine or vehicle was added for 5 min or 30 min. Cells then were lysed in Laemmli sample buffer, cell lysate was subject to 8% SDS-PAGE and resolved protein bands were then transferred onto nitrocellulose membranes. Membranes were incubated with primary antibodies against  $\beta$ -arrestin1 (1:5000),  $\beta$ -arrestin2 (1:6000), GRK2 (1:2000, to detect  $\beta$ ARKct), 14-3-3 $\zeta$  (1:2000), pERK1/2 (1:1000) and total

ERK1/2 (1:1000) overnight followed by goat anti-mouse IgG conjugated with infrared dye 680 or goat anti-rabbit IgG conjugated with infrared dye 800CW secondary antibodies (1:10,000). Images were captured with the Odyssey Infrared Imaging System (LI-COR Biosciences, Lincoln, NE).

### **Data Analysis and Statistics**

Data were graphed and analyzed with GraphPad Prism5 (La Jolla, CA). One-way ANOVA was used to analyze one-factor experiment, followed by Newman-Keuls post-test. Two-way ANOVA and Bonferroni *post-hoc* analysis was used to analyze two-factor experiments.

## Results

### **U50,488H- and etorphine-induced neurite outgrowth.**

We examined dose-response relationship of U50,488H and etorphine in inducing neurite outgrowth. The ranges of concentrations (0.01, 0.1, 1 and 10  $\mu\text{M}$ ) used were about 3- to 300-fold of the  $\text{EC}_{50}$  values of U50,488H and etorphine in promoting [ $^{35}\text{S}$ ]GTP $_{\gamma}\text{S}$  binding, which were 30 nM and 3.4 nM, respectively (DiMattio et al., 2015). Cells were treated with the agonists and then grown in medium plus 0.1% FBS for differentiation for 24 hr. The three concentrations of U50,488H (0.1, 1 and 10  $\mu\text{M}$ ) and two concentrations of etorphine (1 and 10  $\mu\text{M}$ ) significantly increased neurite lengths. U50,488H at 0.1, 1 and 10  $\mu\text{M}$  induced longer neuronal processes than etorphine at each concentration (Figure 2) (two-way ANOVA, agonist main effect  $F_{1,24}=50.13$ ,  $p<0.0001$ ; dose main effect  $F_{4,24}=21.15$ ,  $p<0.0001$ ; agonist x dose interaction  $F_{4,24}=9.71$ ,  $p<0.0001$ ). The doses that produced the largest responses for each drug (10  $\mu\text{M}$  U50,488H and 1  $\mu\text{M}$  etorphine) were used for all the following experiments. Etorphine at 1  $\mu\text{M}$  and 10  $\mu\text{M}$  showed similar response levels, thus 1  $\mu\text{M}$  etorphine was chosen for the following experiments. Due to their affinity and  $\text{EC}_{50}$  values in [ $^{35}\text{S}$ ]GTP $_{\gamma}\text{S}$  binding, we did not use higher concentrations. Untransfected N2A cells did not produce any neurite outgrowth following U50,488H and etorphine treatment (Figure 3).

### **U50,488H- and etorphine-induced neurite outgrowth is mediated by the KOPR.**

Pretreatment with the selective KOPR antagonist NorBNI before agonist treatment significantly reduced U50,488H- and etorphine-promoted neurite outgrowth, indicating that the effects are mediated by the KOPR (Figure 4) (two-way ANOVA,

agonist main effect  $F_{2,12}=51.24$ ,  $p<0.0001$ ; NorBNI main effect  $F_{1,12}=38.81$ ,  $p<0.0001$ ;  
agonist x NorBNI interaction  $F_{2,12}=6.69$ ,  $p=0.0112$ ).

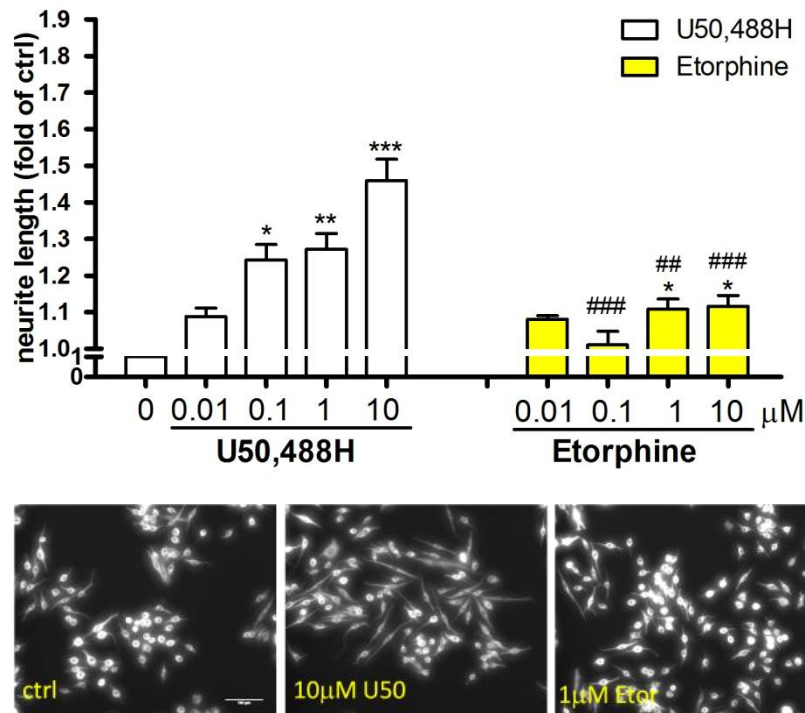


**Figure 2. Effects of U50,488H and etorphine on neurite outgrowth: dose-response relationship** N2A-3HA-hKOPR cells were treated with U50,488H and etorphine at different concentrations (0.01 μM, 0.1 μM, 1 μM and 10 μM) for 10 min and then cells were cultured in 0.1% serum medium for 24 hr, a condition that induces differentiation. In each experiment, neurite lengths of 700-1000 cells were measured using the Neurite-Tracer NIH ImageJ plugin software. Representative images are shown in the bottom. Each value represents the mean ± S.E.M of 3-4 independent experiments. Data were analyzed with two-way ANOVA followed by Bonferroni *post-hoc* test (\*: $p < 0.05$ , \*\*: $p < 0.01$ , \*\*\*: $p < 0.001$ , compared to the untreated group; ##: $p < 0.01$ , compared 1 μM U50,488H vs 1 μM etorphine; ###: $p < 0.001$ , compared 0.1 μM U50,488H vs 0.1 μM etorphine and 10 μM U50,488H vs 10 μM etorphine).

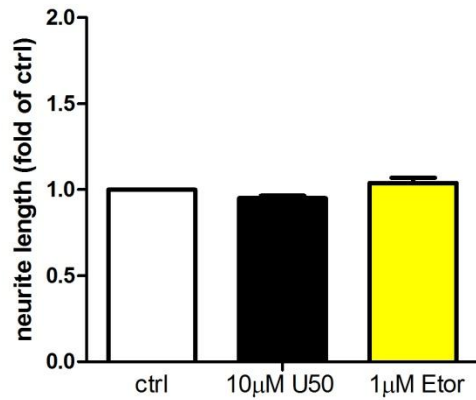


**Figure 3. Effect of KOPR agonists on untransfected N2A cells** Untransfected N2A cells were incubated with vehicle, 10 µM U50,488H or 1 µM etorphine for 10 min. Cells were then cultured in 0.1% serum medium for 24 hr and neurite lengths were measured. Each value represents the mean  $\pm$  S.E.M. of 3 independent experiments and 700-1000 cells/ group in each experiment were measured. Data were analyzed by one-way ANOVA followed by Newman-Keuls *post hoc* test.

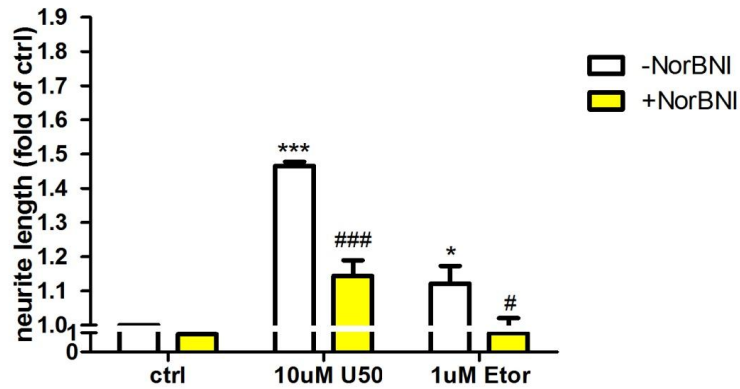


**Figure 4. U50,488H- and etorphine-induced neurite outgrowth is KOPR-mediated.**

N2A-3HA-hKOPR cells were pre-treated with the KOPR antagonist norBNI (1  $\mu$ M) or vehicle for 10 min and 10  $\mu$ M U50,488H, 1  $\mu$ M etorphine or vehicle was added for an additional 10 min. Cells were then cultured in 0.1% serum medium for 24 hr and neurite lengths were measured. Each value represents the mean  $\pm$  S.E.M. of 3 independent experiments and 700-1000 cells/ group in each experiment were measured. Data were analyzed by two-way ANOVA followed by Bonferroni *post-hoc* test (\*: $p$ <0.05, \*\*\*: $p$ <0.001, compared to the no NorBNI-control group; #: $p$ <0.05, compared to the no NorBNI-1  $\mu$ M etorphine group; ###: $p$ <0.001, compared to the no NorBNI-10  $\mu$ M U50,488H alone group).

**Gi/o<sub>α</sub> proteins are involved in U50,488H- and etorphine-induced neurite outgrowth, but not G<sub>βγ</sub> proteins.**

KOPR is a Gi/o-coupled receptor. G protein is a heterotrimer composed of G<sub>α</sub> and G<sub>βγ</sub>. Here, we examined whether G<sub>α</sub> and G<sub>βγ</sub> were involved in U50,488H- or etorphine-induced neurite outgrowth. Pretreatment with PTX, which blocks Gi/o<sub>α</sub>-mediated signaling, completely abolished U50,488- and etorphine-induced neurite outgrowth (Figure 5A) (two-way ANOVA, agonist main effect  $F_{2,18}=8.85$ ,  $p=0.0021$ ; PTX main effect  $F_{1,18}=31.32$ ,  $p<0.0001$ ; agonist x PTX interaction  $F_{2,18}=6.46$ ,  $p=0.0077$ ). This result indicates a critical role of Gi/o<sub>α</sub> in this process.

To determine if G<sub>βγ</sub> complex is involved, the G<sub>βγ</sub> blocker gallein (50 μM) or vehicle was applied to cells for 30 min before agonist treatment. There was no statistically significant difference between vehicle and gallein treatments (Figure 5B) (two-way ANOVA, agonist main effect  $F_{2,24}=42.49$ ,  $p<0.0001$ ; gallein main effect  $F_{1,24}=0.37$ ,  $p=0.5469$ ). βARKct (the C-terminal 194aa of βARK or GRK2) is a G<sub>βγ</sub>-binding peptide and has been used to inhibit G<sub>βγ</sub> signaling (Pitcher et al., 1992). βARKct or the vector pRK5 was transfected into cells and 2 days later agonist-induced neurite outgrowth was examined. Expression of βARKct, which was confirmed by immunoblotting, did not inhibit U50,488H- or etorphine-induced neurite outgrowth (Figure 5C) (two-way ANOVA, agonist main effect  $F_{2,12}=10.41$ ,  $p=0.0024$ ; βARKct main effect  $F_{1,12}=0.13$ ,  $p=0.725$ ). Transfection with the vector control (pRK5) showed no difference with the untransfected group (data not shown). These results indicate G<sub>βγ</sub> is not involved in KOPR agonist-induced differentiation.

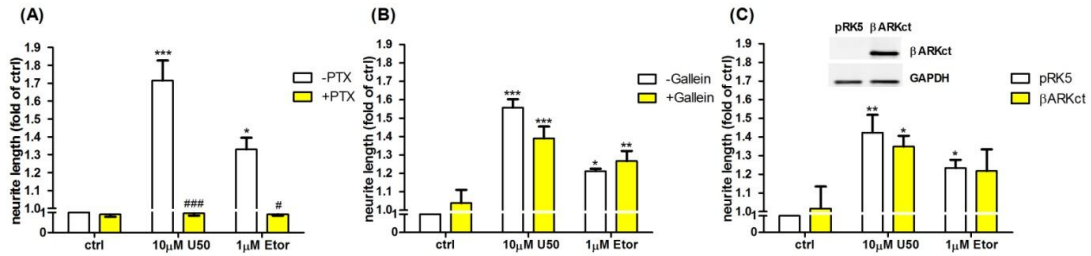


**Figure 5. The roles of G proteins in U50,488H- and etorphine-induced neurite outgrowth** (A) N2A-3HA-hKOPR cells were treated with 50 ng/ml PTX or vehicle for 1 h and vehicle, 10 µM U50,488H or 1 µM etorphine was added for another 10 min. (B) Cells were treated with the  $G_{\beta\gamma}$  inhibitor gallein (50 µM) or vehicle for 30 min and U50,488H, etorphine or vehicle was administered for another 10-min. (C) Cells were transfected with  $\beta$ ARKct or the vector pRK5 using Lipofectamine 2000. Forty eight hours later, cells were treated with U50,488H, etorphine or vehicle. Overexpression of  $\beta$ ARKct was confirmed by immunoblotting using GRK2 antibody because  $\beta$ ARKct is a.a.495-689 of GRK2 with Mr of ~27kDa. (A)(B)(C) Cells were cultured in 0.1% serum medium for 24 hr and neurite lengths were measured. Each value represents the mean  $\pm$  S.E.M (n= 3-5, 700-1000 cells/ group/experiment). Data were analyzed by two-way ANOVA followed by Bonferroni *post-hoc* test (\*: $p$ <0.05, \*\*: $p$ <0.01, \*\*\*: $p$ <0.001, compared to untreated ctrl group; #: $p$ <0.05, compared to no PTX-1 µM etorphine group; ###: $p$ <0.001, compared to no PTX- 10 µM U50,488H group).

**$\beta$ -arrestins were not involved in U50,488H- and etorphine-induced neurite outgrowth.**

Transfection of  $\beta$ -arrestin1 siRNA, which reduced  $\beta$ -arrestin1 by 60% as determined by immunoblotting, did not affect U50,488H- and etorphine-induced neurite outgrowth (Figure 6A) (two-way ANOVA, agonist main effect  $F_{2,21}=31.8$ ,  $p<0.0001$ ; si $\beta$ -arrestin1 main effect  $F_{1,21}=4.48$ ,  $p=0.05$ ; agonist x si $\beta$ -arrestin1 interaction  $F_{2,21}=0.35$ ,  $p=0.71$ ).

$\beta$ -arrestin2 siRNA, which reduced  $\beta$ -arrestin2 level by 30%, increased neurite length in the control, U50,488H- and etorphine-treated groups (Figure 6B) (two-way ANOVA, agonist main effect  $F_{2,21}=25.82$ ,  $p<0.0001$ ; si $\beta$ -arrestin2 main effect  $F_{1,21}=10.3$ ,  $p=0.004$ , agonist x si $\beta$ -arrestin2 interaction  $F_{2,21}=0.01$ ,  $p=0.99$ ). Control siRNA group showed no significant difference from non-transfected group (data not shown). Thus,  $\beta$ -arrestin2 itself may inhibit neurite outgrowth, implying that  $\beta$ -arrestin2 may play a negative regulatory role in the KOPR-independent neurite outgrowth.

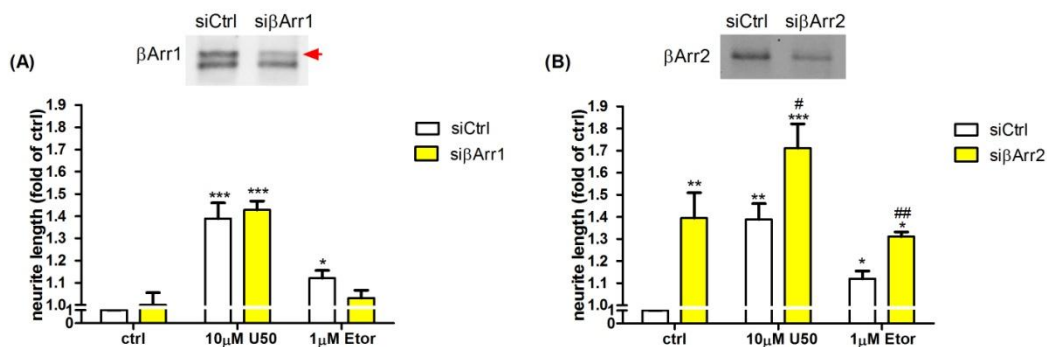


**Figure 6. Roles of  $\beta$ -arrestin1 and  $\beta$ -arrestin2 in U50,488H- and etorphine-induced neurite outgrowth** N2A-3HA-hKOPR cells were transfected with  $\beta$ -arrestin1 and  $\beta$ -arrestin2 siRNA or control siRNA (siCtrl) using Lipofectamine 2000. Forty-eighty hours after transfection, cells were treated with vehicle, 10  $\mu$ M U50,488H or 1  $\mu$ M etorphine for 10 min. Cells were then cultured in 0.1% serum medium for 24 hr and neurite lengths were measured. Each value represents the mean  $\pm$  S.E.M (n= 4, 700-1000 cells/ group/ experiment). The data were analyzed by two-way ANOVA followed by Bonferroni *post-hoc* test (\*: $p$ <0.05, \*\*: $p$ <0.01, \*\*\*: $p$ <0.001 compared to control siRNA-vehicle group; #: $p$ <0.05, ##: $p$ <0.01, compared to the corresponding control siRNA group). Knockdown of  $\beta$ -arrestin1 and 2 was confirmed by immunoblotting.

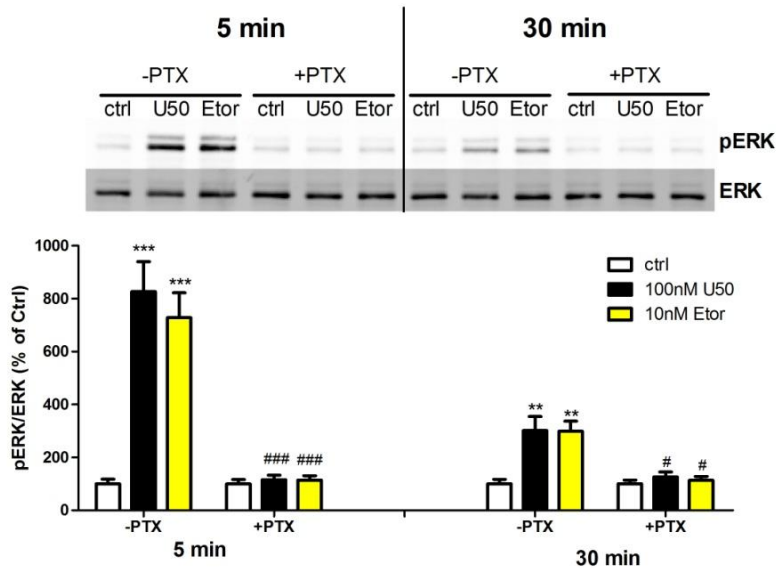
### **ERK1/2 play roles in the KOPR-mediated neurite outgrowth.**

The mitogen-activated protein kinase (MAPK) family regulates a myriad of cellular functions, including cell proliferation and differentiation (Raman et al., 2007). KOPR activation has been shown to activate ERK1/2 and p38 MAPK (Belcheva et al., 1998; Bruchas et al., 2006). Incubation of N2A-3HA-hKOPR cells with U50,488H and etorphine for 5 min and 30 min increased pERK1/2 levels and PTX blocked KOPR agonist-induced ERK1/2 phosphorylation (Figure 7A) (two-way ANOVA, for 5 min: agonist main effect  $F_{2,12}=21.44$ ,  $p=0.0001$ ; PTX main effect  $F_{1,12}=77.26$ ,  $p<0.0001$ ; agonist x PTX interaction  $F_{2,12}=19.63$ ,  $p=0.0002$ ; for 30min, agonist main effect  $F_{2,12}=9.24$ ,  $p=0.0037$ ; PTX main effect  $F_{1,12}=24.68$ ,  $p=0.0003$ ; agonist x PTX interaction  $F_{2,12}=6.18$ ,  $p=0.0143$ ). This indicates that KOPR-induced ERK1/2 activation is mediated by Gi/o protein. Knockdown of  $\beta$ -arrestin1 or 2 did not affect U50,488H- or etorphine-induced ERK activation at 5 min and 30 min (data not shown). This result indicates KOPR-mediated ERK activation is not mediated by  $\beta$ -arrestin.

We used inhibitors of ERK1/2 kinase and p38 MAPK kinase (PD98059 and SB203580, respectively) to examine their involvements in neurite outgrowth. Treatment with PD98059 (50  $\mu$ M, 30 min), which completely abolished U50,488H- or etorphine-induced ERK activation (data not shown), reduced U50,488H- and etorphine-induced neurite outgrowth (Figure 7B) (two-way ANOVA, agonist main effect  $F_{2,32}=60.46$ ,  $p<0.0001$ ; ERK1/2 kinase inhibitor main effect  $F_{1,32}=14.62$ ,  $p=0.0006$ ; agonist x inhibitor interaction  $F_{2,32}=5.21$ ,  $p=0.011$ ). In contrast, the p38 MAPK kinase inhibitor SB203580 (5  $\mu$ M, 1hr) did not inhibit agonist-induced neurite outgrowth (Figure 8) (two-way ANOVA, agonist main effect  $F_{2,11}=25.88$ ,  $p<0.0001$ ; inhibitor main effect  $F_{1,11}=3.31$ ,

$p=0.09$ ; agonist x inhibitor interaction  $F_{2,11}=1.79$ ,  $p=0.21$ ). These results indicate that U50,488H- and etorphine-induced neurite outgrowth is mediated in part by the ERK1/2 signal pathways, but not by the p38 MAPK pathway.

(A)



(B)

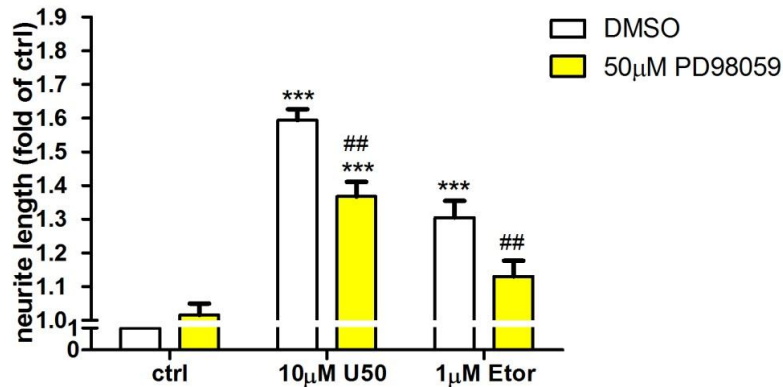


**Figure 7. (A) U50,488H and etorphine enhanced ERK1/2 phosphorylation in PTX-sensitive manner.** N2A-3HA-hKOPR cells were treated with 200 ng/ml PTX or vehicle for 2 h before 5-min or 30-min incubation with vehicle, 100 nM U50,488H or 10 nM etorphine and then lysed with 2X Laemmli sample buffer and subjected into 8% SDS-PAGE. Immunoblotting was performed with pERK1/2 and total ERK1/2 antibodies followed by secondary antibodies. Each value represents the mean  $\pm$  S.E.M (n= 3). Data were analyzed by two-way ANOVA followed by Bonferroni *post-hoc* test. (\*\*: $p < 0.01$ ,

\*\*\*: $p < 0.001$ , compared to no PTX-ctrl group; #: $p < 0.05$ , compared to no PTX-U50 or no PTX-Etor group at 30 min, ###: $p < 0.001$ , compared to no PTX-U50 or no PTX-Etor group at 5 min). (B) **ERK1/2 played a role in U50,488H- or etorphine-induced neurite outgrowth** Cells were pretreated with the MEK1/2 inhibitor PD98059 (50  $\mu$ M) or vehicle (DMSO) for 30 min followed by 10 min incubation with U50,488H, etorphine or vehicle. Cells were differentiated in 0.1% serum medium for 24 hr and neurites were measured. Each value is the mean  $\pm$  S.E.M (n= 4-8). Data are analyzed by two-way ANOVA followed Bonferroni *post-hoc* test (\*\*\*: $p < 0.001$ , compared to DMSO-ctrl group; #: $p < 0.01$ , compared to DMSO-U50 or DMSO-Etor group).

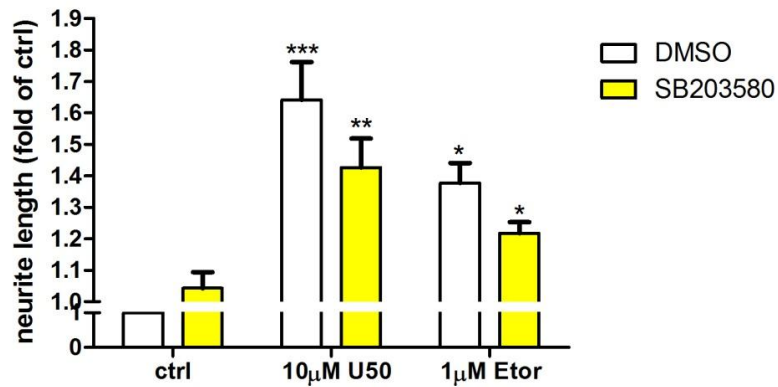


**Figure 8. Effect of p38 MAPK inhibition on U50,488H- and etorphine-induced neurite outgrowth** N2A-3HA-hKOPR cells were pretreated with the p38 inhibitor SB203580 (5 µM) or vehicle (DMSO) for 1 hr followed by U50,488H, etorphine or vehicle incubation for 10 min. Cells were differentiated in 0.1% serum medium for 24 hr and neurites were measured. The data shown are the mean  $\pm$  S.E.M (n= 3) and are analyzed by two-way ANOVA followed by Newman-Keuls *post-hoc* test (\*: $p$ <0.05, \*\*: $p$ <0.01, \*\*\*: $p$ <0.001, compared to the DMSO-ctrl group).

## **Lack of involvement of PKC or PI3K signal pathways in KOPR-induced neuronal differentiation**

Activation of KOPR has been shown to inhibit calcium currents through PKC in rat dorsal root ganglion neurons and to activate ERK signaling via PKC in astrocytes (King et al., 1999; Belcheva et al., 2005). The role of PKC in KOPR-mediated neurite outgrowth was examined. The PKC inhibitor GF109203X did not inhibit KOPR agonist-promoted neurite outgrowth (Figure 9) (two-way ANOVA, agonist main effect  $F_{2,12}=79.14$ ,  $p<0.0001$ ; inhibitor main effect  $F_{1,12}=0.03$ ,  $p=0.87$ ; agonist x inhibitor interaction  $F_{2,12}=0.09$ ,  $p=0.91$ ). This data indicate that PKC does not play a role in KOPR-mediated neurite outgrowth.

U50,488H reduced myocyte apoptosis caused by simulated ischemia/reperfusion through PI3K-Akt signal pathway (Tong et al., 2011). Effect of PI3K inhibition on KOPR neuronal differentiation was determined. The PI3K inhibitor wortmannin did not affect KOPR-induced neurite outgrowth (Figure 10) (two-way ANOVA, agonist main effect  $F_{2,18}=13.74$ ,  $p=0.0002$ ; inhibitor main effect  $F_{1,18}=0.73$ ,  $p=0.4$ ; agonist x inhibitor interaction  $F_{2,18}=0.42$ ,  $p=0.66$ ). This result demonstrates that PI3K is not involved in KOPR-promoted neuronal differentiation.

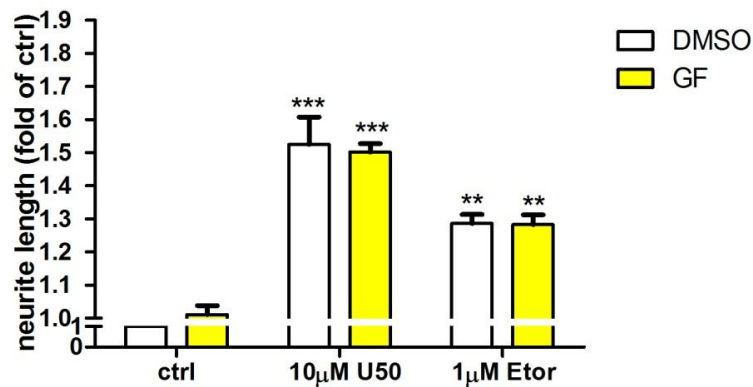


**Figure 9. Effect of PKC inhibition on U50,488H- and etorphine-induced neurite outgrowth** N2A-3HA-hKOPR cells were pretreated with the nonselective PKC inhibitor GF109203X (GF) (2µM) or vehicle (DMSO) for 30 min followed by U50,488H, etorphine or vehicle incubation for 10 min. Cells were differentiated in 0.1% serum medium for 24 hr and neurites were measured. Each value is the mean  $\pm$  S.E.M (n= 3). Data are analyzed by two-way ANOVA followed by Bonferroni *post-hoc* test (\*\*: $p$ <0.01, \*\*\*: $p$ <0.001, compared to the DMSO-ctrl group).

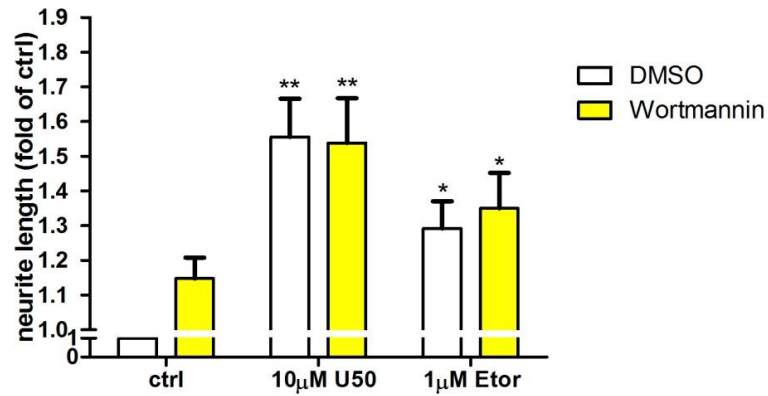


**Figure 10. The role of PI3K in U50,488H- and etorphine-induced neurite outgrowth**  
 N2A-3HA-hKOPR cells were pretreated with the PI3K inhibitor wortmannin (100 nM) or vehicle (DMSO) for 2 hr followed by U50,488H, etorphine or vehicle incubation for 10 min. Cells were differentiated in 0.1% serum medium for 24 hr and neurites were measured. Each value shown is the mean  $\pm$  S.E.M (n= 4) and data are analyzed by two-way ANOVA and Newman-Keuls *post-hoc* test (\*: $p < 0.05$ , \*\*: $p < 0.01$ , compared to the DMSO-ctrl group).

## **The roles of the KOPR interacting proteins 14-3-3 $\zeta$ or GEC1 in U50,488H- and etorphine-induced neurite outgrowth.**

Besides downstream signaling cascades, KOPR interacting proteins may play crucial roles in regulating receptor-mediated signaling. Our lab previously found that KOPR interacted with 14-3-3 $\zeta$  and GEC1, which increase expression of KOPR on plasma membrane by facilitating trafficking of the KOPR along the export pathway (Chen et al., 2006; Li et al., 2012).

14-3-3 proteins are abundant in eukaryotic cells and play important roles in many cellular functions such as cell cycle, apoptosis, differentiation, protein trafficking and neuronal development (Hermeking, 2006; Shikano et al., 2006). We examined if 14-3-3 $\zeta$  affected U50,488H- or etorphine-induced differentiation by overexpression or knockdown of 14-3-3 $\zeta$ , which was confirmed by immunoblotting. Overexpression of 14-3-3 $\zeta$  did not affect U50,488H- or etorphine-induced neurite outgrowth (Figure 11A) (two-way ANOVA, agonist main effect  $F_{2,18}=11.18$ ,  $p=0.0007$ ; 14-3-3 $\zeta$  main effect  $F_{1,18}=0.3$ ,  $p=0.5937$ ; agonist x 14-3-3 $\zeta$  interaction,  $F_{2,18}=0.55$ ,  $p=0.59$ ). Knockdown of 14-3-3 $\zeta$  itself promoted neurite outgrowth and induced longer neurites in U50,488H- and etorphine-treated groups (Figure 11B) (two-way ANOVA, agonist main effect  $F_{2,18}=13.32$ ,  $p=0.0003$ ; si14-3-3 $\zeta$  main effect  $F_{1,18}=84.5$ ,  $p<0.0001$ ; agonist x si14-3-3 $\zeta$  interaction  $F_{2,18}=0$ ,  $p=0.99$ ). These results suggest that 14-3-3 $\zeta$  itself may play a role in neurite outgrowth, but is not involved in KOPR-mediated differentiation.

GEC1 (GABARAPL1) belongs to the microtubule associated protein family and is involved in the process of autophagy, cell proliferation, cell death, neurodegenerative diseases and transport of proteins or vesicles (Le Grand et al., 2011). Whether the

interaction of KOPR with GEC1 affected U50,488H- or etorphine-induced neurite outgrowth was examined by overexpression and siRNA knockdown of GEC1. GEC1 overexpression showed a trend of inducing neurite outgrowth, but the increase did not reach statistical significance. Overexpression of GEC1 did not affect U50,488H- or etorphine-induced neurite outgrowth (Figure 12A) (two-way ANOVA, agonist main effect  $F_{2,12}=9.48$ ,  $p=0.003$ ; GEC1 main effect  $F_{1,12}=1.4$ ,  $p=0.26$ ; agonist x GEC1 interaction  $F_{2,12}=0.7$ ,  $p=0.52$ ). Knockdown of GEC1 showed a trend of increasing neuronal differentiation and did not affect U50,488H- or etorphine-induced neurite outgrowth (Figure 12B). These data suggested GEC1 did not participate in KOPR-mediated neurite outgrowth.

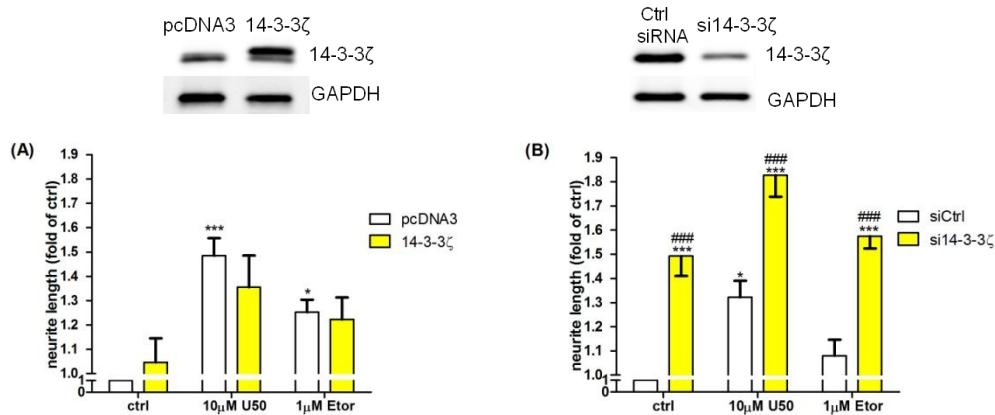


**Figure 11. Role of the KOPR interacting protein 14-3-3ζ in KOPR-mediated neurite outgrowth.** N2A-3HA-hKOPR cells were transfected with pcDNA3, 14-3-3ζ, 14-3-3ζ siRNA or control siRNA (siCtrl) using Lipofectamine 2000 to overexpress or knockdown 14-3-3ζ. Two days after transfection, cells were treated with vehicle, 10 μM U50,488H or 1 μM etorphine for 10 min followed by 24-hr differentiation in 0.1% serum medium. Neurite processes were measured. Each value is the mean ± S.E.M (n= 4) and data are analyzed by two-way ANOVA followed by Bonferroni *post-hoc* test (\*: $p < 0.05$ , \*\*\*: $p < 0.001$ , compared to the ctrl group; ###: $p < 0.001$ , compared to the corresponding control siRNA group). Overexpression and knock down of 14-3-3ζ were confirmed by immunoblotting.

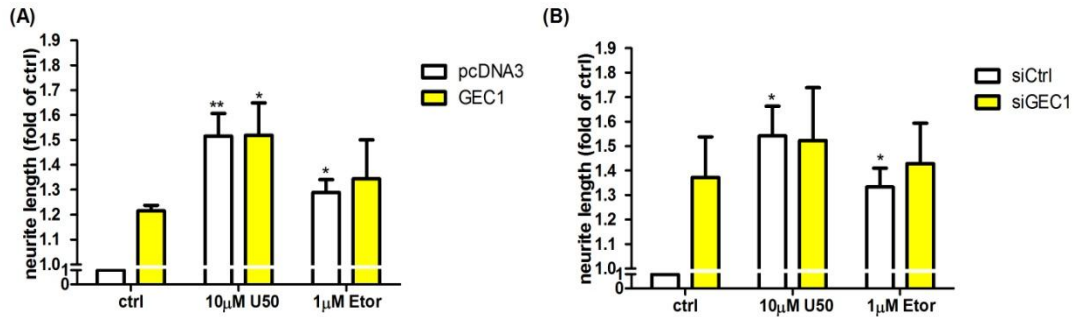


**Figure 12. Role of the KOPR interacting protein GEC1 in KOPR-mediated neurite outgrowth.** N2A-3HA-hKOPR cells were transfected with pcDNA3, GEC1, GEC1 siRNA or control siRNA (siCtrl) using Lipofectamine2000 to overexpress or knockdown GEC1. Two days after transfection, cells were treated with vehicle, 10 µM U50,488H or 1 µM etorphine for 10 min followed by 24-hr differentiation in 0.1% serum medium. Neurite processes were measured. Each value represents the mean± S.E.M (n= 3) and data are analyzed by two-way ANOVA followed by Bonferroni *post-hoc* test (\*: $p < 0.05$ , \*\*: $p < 0.01$ , compared to the pcDNA3-ctrl group or the ctrl siRNA-ctrl group).

## **The role of G protein regulated inducer of neurite outgrowth 1 or 2 (GRIN1 or 2) in U50,488H- or etorphine-induced neurite outgrowth.**

The GRIN family (GRIN1 and 2) has been reported to interact with activated  $G_{\alpha}$  to regulate neurite outgrowth (Chen et al., 1999; Iida and Kozasa, 2004; Nakata and Kozasa, 2005; Masuho et al., 2008). GRIN1 was reported to be involved in MOPR-mediated neurite outgrowth following etorphine treatment in N2a cells (Ge et al., 2009). Our finding that PTX treatment eliminated KOPR agonist-induced neurite outgrowth (Figure 4A) demonstrates the pivotal role of  $G_i/o_{\alpha}$ -proteins in this process. Therefore, we examined if GRIN participated in KOPR-mediated neuronal differentiation. Knockdown of GRIN1 did not affect U50,488H- and etorphine-induced neurite outgrowth (Figure 13A) (two-way ANOVA, agonist main effect  $F_{2,18}=49.47$ ,  $p<0.0001$ ; siGRIN1 main effect  $F_{1,18}=1.66$ ,  $p=0.21$ ; agonist x siGRIN1 interaction  $F_{2,18}=2.59$ ,  $p=0.1$ ). This result indicates that GRIN1 does not play a role in KOPR-mediated neurite outgrowth.

GRIN2 has been found to be involved in neurite outgrowth following activation of the CB1 cannabinoid receptor (Hwangpo et al., 2012). We explored the role of GRIN2 in KOPR-mediated neuronal differentiation. Knockdown of GRIN2 did not affect U50,488H- or etorphine-induced neurite outgrowth (Figure 13B) (two-way ANOVA, agonist main effect  $F_{2,18}=15.67$ ,  $p=0.0001$ ; siGRIN2 main effect  $F_{1,18}=0.36$ ,  $p=0.56$ ; agonist x siGRIN2 interaction  $F_{2,18}=0.47$ ,  $p=0.64$ ). These data indicate that GRIN2 is not involved in KOPR-promoted neuronal differentiation.

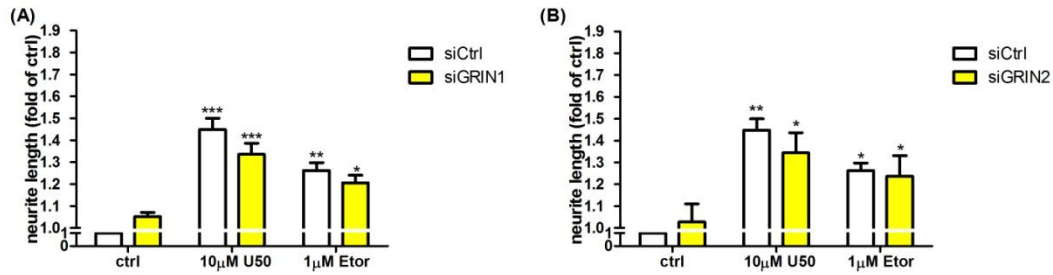


**Figure 13. Role of the  $\alpha$ -binding proteins GRIN1 and GRIN2 in KOPR-mediated neurite outgrowth** N2A-3HA-hKOPR cells were transfected with GRIN1 or GRIN2 siRNAs or control siRNA (siCtrl) using Lipofectamine 2000 to knockdown GRIN1 or GRIN2. Two days after transfection, cells were treated with vehicle, 10  $\mu$ M U50,488H or 1  $\mu$ M etorphine for 10 min followed by 24-hr differentiation in 0.1% serum medium. Neurite processes were measured. Each value represents the mean  $\pm$  S.E.M (n= 4) and data are analyzed by two-way ANOVA followed by Bonferroni *post-hoc* test (\*: $p$ <0.05, \*\*: $p$ <0.01, \*\*\*: $p$ <0.001, compared to the control siRNA-ctrl group).

## **To examine if Rap1-STAT3 pathway is involved in KOPR agonist-induced neurite outgrowth**

Accumulating evidence has shown that Gi/o-protein coupled receptors (eg. CB1 receptor, 5-HT1A receptor, and MOPR) contribute to neurite outgrowth via Gi/o-Rap1-STAT3 pathway in N2A cells (Fricker et al., 2005; He et al., 2005; Rios et al., 2006). Whether KOPR-mediated neurite outgrowth involves Rap1-STAT3 signaling was examined.

Cells were transfected with Rap1 or a dominant negative (DN) mutant of Rap1 and their effects on KOPR-mediated neurite outgrowth were examined. Expression of Rap1 or Rap1-DN mutant did not affect U50,488H- and etorphine-caused neurite outgrowth (Figure 14) (two-way ANOVA, agonist main effect  $F_{2,30}=12.07$ ,  $p=0.0001$ ; Rap1 main effect  $F_{2,30}=0.44$ ,  $p=0.65$ ; agonist x Rap1 interaction  $F_{4,30}=1$ ,  $p=0.42$ ). These results indicate that Rap1 is not involved in KOPR-mediated neurite outgrowth. However, Rap1-DN mutant alone increased neurite outgrowth, indicating Rap1 itself plays an inhibitory role in KOPR-independent neurite outgrowth.

Whether STAT3 is involved in KOPR neuronal differentiation was examined. Knockdown of STAT3 by siRNA showed a trend of decreasing U50,488H- and etorphine-promoted neurite outgrowth, but the reduction did not reach statistical significance (Figure 15) (two way ANOVA, agonist main effect  $F_{2,24}=7.06$ ,  $p=0.004$ ; siSTAT3 main effect  $F_{1,24}=6.55$ ,  $p=0.02$ ; agonist x siGRIN2 interaction  $F_{2,24}=0.48$ ,  $p=0.63$ ). These results show that STAT3 does not participate in KOPR-induced neurite outgrowth.

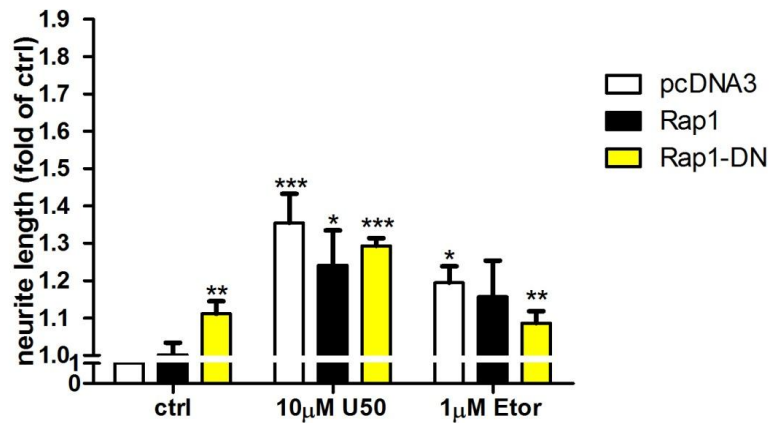


**Figure 14. Effect of Rap1 on U50,488H- or etorphine-induced neurite outgrowth**  
 N2A-3HA-hKOPR cells were transfected with pcDNA3, Rap1 or Rap1 dominant negative form (DN) using Lipofectamine 2000 to overexpress RAP1 and Rap1-DN. Two days after transfection, cells were treated with vehicle, 10 µM U50,488H or 1 µM etorphine for 10 min followed by 24-hr differentiation in 0.1% serum medium. Neurite processes were measured. Each value represents the mean± S.E.M (n= 3) and data are analyzed by two-way ANOVA followed by Newman-Keuls *post-hoc* test (\*: $p < 0.05$ , \*\*: $p < 0.01$ , \*\*\*: $p < 0.001$  compared to pcDNA3-ctrl group).

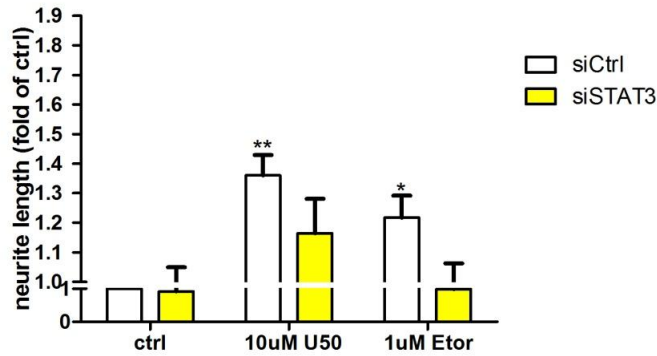


**Figure 15. Effect of STAT3 on U50,488H- or etorphine-induced neurite outgrowth**  
 N2A-3HA-hKOPR cells were transfected with STAT3 siRNAs or control siRNA (siCtrl) using Lipofectamine2000 to knock down STAT3. Forty eight hr after transfection, cells were incubated with vehicle, 10  $\mu$ M U50,488H or 1  $\mu$ M etorphine for 10 min followed by 24-hr differentiation in 0.1% serum medium. Neurite processes were measured. Each value represents the mean  $\pm$  S.E.M (n= 3) and data are analyzed by two-way ANOVA and Newman-Keuls *post-hoc* test (\*: $p$ <0.05, \*\*: $p$ <0.01, compared to the control siRNA-ctrl group).

## Discussion

In this study, we found that U50,488H and etorphine caused neurite outgrowth in N2A cells stably transfected with the KOPR. The effects of both agonists are mediated by the KOPR, Gi/o alpha subunits and in part by ERK1/2 pathway, but  $\beta\gamma$  subunits of G proteins,  $\beta$ -arrestins, p38 MAPK, PKC, PI3K, 14-3-3 $\zeta$ , GEC1, GRIN1/2, Rap1 and STAT3 did not play significant roles. Therefore, since both agonists share the same signaling pathway to promote neurite outgrowth, the lower effect of etorphine is due to lower efficacy of etorphine compared with U50,488H, but not due to activation of different signaling pathways. Some effectors and interacting proteins ( $\beta$ -arrestin2, GEC1, 14-3-3 $\zeta$  and Rap1) inhibited neurite outgrowth in the KOPR-independent manner (Figure16).

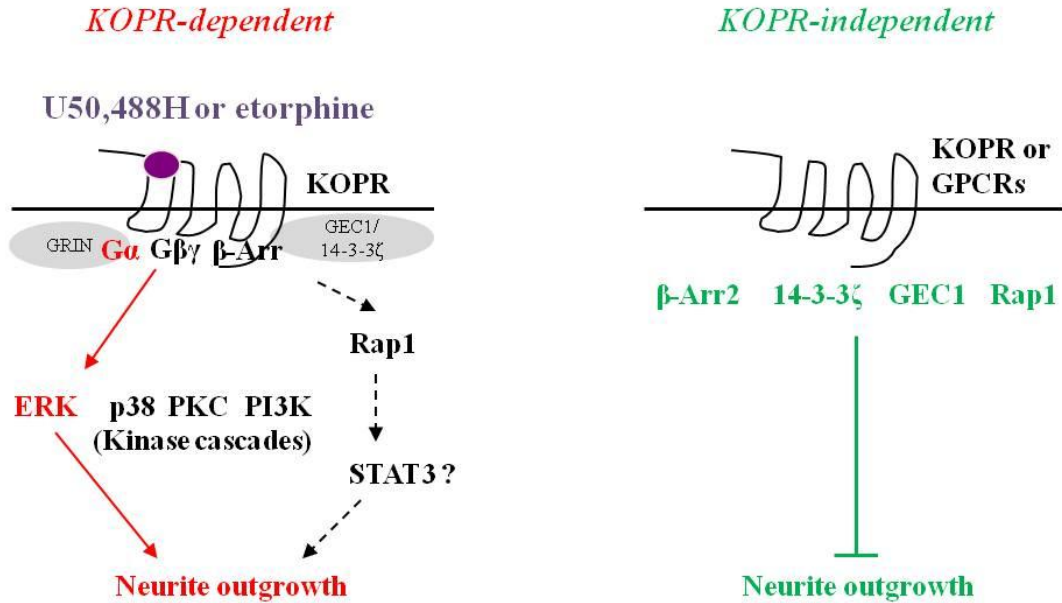


**Figure 16. Summary of KOPR-dependent and KOPR-independent neurite outgrowth** KOPR agonists (U50,488H and etorphine) bind KOPR to activate Gi/o $\alpha$  protein and then ERK1/2 signaling to enhance neurite outgrowth (shown in the red color in the left figure). G $\beta\gamma$  subunits and  $\beta$ -arrestin1/2 did not affect KOPR-mediated neuronal differentiation. The downstream kinase cascades (p38, PKC and PI3K) did not affect KOPR-mediated neurite extension. KOPR-interacting proteins (GEC1 and 14-3-3 $\zeta$ ) and G $\alpha$ -interacting proteins (GRIN1 and GRIN2) are not involved in KOPR-mediated neurite outgrowth. In the Rap1-STAT3 signal pathway, Rap1 did not have any effect on KOPR-mediated neurite outgrowth, while STAT3 showed a trend of increasing this process. Knockdown by siRNAs of  $\beta$ -arrestin2, GEC1 and 14-3-3 $\zeta$  or expression of Rap1-DN mutant increases neurite extension (shown in the green color in the right figure), suggesting  $\beta$ -arrestin2, GEC1, 14-3-3 $\zeta$  and Rap1 may negatively regulate neurite outgrowth in the KOPR-independent manner.

### **KOPR-mediated neurite outgrowth is G protein-, but not $\beta$ -arrestin-dependent**

U50,488H- and etorphine-induced neurite outgrowth were abolished by norBNI and PTX, indicating that Gi/o mediates KOPR-induced neurite outgrowth. Expression of the G $\beta\gamma$  scavenger protein  $\beta$ ARKct or knockdown of  $\beta$ -arrestin1 or  $\beta$ -arrestin2 did not affect agonist-mediated neurite extension. However, knockdown of  $\beta$ -arrestin2 alone promoted basal neurite outgrowth and appeared to have additive effects with U50,488H and etorphine in promoting neurite outgrowth (Figure 6B). These results suggest that  $\beta$ -arrestin2 may play an inhibitory role in KOPR-independent neurite outgrowth. Alternatively, at the basal states, there may be constitutively active KOPR (and possibly other GPCRs) that is negatively regulated by  $\beta$ -arrestin2 and when  $\beta$ -arrestin2 was knocked down, KOPR-mediated increased neurite outgrowth was revealed. This interpretation is consistent with the previous findings of Li et al. (1999), who showed that expression of a dominant negative mutant of  $\beta$ -arrestin2 reduced the intracellular pool of the KOPR at the basal state, suggesting that without agonist treatment, there is a low level of  $\beta$ -arrestin-dependent KOPR internalization, likely due to constitutive KOPR activity.

PTX blocked KOPR-mediated neurite outgrowth, indicating that Gi/o $\alpha$  proteins are involved in promoting neurite outgrowth. However, forskolin and dibutyryl cyclic AMP (db-cAMP), which increase cAMP level and PKA activation, induce neurite outgrowth in N2A cells (Valero et al., 2012). Thus, reduction in cAMP levels caused by Gi/o activation is not likely to be involved in KOPR-mediated neurite outgrowth. Gi/o-coupled KOPR-mediated and forskolin-induced neurite outgrowth may be through different downstream signal pathways.

$\beta$ ARKct, a  $G_{\beta\gamma}$  scavenger, did not affect agonist-induced neurite extension, indicating that  $G_{\beta\gamma}$  are not involved in the process. Activated  $G_{\beta\gamma}$  can bind to GRK2 subfamily proteins to activate GRK2 and GRK3. Therefore, GRK2 and GRK3 may not be involved in KOPR-mediated neurite outgrowth via  $G_{\beta\gamma}$  activation.  $\beta$ -arrestin2 promoted more neurite outgrowth.  $\beta$ -arrestins recruitment followed GRK-mediated GPCR phosphorylation. Taken together, these results suggest that GRK5 and GRK6, but not the GRK2 subfamily (GRK2 and GRK3), play a role in  $\beta$ -arrestin2-mediated neurite outgrowth.

KOPR-induced neurite outgrowth is mediated by  $G_i/o_\alpha$ -protein, but not  $G_{\beta\gamma}$ ,  $\beta$ -arrestin and PKC. The finding that  $\beta$ -arrestin and PKC are not involved in neurite outgrowth is consistent with the finding that PKC mediated part of U50,488H-promoted KOPR phosphorylation (shown in chapter 2), which in turn appears to recruit  $\beta$ -arrestin, leading to  $\beta$ -arrestin-mediated signaling. This  $\beta$ -arrestin-mediated signaling is not involved in KOPR-mediated neurite outgrowth.

### **Roles of KOPR- and $G_o_\alpha$ -interacting proteins in neurite outgrowth**

Expression of the KOPR-interacting proteins 14-3-3 $\zeta$  and GEC1 did not affect KOPR-mediated neurite outgrowth. However, knockdown of 14-3-3 $\zeta$  promoted longer outgrowth of neurites (Figure 11), indicating that 14-3-3 $\zeta$  itself may inhibit neurite outgrowth. It is consistent with the report that 14-3-3 $\zeta$  binds to cell adhesion molecule L1 and regulates L1-dependent neurite outgrowth (Ramser et al., 2010). Knockdown of GEC1 alone showed a trend of increasing neurite outgrowth (Figure 12). The N-terminal region of GEC1 binds to tubulin and promotes tubulin polymerization (Mansuy et al.,

2004), suggesting a possible role of GEC1 in neurite outgrowth. Thus, 14-3-3 $\zeta$  and GEC1 may regulate neurite outgrowth in a KOPR-independent manner.

KOPR-caused neuronal differentiation is Gi/o $\alpha$ -dependent. GRIN1 and 2 have been shown to interact with activated form of Go $\alpha$  protein to stimulate neurite outgrowth (Chen et al., 1999; Iida and Kozasa, 2004; Nakata and Kozasa, 2005; Masuho et al., 2008). Our results showed that KOPR-mediated neurite extension is not through GRIN1 and GRIN2 (Figure 13), which is different from MOPR- and CB1-mediated neurite outgrowth. GRIN1 was involved in etorphine-induced MOPR-mediated neurite outgrowth and GRIN2 participated in CB1-mediated neurite outgrowth (Ge et al., 2009; Hwangpo et al., 2012).

### **The role of MAPK in KOPR-mediated cellular functions**

Stimulation of the KOPR by agonists activates MAP kinase family, including ERK1/2 and p38 MAPK (Belcheva et al., 1998; Bruchas et al., 2006). In our study, neurite outgrowth in N2A cells promoted by a KOPR agonist (U50,488H or etorphine) is in part ERK1/2-mediated (Figure 7B), but p38 MAPK is not involved (Figure 8). U69,593 inhibited mouse embryonic stem cell (ESC)-derived neurogenesis via the p38 MAPK pathway and astrogenesis via the ERK1/2 pathway, whereas it stimulated ESC-derived oligodendrogenesis via both p38 and ERK1/2 pathways (Hahn et al., 2010). Thus, differentiation in different cell systems is regulated by different MEK kinase pathways.

Here we found that U50,488H and etorphine shared the same signaling pathway to promote neurite outgrowth, and the differential effects are due to the lower efficacy of etorphine. This is different from the finding of Coscia and colleagues (McLennan et al.,

2008) on the differences in signaling and proliferation of immortalized astrocytes between the KOPR agonists U69,593 and MOM-Sal B. These researchers showed that KOPR activation by U69,593, promoted proliferation of immortalized astrocytes via  $G_{\beta\gamma}$  and  $\beta$ -arrestin2-promoted sustained ERK1/2 phosphorylation, whereas MOM-Sal B induced only transient ERK1/2 phosphorylation and did not cause cell proliferation (McLennan et al., 2008). In contrast, in primary astrocytes U69,593 and MOM-Sal B showed similar effects. Both caused sustained ERK1/2 phosphorylation and proliferation of primary astrocytes, which are mediated by  $G_{\beta\gamma}$  and  $\beta$ -arrestin2 (McLennan et al., 2008). Therefore, there are both cell- and agonist-specific effects in their studies.

### **Gi/o $_{\alpha}$ -coupled GPCR-mediated neurite outgrowth**

Our finding that activation of the KOPR, a Gi/o $_{\alpha}$ -coupled receptor, resulted in neurite outgrowth is consistent with the reports that many other Gi/o $_{\alpha}$ -coupled receptors participate in neurite outgrowth (He et al., 2006). D2 dopamine receptor increased neurite outgrowth in cultured cortical neurons (Reinoso et al., 1996). Activation of the CB1 or 5-HT1A receptor causes neurite outgrowth in N2A cells via Gi/o-Rap1-STAT3 pathway (Fricker et al., 2005; He et al., 2005). We have found that KOPR-caused neurite outgrowth is not mediated by Rap1 and STAT3 (Figure 14 and Figure 15), whereas stimulation of the  $\delta$  opioid receptor induced neurite outgrowth via Gi/o-STAT5B pathway in N2A cells (Georganta et al., 2013). Thus, Gi/o $_{\alpha}$ -coupled receptors activate different signaling pathways to regulate neurite outgrowth.

### **Similarities and differences between U50,488H and etorphine**

U50,488H caused neurite outgrowth to a greater extent than etorphine and both drugs produced the effect by acting on the KOPR via  $G_i/o_\alpha$  protein-mediated pathway. Both U50,488H and etorphine enhanced KOPR-mediated [ $^{35}$ S]GTP $\gamma$ S binding to N2A-3HA-hKOPR cell membranes, a functional measurement of  $G_\alpha$  protein activation, and in this assay the  $E_{max}$  value of etorphine was 72.2% of that of U50,488H (DiMattio et al., 2015). These results indicate etorphine is a partial agonist in the neurite outgrowth and [ $^{35}$ S]GTP $\gamma$ S binding assays. However, in the same cell line, both U50,488H and etorphine enhanced ERK1/2 phosphorylation via PTX-sensitive  $G_\alpha$  proteins with the same  $E_{max}$  values, indicating that both are full agonists in this assay. Thus etorphine is a low-efficacy partial agonist in promoting neurite outgrowth, a high-efficacy partial agonist in inducing [ $^{35}$ S]GTP $\gamma$ S binding and a full agonist in enhancing ERK1/2 phosphorylation, although in N2A cells all the three end points are manifestations of activation of PTX-sensitive  $G_\alpha$  proteins. These results are consistent with the notion that the efficacy of a drug depends on the end point examined. There may be spare receptors for ERK1/2 phosphorylation, but not for [ $^{35}$ S]GTP $\gamma$ S binding and neurite outgrowth. Alternatively, there may be signal amplification for ERK1/2 phosphorylation downstream of  $G_\alpha$  proteins, but not for [ $^{35}$ S]GTP $\gamma$ S binding and neurite outgrowth.

In conclusion, in N2A cells, U50,488H and etorphine activate the same KOPR-mediated signaling pathway to cause neurite outgrowth and the differential effects are due to different efficacy of the two agonists.

**CHAPTER 2**  
**STUDIES ON RECEPTOR PHOSPHORYLATION**  
**FOLLOWING KAPPA OPIOID RECEPTOR ACTIVATION**

**Introduction**

**Phosphorylation of GPCR**

Phosphorylation on GPCRs caused by agonists, commonly on serine and threonine residues within the C-terminal tail and, to lower extents, the third intracellular loop, has been well established (Butcher et al., 2011). Phosphorylation of GPCRs is a major regulatory mechanism to drive different signaling outcomes. Agonists occupy GPCRs, leading to recruitment of kinases to plasma membranes. Kinases phosphorylate GPCRs at multiple phosphorylation sites with GRKs being the major kinases.  $\beta$ -arrestins are recruited to phosphorylate GPCRs, leading to  $\beta$ -arrestin-mediated signaling and also as a result, G proteins are uncoupled from phosphorylated GPCRs, which is termed desensitization.  $\beta$ -arrestin also binds to clathrin, which in turn moves GPCR into clathrin-coated pits, leading to receptor internalization, trafficking and downregulation (Lefkowitz, 1998; Lefkowitz, 2004; Lefkowitz and Shenoy, 2005).

Many strategies have been used to directly map phosphorylation sites on ligand-activated GPCRs. Tryptic phosphosite mapping has been employed for the bradykinin B2 receptor (Blaukat et al., 2001). Tryptic digestion of purified receptors followed by high performance liquid chromatography (HPLC) and tandem mass spectrometry (MS/MS) has been used for the  $\beta$ 2-adrenergic receptor, and the chemokine receptor CXCR4 (Trester-Zedlitz et al., 2005; Busillo et al., 2010) and the MOPR (Lau et al., 2011). Immunoblotting or immunohistochemistry with phosphospecific antibodies has been utilized for the  $\beta$ 2-adrenergic receptor, CXCR4, and somatostatin 2A receptors and

MOPR (Tran et al., 2004; Busillo et al., 2010; Doll et al., 2011; Ghosh and Schonbrunn, 2011). Site-directed mutagenesis was used extensively in earlier studies.

In recent years, evidence supports the concept of receptor phosphorylation “**barcode**”, which states that when agonists bind to GPCR and cause receptor conformation changes, different GRKs phosphorylate GPCRs in specific phosphorylation patterns, leading to recruitment of distinct  $\beta$ -arrestin conformations for specialized signaling outcomes (Figure 17) (Reiter et al., 2012; Wisler et al., 2014). For the  $\beta_2$ -adrenergic receptor expressed in HEK293 cells, GRK2-promoted phosphorylation contributes to receptor internalization, whereas GRK6-induced phosphorylation is essential for  $\beta$ -arrestin-mediated ERK1/2 signaling, and phosphorylation caused by both GRKs are responsible for receptor desensitization. The  $\beta_2$ -adrenergic receptor full agonist isoproterenol recruits GRK2 and GRK6 to phosphorylate receptor, whereas a weak  $\beta$ -arrestin-biased agonist, carvedilol, only recruits GRK6 (Nobles et al., 2011). Studies on the CXCR4 showed that GRK3 and GRK6 positively regulated ERK1/2, while GRK2 negatively regulated ERK1/2 signaling (Busillo et al., 2010). In addition, it was reported that the M3 muscarinic receptor was phosphorylated to different levels at different phosphorylation sites in different cells (CHO, MIN6 insulinoma cells and primary CG neurons) and tissues (hippocampus, cortex, pancreas and salivary) (Butcher et al., 2011). These findings suggest that GPCRs phosphorylated by GRKs generate specialized phosphorylation barcodes in agonist-, cell type- and tissue-specific fashions that may provide a mechanism for agonist-, cell- and tissue-specific receptor signaling and regulation.

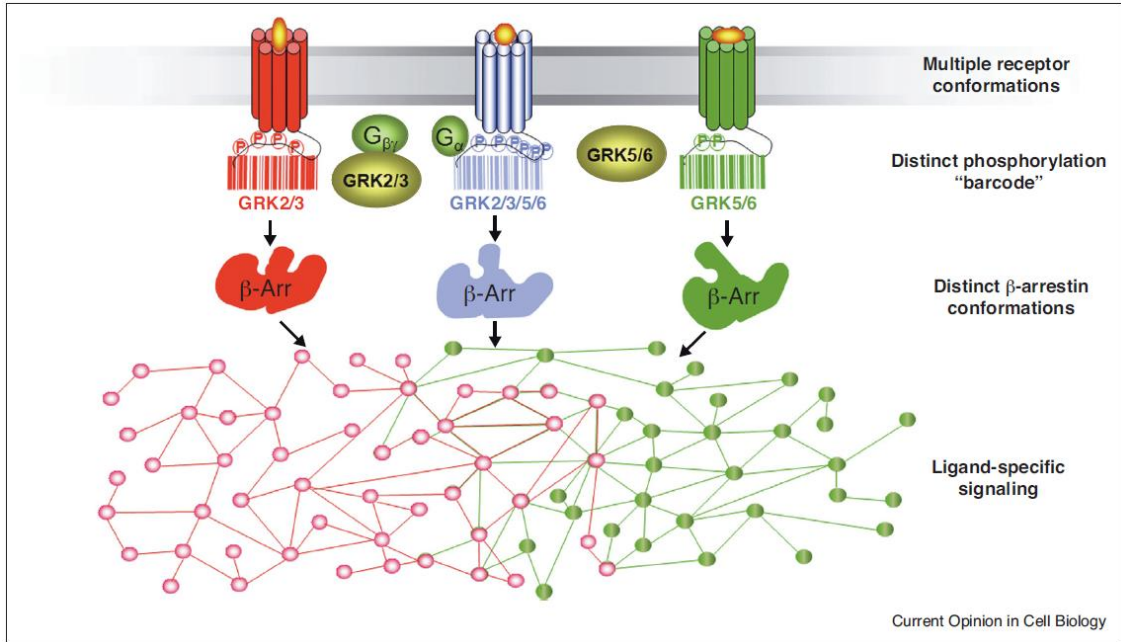


**Figure 17. The barcode hypothesis** (Wisler et al., 2014)

## **G protein receptor kinase (GRK)**

GRKs are serine/threonine kinases. Based on their gene structures and sequences, the GRK family has been classified into 3 subfamilies: visual subfamily (GRK1 and GRK7), GRK2 subfamily [ $\beta$ -adrenergic receptor kinase ( $\beta$ ARK) subfamily, GRK2 and GRK3] and GRK4 subfamily (GRK4, GRK5 and GRK6). Visual subfamily and GRK4 are expressed in retina and testis, respectively. Other subtypes (GRK2, 3, 5 and 6) have ubiquitous distribution.

Structurally, all the GRKs are composed of three major regions (Figure 18): the N-terminal domain, the regulator of G protein signaling (RGS) homology (RH) domain, and the C-terminal domain. The N-terminal domain, highly conserved among all the GRKs, has a short 25-residue proximal NH<sub>2</sub>-terminal region which is unique to GRK enzymes and is involved in GPCR binding. RH domain is divided by a Ser/Thr kinase domain (KD) of about 500-520 residues, which belongs to the AGC (protein kinase A, protein kinase G and protein kinase C) kinase family and is shared among all the GRKs. Specific lysine residue (K) in the kinase domain of each GRK is responsible for the catalytic activity (shown in the kinase domain of Figure 18). The C-terminal domain is diverse among GRKs. Visual GRKs have short C-terminal prenylation sequences. GRK2 subfamily in the C-terminal domain has pleckstrin homology (PH) domains implicated in anionic phospholipids binding and G $_{\beta\gamma}$ -binding, allowing translocation of GRK2 or GRK3 to the inner side of plasma membranes. GRK4 and GRK6 contain palmitoylation sites and lipid-binding capabilities. GRK5 has a phospholipid binding domain at residues 552-562, which targets GRK5 to membranes. Nuclear localization signal and nuclear export signal are identified within GRK5 (Premont et al., 1995; Sato et al., 2015).

Generally, GRKs are recruited to membranes toward activated GPCRs using residues and domains within their C-terminal domains. GRKs phosphorylate at Ser/Thr residues in the C-terminal domains and third intracellular loops of GPCRs. GRKs appear not to have high receptor specificity. There is no clear consensus sequence in receptor substrate of GRKs. However, in some case, GRK2 and GRK3 have been reported to show preference for Ser or Thr residues downstream of acidic residues (Eason et al., 1995), whereas GRK5 and GRK6 prefer residues downstream of basic residues (Kunapuli et al., 1994; Pitcher et al., 1998). Recently, the concept of GPCR phosphorylation barcode may provide one possible way to explain GRK selectivity (Reiter et al., 2012; Wisler et al., 2014). Differentially activated receptor conformations recruit different GRKs to cause distinct phosphorylation patterns, leading to recruitment of different  $\beta$ -arrestin conformations and diverse downstream signaling or receptor trafficking.

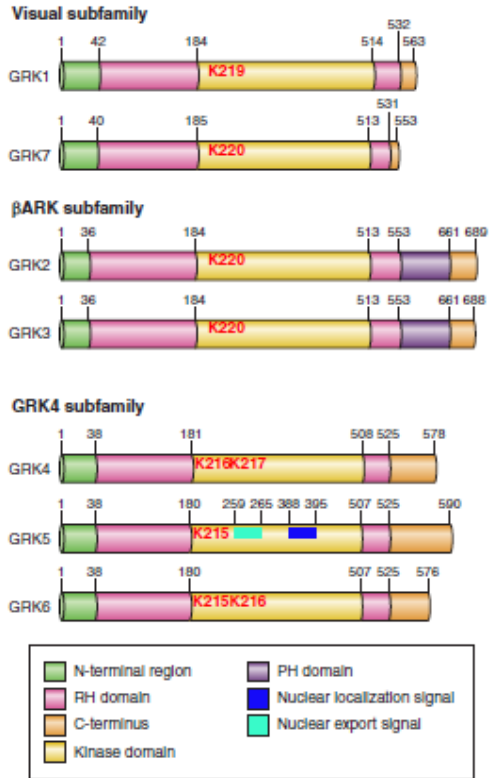


**Figure 18. GRKs subfamily** (Sato et al., 2015)

## **Protein kinase C (PKC)**

PKC is a group of serine/threonine kinases, which belongs to the AGC kinase family. According to the second messengers that regulate their activities, PKC is classified into three major groups: the conventional isoforms (PKC $\alpha$ , PKC $\beta$  and PKC $\gamma$ ), which are regulated by calcium, diacylglycerol (DAG) and phospholipids, the novel forms (PKC $\delta$ , PKC $\epsilon$ , PKC $\eta$  and PKC $\theta$ ), which are regulated by DAG and phospholipids, and the atypical isoforms (PKC $\zeta$  and PKC $\iota/\lambda$ , PKC $\lambda$  is the mouse ortholog of human PKC $\iota$ ), which are insensitive to calcium and DAG. Most PKC isoforms are expressed ubiquitously in all tissues.

Structurally, there are two major regions, a regulatory region in the N-terminal domain and a catalytic region in the C-terminal domain (Figure 19). In the regulatory region, there are one pseudosubstrate motif and one C1 (DAG-binding) and one C2 (calcium-binding) domains. The pseudosubstrate motif closely resembles substrate-phosphorylation motif with an alanine residue instead of serine-threonine phosphorylation site and bind the catalytic region to keep it in the inactive state. Conventional PKC isoforms have C1 and C2 domains while novel and atypical isoforms only have C1 domain. Conventional and novel PKC isoforms have tandem C1 domains (C1a and C1b) to bind DAG, whereas atypical isoforms only have one C1 domain, which cannot bind to DAG. The catalytic region is composed of conserved C3 (ATP-binding site) and C4 (substrate-binding site) domains. For conventional PKCs, DAG bind to the C1 domain, leading to conformation changes that facilitate dissociation of the pseudosubstrate motif from the catalytic domain and increase catalytic activity of PKC. The C2 domain binds phospholipids in a calcium-dependent manner for PKC activation.

For calcium-independent novel PKCs, there is C2-like structure binding to phospholipids. For DAG- and calcium-independent atypical PKCs, the catalytic activity is regulated by intracellular localization, which is controlled by nuclear localization signals (NLS) and nuclear export signals (NES) as well as the interaction with regulatory proteins (Spitaler and Cantrell, 2004).

A hallmark of PKC activation is translocation from cytosol to cellular particulate fraction involving plasma membranes and intracellular organelles (e.g. mitochondria and Golgi). The consensus phosphorylation sequences for PKCs are (R/K)(R/K)X(S/T), (R/K)XX(S/T), (R/K)X(S/T)(R/K), (R/K)XX(S/T)XR/K and (R/K)X(S/T). PKCs prefer a basic amino acid (Arg and/or Lys) at the position -2 and/or -3 N-terminal of the phosphorylation sites (Ser and Thr) within the substrate proteins (Kang et al., 2012). Phosphorylation of substrate proteins by PKC causes conformational change resulting in functional changes. GPCRs are one of the candidate substrates for PKC. MOPR and CXCR4 have been reported to be phosphorylated by PKC (Busillo et al., 2010; Chen et al., 2013).

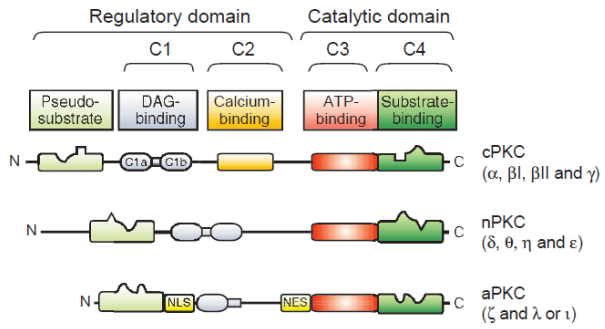


**Figure 19. PKC isoforms** (Spitaler and Cantrell, 2004)

## **KOPR-mediated pharmacological effects**

KOPR agonists have been shown to produce antinociception (von Voigtlander et al., 1983; Dykstra et al., 1987) without respiratory depression and physical dependence as MOPR agonists do (Koob and Bloom, 1988; Kong et al., 1994). KOPR agonists also have therapeutic potentials as antipruritic and water diuretic agents (Gmerek and Cowan, 1988). However, they also have some undesirable side effects, such as dysphoria (Dykstra et al., 1987), sedation, and motor incoordination (Kieffer, 1999). These side effects limited the therapeutic development of KOPR agonists. Chavkin and colleagues have postulated that KOPR-induced analgesia is G protein-dependent, whereas aversion is  $\beta$ -arrestin-p38-mediated (Bruchas and Chavkin, 2010). G protein-biased KOPR agonists may provide a way to optimize KOPR therapeutic potentials. In addition, understanding the underlying mechanisms of  $\beta$ -arrestin-mediated signaling will allow us to explore avenues to minimize the side-effects. KOPR phosphorylation is the initial step for  $\beta$ -arrestin recruitment, thus it is important to characterize in details mechanisms of agonist-promoted KOPR phosphorylation.

U50,488H has been reported to induce phosphorylation of the human KOPR (hKOPR) expressed in CHO cells using the method of metabolic labeling with  $^{32}\text{P}$ -orthophosphate (Li et al., 2002). Etorphine promotes much lower levels of KOPR phosphorylation than U50,488H and reduces U50,488H-promoted KOPR phosphorylation (Li et al., 2003). Chavkin et al. reported that U50,488H induced phosphorylation of S369 in the rat KOPR (rKOPR) stably transfected into HEK293 cells by immunoblotting using phospho-specific antibody. S369A mutation or expression of GRK2 dominant negative mutant GRK2 (K220R) decreased U50,488H-mediated rKOPR

desensitization and internalization (McLaughlin et al., 2003). In *Xenopus* oocytes, co-expression of GRK3 or GRK5 and  $\beta$ -arrestin2 enhanced U69,593-induced rKOPR desensitization, which was attenuated by S369A mutation in the rKOPR. In contrast, U69,593-induced KOPR desensitization was not affected by substitution with Ala of S356, T357 or T363 in the C-terminal domain or S255, S260 and S262 in the third intracellular loop (Appleyard et al., 1999). These studies demonstrate that agonist-promoted KOPR phosphorylation at S369 contributes to KOPR desensitization and internalization, which are mediated by GRK- $\beta$ -arrestin-dependent mechanisms. Human and rodent (mouse and rat) KOPRs show some sequence differences in the C-terminal domains (the sequences shown in the table 1). The human and mouse KOPRs differ in two positions: Ser<sup>358</sup> and Tyr<sup>369</sup> in the human KOPR, but Asn<sup>358</sup> and Ser<sup>369</sup> in the mouse KOPR.

Our lab has recently determined sites of U50,488H-promoted phosphorylation of the mouse KOPR (mKOPR) expressed in N2A cells to be S356, T357, T363 and S369 by LC-MS/MS and phospho-KOPR specific antibodies (Chen et al., 2016). Antibodies recognizing KOPR phosphorylated at S356/T357, T363 and S369 are shown to be highly specific (Chen et al., 2016). In this study, we focused on dose-response relationship and time course of U50,488H-promoted mKOPR phosphorylation at each site and the protein kinases (GRK and PKC) involved in mKOPR phosphorylation *in vitro*. In addition, we also examined the role of PKC in U50,488H-promoted KOPR phosphorylation in mouse brains and in KOPR-mediated pharmacological effects in CD1 mice.

## Materials and Methods

### Materials

Mouse neuro2A neuroblastoma (N2A) cells were purchased from the A.T.C.C. (Manassas, VA). U50,488H and norbinaltorphimine (nor-BNI) were provided by the National Institute on Drug Abuse (Bethesda, MD). Horseradish peroxidase (HRP)-conjugated goat anti-rabbit or anti-mouse IgG antibodies were purchased from Jackson ImmunoResearch Laboratories (West Grove, PA). Minimal essential medium (MEM), blasticidin and Lipofectamine™ 2000 were purchased from Invitrogen/Thermo Fisher Scientific (Waltham, MA). Fetal bovine serum was purchased from Atlanta Biochemicals (Flowery Branch, GA). Protease inhibitor tablet, bicinchoninic acid assay (BCA) reagents and enhanced chemiluminescence (ECL) reagent Supersignal West Pico were purchased from Pierce/Thermo Fisher Scientific (Waltham, MA). The nickel-nitrilotriacetate (Ni-NTA) agarose was purchased from Qiagen (Hilden, Germany). Dodecyl- $\beta$ -Dmaltoside (DDM), Go6976, Pansorbin and PVDF membranes was purchased from EMD Millipore (Billerica, MA). Odyssey blocking buffer, secondary antibody goat anti-mouse IgG-800CW, Sapphire and DRAQ5 were from LI-COR Bioscience (Lincoln, NE). Chelerythrine chloride (CHL) was from Enzo Life science (Farmingdale, NY).

The rabbit total mKOPR (PA847) and phospho-specific KOPR antibodies were custom-generated by Covance (Conshohocken, PA) and purified in our own laboratory (Chen et al., 2016). Total mKOPR antibody (PA847) were generated against a.a.371-380 in the C-terminal domain of the mKOPR. Phospho-specific antibodies were generated against phosphopeptides in the C-terminal domain of the mKOPR as follows: pS356/pT357 antibody against a.a.352-360 containing pS356 and pT357; pT363

antibody against a.a.359-367 with pT363; pS369 antibody against a.a.365-373 with pS369.

siRNAs against GRK2, GRK3, PKC $\alpha$  and PKC $\epsilon$  and GRK2 antibody (sc-562) and GRK3 antibody (sc-563) were purchased from Santa Cruz Biotechnology (Santa Cruz, CA). The sequences of GRK2 siRNAs are: GACGUGUUC CAGAAGUUCAtt, UGAACUUCUGGAACACGUCtt, GAGUACCCAAGAUGAAGAAAtt, UUCUUCAUCUUGGGUACUCtt, GUACCCAAGAUGAAGAACAAtt, UGUUCUUCAUCUUGGGUACtt. The GRK3 siRNAs sequences of are CUGCGAACAUCCUCCUAGAtt, UCUAGGAGGAUGUUCGCAGtt, CAGGACCUCUAUAAGAACUtt, AGUUCUUAUAGAGGUCCUGtt, CGUCUAGGGUAAUUAUGAAAtt, UUCAUAAUUACCCUAGACGtt. The sequences of PKC $\alpha$  siRNAs are GACAUA AAGUACAGAGUAUtt, AUACUCUGUACUUUAUGUCtt, GUAGGUACCCUCCUAAGAtt, UCUUAGGAAGGGUACCUACTt, GGAAGUACAAUGUAUAGUAAtt, UACUAUACA UUGUACUUCtt. The sequences of PKC $\epsilon$  siRNAs are GGAAGGCCUUGUCAUUUGATT, UCAA AUGACAAGGCCUUCCTT, CUGGAUGAGUUCAACUUCATT, UGAAGUUGAACUCAUCCAGTT, GAA GGACGUUAUCCUACAATT, and UUGUAGGAUAACGUCCUUCTT. Polymerase chain reaction (PCR) primers for PKC isoforms (PKC $\alpha$ , PKC $\beta$ , PKC $\gamma$ , PKC $\zeta$ , PKC $\iota/\lambda$ , PKC $\delta$ , PKC $\epsilon$ , PKC $\theta$  and PKC $\eta$ ) also were purchased from Santa Cruz (Santa Cruz, CA). GRK4/5/6 antibody was purchased from Millipore (Billerica, MA). siRNAs against GRK5 and GRK6 and TRIzol<sup>®</sup> Reagent were bought from Life Technologies (Carlsbad, CA). The sequences of GRK5 siRNA are GGACCAUAGACAGAGAUUAtt, and UAAUCUCUGUCUAUGGUCtt. The sequences of GRK6 siRNAs are GGCAAGAGCAAGAAAUGGctt, and GCCAUUUCUUGCUCUUGCCtt.

Mouse monoclonal anti-FLAG M1 affinity antibody, GF109203X, penicillin/streptomycin, pyruvic acid, NaHCO<sub>3</sub>, Phorbol-12-myristate-13-acetate (PMA), phosphatase inhibitors [tetrasodium pyrophosphate, glycerophosphate disodium, NaF and orthovanadate (Na<sub>3</sub>VO<sub>4</sub>)], dithiothreitol (DTT), imidazole, ethylenediaminetetraacetic acid (EDTA), paraformaldehyde and compound 48/80 were purchased from Sigma-Aldrich (St. Louis, MO).

### **Cell Culture**

The mouse KOPR (mKOPR) construct was generated previously (Chen et al., 2016). Briefly, the mKOPR was epitope-tagged with FLAG including a signal peptide at the N-terminus to facilitate receptor purification. The construct was cloned into KpnI/AgeI sites of the vector pcDNA3/6His with a blasticidin resistance gene. Thus the mKOPR has a FLAG tag at the N-terminus and 6×His at the C-terminus (FmK6H). N2A cells stably transfected with FmK6H (FmK6H-N2A cells) were established previously in our lab (Chen et al., 2016). Cells were grown in 10% fetal bovine serum, 2.2g/L NaHCO<sub>3</sub>, 110mg/L pyruvic acid, 1µg/mL blasticidin, MEM and 100 units/ml penicillin/streptomycin in a humidified atmosphere with 5% CO<sub>2</sub>, 95% air at 37°C. Saturation binding of [<sup>3</sup>H]diprenorphine to membranes was performed and K<sub>d</sub> and B<sub>max</sub> values were determined to be 0.30±0.06 nM and 5.48±0.52 pmole/mg protein (mean ± s.e.m., n=3), respectively.

### **Drug treatment**

*Effects of U50,488H on KOPR phosphorylation: time course and dose-response*

### relationship

About  $1 \times 10^7$  cells were incubated in serum-free medium for at least for 1 hr. For time-course experiments, cells were treated with vehicle or 0.1  $\mu\text{M}$  U50,488H for different time intervals (0, 0.5, 1, 2, 5, 10 min) at 37°C. For concentration-response relationship, cells were treated with vehicle or different concentrations of U50,488H (0.01, 0.1, 0.3, 1, 3, 10  $\mu\text{M}$ ) for 2 min at 37°C.

### Roles of GRKs on U50,488H-promoted KOPR phosphorylation

For knockdown of GRK isoforms experiments,  $5 \times 10^5$  cells/ well in 6-well plates were left untransfected or transfected with control siRNA or siRNA targeting GRK2, GRK3, GRKs2+3 or GRK6 (75 pmole siRNA) using Lipofectamine 2000. Because N2A cells had very low levels of GRK5, effects of both overexpression and overexpression / knockdown of GRK5 were examined. Cells were co-transfected with pcDNA3 + control siRNA, GRK5 cDNA + control siRNA, pcDNA3 + GRK5 siRNA and GRK5 cDNA + GRK5 siRNA (1  $\mu\text{g}$  cDNA + 100 pmole siRNA) using Lipofectamine 2000. Forty eight hours after transfection, cells were treated with vehicle or 3  $\mu\text{M}$  U50,488H for 2 min at 37°C.

### Effects of protein kinase C (PKC) activation on KOPR phosphorylation

Phorbol-12-myristate-13-acetate (PMA), a PKC activator, was used to examine if activation of PKC affects KOPR phosphorylation. PMA is a diester of phorbol and a structural analogue of diacylglycerol (DAG), which activates PKC via C1 DAG/phorbol ester binding domain. For dose-response relationship,  $1 \times 10^7$  cells were incubated in serum-free medium for at least for 1 hr and then treated with different concentrations (0.001, 0.01, 0.1, 1 and 10  $\mu\text{M}$ ) of PMA for 30 min at 37°C. For time-course experiments,

after being in serum-free medium for 1 h, cells ( $\sim 1 \times 10^7$ ) were treated with 0.1  $\mu\text{M}$  PMA for different intervals (0, 1, 5, 10 and 30 min) at 37°C. For comparison,  $1 \times 10^7$  cells were treated with 3  $\mu\text{M}$  U50,488H for the same intervals as the PMA experiments. These two treated groups underwent SDS-PAGE and immunoblotting together to compare heterologous and homologous phosphorylation.

#### Effects of PKC inhibition on U50,488H-induced KOPR phosphorylation

Two nonselective PKC inhibitors (GF109203X and chelerythrine chloride, CHL) and one selective PKC $\alpha$  and PKC $\beta$ 1 inhibitor (Go6976) were used to examine the role of PKC in U50,488H-induced KOPR phosphorylation. Cells ( $\sim 1 \times 10^7$ ) were incubated with serum-free medium for 1 hr followed by incubation with vehicle or a PKC inhibitor (4  $\mu\text{M}$  GF109203X, 1  $\mu\text{M}$  CHL or 100 nM Go6976) for 30 min and cells then were treated with vehicle or 3  $\mu\text{M}$  U50,488H for 2 min at 37°C.

For knockdown of PKC $\alpha$  or PKC $\epsilon$ ,  $\sim 5 \times 10^5$  cells were transfected with control siRNA or PKC $\alpha$  siRNA or PKC $\epsilon$  siRNA using Lipofectamine 2000. Forty eight hours later, cells were treated with 3  $\mu\text{M}$  U50,488H for 2 min at 37°C.

All the vehicle- and drug-treated cells were lysed for receptor purification and subsequent immunoblotting as described below.

#### **Receptor purification and Western blot**

After vehicle or drug treatment, cells were lysed with 1 ml lysis buffer [1% DDM, phosphatase inhibitors, protease inhibitors (20 mM tetrasodium pyrophosphate, 20 mM glycerophosphate disodium, 20 mM NaF and 2 mM Na<sub>3</sub>VO<sub>4</sub>), 20 mM Tris-HCl buffer, pH 7.4]. Cell lysate were supplemented with 10  $\mu\text{M}$  naloxone to stabilize the receptor

and then centrifuged at 12,000rpm (13,000 X g) for 10min. The supernatant were incubated with 50 µl Ni-NTA agarose in a 1.5-ml Eppendorf tube for 1 hr and then washed 3 times to remove non-specific binding with wash buffer [20 mM Tris-HCl, pH 7.4, 0.5N NaCl, phosphatase inhibitors (2 mM tetrasodium pyrophosphate, 2 mM glycerophosphate, 2 mM NaF and 0.2 mM Na<sub>3</sub>VO<sub>4</sub>), 0.1% DDM, 20 mM imidazole] by resuspension and centrifugation. Samples were incubated with 100 µl elution buffer (0.3 M imidazole, 66 mM Tris-free base, 0.3 M NaCl and 0.05% DDM) at 4°C for 15 min. Laemmli sample buffer (5X, 10% SDS, 0.25 M Tris, pH 7.4, 50% glycerol and 0.01% Bromophenol Blue, 25 µl) was added to eluted samples. Sample (30 µl) were resolved with 8% SDS-PAGE and then transferred onto PVDF membranes. Membranes were incubated with phospho-specific KOPR antibodies (1 µg/ml, pS356/pT357, pT363 and pS369) overnight followed by HRP-conjugated secondary anti-rabbit IgG antibodies and then reacted with ECL reagents. Images were captured with LAS 1000 plus Image Analyzer (Fuji Photo Film Co. Ltd., Tokyo, Japan). Membranes were stripped with stripping buffer (0.1 M glycine, pH 2 and 1% SDS) at room temperature and immunoblotted again for total mouse KOPR using antibody PA847 (1:10,000), followed by HRP-conjugated secondary anti-rabbit IgG antibodies and ECL reagents. Staining intensity of phospho-KOPR was normalized against that of the total KOPR in the same lane.

#### **Detection of endogenous GRKs and the specificity of GRK siRNAs in N2A cells**

Cells (~1×10<sup>7</sup>) were lysed with 2X Laemmli sample buffer (4% SDS, 100 mM DTT, 10% glycerol, 62.5 mM Tris, 0.01% Bromophenol Blue, pH 7.4) and protein

concentration of the lysate was determined with the BCA method. For immunoblotting of GRK5 and GRK6, cells ( $\sim 5 \times 10^5$ ) were transfected with GRK5 or GRK6 cDNA (1  $\mu\text{g}$ ) using Lipofectamine 2000 for 48 hr as the positive controls because the antibodies recognize GRKs4/5/6. Some cells ( $\sim 5 \times 10^5$ ) were untransfected or transfected with control siRNA or siRNAs against GRK2, GRK3, GRK2+3, GRK5 and GRK6 (75 pmole) by Lipofectamine 2000 for 48 hr. Cells were lysed with 2X Laemmli sample buffer and then protein concentration was examined by BCA assay. For endogenous GRKs detection, aliquots of cell lysate (15 or 30  $\mu\text{g}$  protein for GRK2 and GRK3 detection, 80  $\mu\text{g}$  for GRKs5/6 detection, and 2  $\mu\text{l}$  GRK5 or GRK6 overexpression cell lysate) were resolved with 8% SDS-PAGE. For examination of GRKs siRNA specificity, aliquots of cell lysate from nontransfection, control siRNA, siGRK2, siGRK3, siGRK2+3, siGRK5 and siGRK6 (30  $\mu\text{g}$  protein for GRK2 and GRK3 detection and 80  $\mu\text{g}$  for GRK6 detection) were resolved with 8% SDS-PAGE. Protein bands thus resolved were transferred onto PVDF membranes. Membranes were incubated with GRK2 (1:1000), GRK3 (1:1000) or pan-GRK4/5/6 (1:2000) antibodies overnight at 4°C followed by HRP-conjugated secondary anti-rabbit IgG antibodies and then ECL reagents. Images were captured with a Fuji LAS 1000 plus Image Analyzer (Fuji Photo Film Co. Ltd., Tokyo, Japan).

### **Reverse transcription- polymerase chain reaction (RT-PCR)**

Cells ( $\sim 1 \times 10^7$ ) were solubilized with 1 ml Trizol reagent followed by chloroform phase extraction. Isopropanol (100%, 0.5 mL) was added to the aqueous phase to precipitate RNA (gel-like pellet). RNA pellet was washed with 75% ethanol and then dried in the air for 10 min. RNA was resuspended in RNAase-free water at 55°C for 10

min. RNA was used for RT- two-step PCR for detection of different isoforms of PKC (conventional PKCs: PKC $\alpha$ , PKC $\beta$  and PKC $\gamma$ ; atypical PKCs: PKC $\zeta$  and PKC $\iota/\lambda$ ; novel PKCs: PKC $\delta$ , PKC $\epsilon$ , PKC $\theta$  and PKC $\eta$ ). RT-PCR was performed according to the semi-quantitative nested RT-PCR protocol of the manufacturer (Santa Cruz). Nested PCR is modified from the regular PCR using two pairs of primers to reduce mispriming, leading to the generation of specific PCR products. The first pair of primers (primer pair A) are for amplification of a larger DNA fragment. The second pair of primers (nested primers, primer pair B) are for amplification of a shorter fragment from the first run PCR product. Thus, the second run of PCR can exclude nonspecific fragments from the first run PCR products. Total RNA (5 ng) was reverse-transcribed into cDNA first. For the first PCR reaction, 2  $\mu$ l cDNA was amplified with the primer pair A. The first PCR product (5  $\mu$ l) was used as the template for the second PCR reaction using the primer pair B. For the control, no PCR primers were added (RT-ctrl). The PCR cycle was as follows: initial denature at 95°C for 30 sec followed by 35 cycles (95°C, 45 sec; 55°C, 45 sec; 72°C, 1 min) and then the final elongation at 72°C for 10 min. PCR products were resolved with 1% agarose gel electrophoresis and the image was captured with the Fuji Image Analyzer.

### **On cell western for receptor internalization**

Cells were seeded into 96-well plate (Falcon) at  $3 \times 10^4$  cells/well and grown for 2 days to confluence. Cells were incubated with 4  $\mu$ M GF109203X or 1  $\mu$ M CHL in serum-free medium for 30 min and then treated with 10  $\mu$ M U50,488H for 1 h. Cells were washed with cold PBS containing Mg<sup>2+</sup> and Ca<sup>2+</sup> followed by anti-FLAG M1 antibody (1:500) incubation for 1 hr at 4°C to label cell surface KOPR. Cells were fixed with 4%

paraformaldehyde for 10 min at room temperature and then incubated with Odyssey blocking buffer for 1 hr followed by secondary antibody goat anti-mouse IgG-800CW (1:800), which reacted with anti-FLAG M1 antibody and yielded green color. Cells were also stained with cellular cytosol control Sapphire (1:700) and cytosol and nuclei control 5mM DRAQ5 (1:10,000) in blocking buffer for 1 hr at room temperature, which yielded red color and were used for normalization of cell numbers in each well. Cells were washed five times with TBST (20 mM Tris, 0.9% NaCl, 0.1% Tween20, pH 7.6) and then one time with water. Two signals [surface KOPR (green) and cellular stain (red)] were measured using Odyssey Infrared Image System and software (LI-COR Bioscience, Lincoln, NE). The ratio of the intensity of KOPR (green) over the intensity of cellular stain (red) was used as a measure of cell surface receptors. Receptor internalized (% of total cell surface receptor) was calculated as follows.

$$\text{Receptor Internalized (\% of total cell surface receptor)} = \frac{\text{control} - \text{treated}}{\text{control}} \times 100\%$$

## **Animals**

Male adult CD1 mice (8 weeks) were purchased from Charles River (Wilmington, MA). Mice were housed 5 per cage in a temperature- and relative humidity-controlled room with a 12-hr light/dark cycle. Animals were acclimated for about seven days before tests. All animals were provided food and tap water *ad libitum*. All the animal experiments were performed according to the National Institutes of Health guidelines for the Care and Use of Laboratory Animals and with an approved protocol from Temple University Institutional Animal Care and Use Committee.

### **Effect of PKC inhibition on U50-induced KOPR phosphorylation in mouse brain**

Male adult CD1 mice were pretreated with H<sub>2</sub>O or CHL (5 mg/kg, s.c.) for 1 hr followed by saline or U50,488H (10 mg/kg, s.c.) administration for 15 min. Mice were euthanized with gaseous CO<sub>2</sub>. Whole brains without cerebellum were removed, immediately frozen in liquid nitrogen and then stored at -80°C for receptor purification.

Because of very low level of KOPR in mouse brains (~40 fmole/mg protein), five brains were pooled as one sample. KOPR was purified with tandem immunoprecipitation of KOPR and then subject to western blotting with phospho-KOPR specific antibodies. Brains were homogenized with 15 ml buffer A [modified RIPA with the following composition: 1% NP-40, 1% sodium deoxycholate, 0.1% SDS, 25mM Tris, pH 7.4, 10 mM EDTA, phosphatase inhibitors (15 mM tetrasodium pyrophosphate, 20 mM glycerophosphate disodium, 50 mM NaF, 1 mM Na<sub>3</sub>VO<sub>4</sub>), and protease inhibitors tablet, pH adjusted to 8.0], then incubated with 0.5 ml Pansorbin for 1 hr at 4°C for pre-clearing of materials interacting with Pansorbin and centrifuged at 50,000 x g for 30 min. Supernatants were incubated with purified rabbit PA847 anti-mouse KOPR antibody at 2.5 µg/ml overnight at 4°C for immunoprecipitation of KOPR as the first step of receptor purification and centrifuged at 50,000 x g for 30 min to remove particulates. Pansorbin (200 µl) was added to the supernatant, incubated for 2 hr and then centrifuged at 20,000 x g for 10 min. The pellet was re-suspended in 1 ml buffer A, transferred to Eppendorf tubes, and washed by centrifugation and re-suspension two times with buffer A and once with buffer C (25 mM Tris, pH 7.4, 0.1% DDM, 0.25M NaCl, 1 mM EDTA). Pellets were resuspended in 100 µl buffer E [4% SDS, 25 mM Tris-HCl buffer, pH7.4, 10% glycerol, 1 mM EDTA, 0.1 M DTT (freshly added)], incubated for 30 min at room

temperature to dissociate immunoprecipitated proteins from Pansorbin and centrifuged at 12,000 x *g* for 2 min to remove Pansorbin. Supernatant was transferred to a fresh Eppendorf tube, heated at 55°C for 30 min, added dropwise to 1.8 ml of buffer B (25 mM Tris, pH 7.4, 2% DDM, 0.15M NaCl, 1 mM EDTA) containing 10 µg guinea pig antibodies against the KOPR (371-380) peptide (custom-generated, Ab5699) and incubated overnight at 4°C for the second immunoprecipitation. Pansorbin (50 µl) was added to the mixture, incubated for 2 h and centrifuged at 12,000 x *g* for 2 min. The supernatant was removed and the pellet was washed twice with buffer B and once with buffer C by resuspension and centrifugation. KOPR was eluted from Pansorbin by incubation and vortexing with 50 µl buffer D [25 mM Tris, pH 7.4, 0.05% DDM, 0.25M NaCl, 1 mM EDTA, 0.1 mg/ml KOPR(371-380) peptide (amino acid sequence: RDVGGMNKPV)] for 10 min twice and 100ul for 30 min once at room temperature and centrifuged for collection of supernatants. The combined eluate was concentrated to 20 µl using an Amicon Concentrator with a 50-kDa cutoff, mixed with 20 µl buffer F [8% SDS, 25 mM Tris-HCl buffer, pH7.4, 20% glycerol, 1 mM EDTA, 0.1 M DTT (freshly added)], heated at 55°C for 20 min. Eluted samples were subjected to SDS-PAGE (precast gel 4-12%, Invitrogen) and then transferred onto PVDF membranes, which incubated for 1 hr with 3% BSA blocking buffer in TBS-T containing normal guinea pig IgG (10 µg/ml). Membranes were incubated overnight with anti-pT363 or anti-pS369 (1 µg/ml) at 4°C followed by incubation with HRP-conjugated mouse monoclonal anti-rabbit IgG and reaction with ECL reagents. Images were captured with a Fuji LAS 1000 plus Image Analyzer and the intensity of each band was quantified using the ImageGauge software (Version 4.1, Fuji Photo Film Co.). The blot was stripped and re-blotted for the total

mouse KOPR using rabbit PA847 antibody (0.1 µg/ml) for 1 hr. For quantitation, p-KOPR staining intensity was normalized against that of the total KOPR in the same lane. The resulting data were then normalized against those of U50,488H.

### **Formalin test**

Male adult CD1 mice were injected subcutaneously with the PKC inhibitor CHL (1 mg/kg) or H<sub>2</sub>O in the home cage in the test room for 1 h. Mice were treated with U50,488H (1 mg/kg, s.c.) or saline for 5 min in the test chamber and then injected with 5% formalin into the bottom of their left hind paws under isoflurane anesthesia. Mice recovered from anesthesia in about 1 min and then started flinching the injected paw for 15-20 min, which is considered as phase I reaction. When the phase I reaction was over, mice licked the injected paw, which is the phase II reaction and is inhibited by KOPR agonists (Wheeler-Aceto and Cowan, 1991). Mice were recorded for 20 min for the time they spent on licking their injected hind paws as a measure of U50,488H-induced analgesic effect.

### **Anti-scratching test**

Male adult CD1 mice were treated with the PKC inhibitor CHL (5 mg/kg, s.c.) or water and placed in test cages for 1 hr. Mice were injected with 5 mg/kg U50,488H or saline (s.c.) for 20 min followed by injection with 0.1 ml of the pruritogen compound 48/80 (0.5 mg/ml, s.c.) into the nape of the neck. Mice started to scratch in a few seconds and the number of scratching bouts was counted for 30 min.

### **Tolerance to the anti-scratching effect of U50,488H**

Whether repeated U50,488H treatment induced tolerance to its anti-scratching effect was examined. Mice were treated once a day for 6 days with saline or 5 mg/kg U50,488H (s.c.). On day 1 and day 6, mice were tested for their anti-scratching behavior. On the test days, mice were acclimated in test chamber for 1 h followed by injection of saline or U50,488H. Twenty min later, mice were injected with compound 48/80 to cause scratching. The number of scratching bouts was counted for 30 min.

### **Novelty-induced locomotor activity**

#### Apparatus

Home cage locomotor activity system (Omnitech Electronics Inc., Columbus, OH) was used. Each locomotor chamber frame can accommodate a transparent plastic cage (45cm× 20cm× 20cm) and has a pair of sensor panels with a set of 16 light beams in a horizontal direction. When a mouse interrupts light beams, the connected Fusion software records and determines the location of mice along X-axis. Breaking of two consecutive light beams by a mouse is interpreted as ambulatory activity, while repeated breaking of the same light beam is recorded as stereotypic activity. The total activity is composed of ambulatory activity and stereotypic activity. The total travel distance (cm) is the distance traveled along the horizontal direction.

#### Procedure

Male adult CD1 mice were injected with the PKC inhibitor CHL (1 mg/kg, s.c.) or water in the home cages. One hour later, mice were treated with 5 mg/kg U50,488H (s.c.) or saline and were immediately placed into locomotor activity chambers for activity recording in 5-min bins for 1 hr. Total distance traveled (cm), total activity, ambulatory

activity and stereotypy activity (the number of beam breaking) were recorded by Fusion software. Data were analyzed with GraphPad Prism5 (La Jolla, CA) to calculate the area under curve (AUC) of first 30-min period for all the groups.

### **Rotarod performance assay**

Male adult CD1 mice were trained to run on a rotarod apparatus (Ugo-Basile mouse rotar-rod, Stoelting Co., Wood Dale, IL) 2 days before the test day. On the training day, mice were acclimated in the test room for 1 hr and then placed on the rotarod for 5 min with the rotation revolution changing from 3 to 30 rpm. Each mouse was trained for 3 trials with a break of 5 min between trials. Mice that stayed on the rotarod for less than 255 sec (85% of the 5-min period) were excluded from testing. On the test day, mice were tested on the rod first to measure the baseline. All the mice were able to stay on the rotarod for almost the entire 5 min, so the baselines were close to 300 sec for all the groups. Mice were subcutaneously injected with the PKC inhibitor CHL (1 mg/kg or 5 mg/kg) or H<sub>2</sub>O for 1 hr prior to subcutaneous administration of U50,488H (10 mg/kg) or saline. Ten, 20 and 30 min after U50,488H injection, mice were tested for the time they stayed on the rotarod for 5 min. Results are shown as the percentage of time staying on the rod following drug or vehicle administration compared with the baseline.

### **Conditioned place aversion (CPA)**

CPA was performed according to our published procedure of conditioned place preference (Xu et al., 2013) with some modifications.

#### Apparatus

A Plexiglas chamber with two identical-size compartments ( $12.7 \times 34.7 \times 12.7 \text{ cm}^3$ ) and a guillotine door ( $5 \times 5.9 \text{ cm}^2$ ) in the middle was used for each mouse. The visual cues for one side were checker coverings on the floor and three walls with a blue light bulb (5-watt) hung at the top. The other side was covered with white coverings and a red bulb hung at the top.

Procedures (see the time scheme on Figure 41A)

Pretest (day 0)

Mice were acclimated in the test room for 1 hr in the dark with blue and red light on. Drug-naïve mice were placed into the chambers and allowed free access to both sides for 15 min for determination of their initial preference. Mice that stayed in one side for over 570 sec (65% of 15 min) were excluded from the subsequent experiment.

Conditioning (day 1- day 6)

The CPA procedure is unbiased and visual cue-counterbalance in design. Half of the mice were conditioned in the chamber of white-red light as drug-paired side; the others were conditioned in the chamber of checker-blue light as drug-paired side. There were two conditioning sessions each day: non-drug-paired side for the morning session and drug-paired side for the afternoon session. For the morning sessions, mice were treated with H<sub>2</sub>O for 1 hr followed by 15-min saline administration in the home cages and then placed into the CPA chamber for 30 min as non-drug treatment conditioning (half in the checker-side; half in the white-side). For the afternoon sessions, mice were treated with drugs. There are 4 basic treatment groups in this experiment: H<sub>2</sub>O-Sal, H<sub>2</sub>O-U50,488H, CHL-Sal and CHL-U50,488H. The dose-response relationship for CHL was examined, thus 1 and 5 mg/kg CHL and saline treated groups and co-treatment of CHL

(0.5, 1 and 5 mg/kg) and U50,488H were examined. Mice were pretreated with vehicle or CHL at different doses (0.5, 1 or 5 mg/kg) for 1 h followed by 5 mg/kg U50,488H or saline in the home cage. Fifteen minutes later, mice were placed into chamber for 30 min for drug-treatment conditioning. If mice were conditioned in the white side for non-drug paired side in the morning, in the afternoon mice were placed into the checker side as drug-paired side and vice versa. Conditioning was carried out for 6 days.

#### Posttest (day7)

Mice were acclimated for 30 min in the test room in the dark. Without any drug treatment, mice were placed into the chambers and allowed free access to both sides for 15 min. The time each mouse staying in either side was recorded. Post-drug preference was determine as drug-paired side minus nondrug-paired side.

#### **Data Analysis and Statistics**

Data were graphed and analyzed with Graph Pad Prism5 (La Jolla, CA). One-way ANOVA was used to analyze one-factor experiment, followed by Newman-Keuls *post-hoc* test. Two-way ANOVA was used to analyze two-factor experiments followed by Bonferroni *post-hoc* test.

## Results

### **U50,488H-induced KOPR phosphorylation is mediated by KOPR.**

Our previous studies showed that phosphorylation of mKOPR in the C-terminal domain induced by U50,488H occurred at pS356, pT357, pT363 and pS369 by LC-MS-MS analysis of purified mKOPR (Chen et al., 2016). Here, whether phosphorylation at these sites was due to KOPR activation was examined. Cells were pretreated with the selective KOPR antagonist NorBNI (1  $\mu$ M) for 1 hr followed by 30-min incubation with 10  $\mu$ M U50,488H and KOPR phosphorylation was examined with immunoblotting using the three phospho-KOPR specific antibodies. NorBNI blocked U50,488H-induced KOPR phosphorylation at S356/T357, T363 and S369 (two way ANOVA, for S356/T357, U50,488H main effect  $F_{1,11}=9.97$ ,  $p=0.009$ ; NorBNI main effect  $F_{1,11}=25.18$ ,  $p=0.0001$ ; U50,488H  $\times$  NorBNI interaction,  $F_{1,11}=28.44$ ,  $p=0.0002$ ; for T363: U50,488H main effect  $F_{1,12}=2094.18$ ,  $p<0.0001$ ; NorBNI main effect  $F_{1,12}=1966$ ,  $p<0.0001$ ; U50,488H  $\times$  NorBNI interaction,  $F_{1,12}=2051.94$ ,  $p<0.0001$ ; for S369: U50,488H main effect  $F_{1,12}=985$ ,  $p<0.0001$ ; NorBNI main effect  $F_{1,12}=1014.7$ ,  $p<0.0001$ ; U50,488H  $\times$  NorBNI interaction,  $F_{1,12}=949$ ,  $p<0.0001$ ) (Figure 20). This indicates that U50,488H-induced KOPR phosphorylation at these sites is KOPR-mediated.

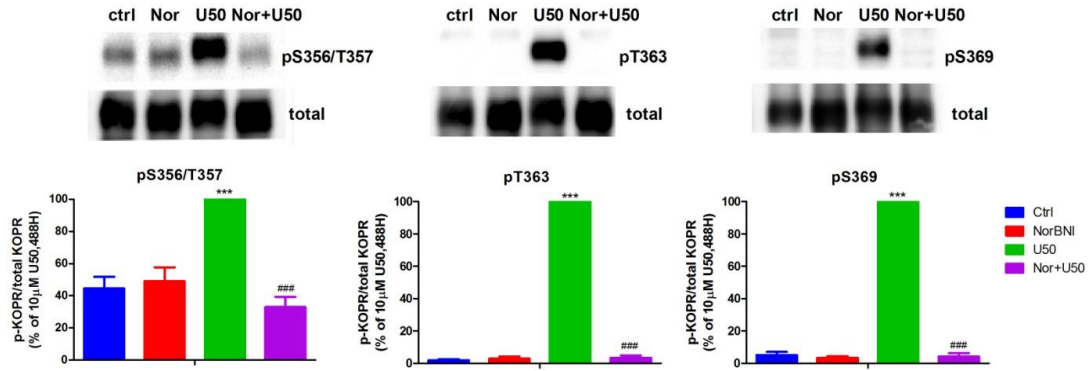


**Figure 20. U50,488H-promoted KOPR phosphorylation was blocked by norBNI.** N2A-FmK6H cells were treated with 1  $\mu$ M norBNI for 1 hr followed by 30-min incubation with 10  $\mu$ M U50,488H. Cells were lysed and receptors were partially purified by use of Ni-NTA agarose. The eluted samples were used for western blot using phospho-specific antibodies: anti-pS356/pT357, anti-pT363 and anti-pS369. Membranes were stripped and immunoblotting was performed with anti-KOPR antibodies. One representative blot is shown. Staining intensity of phospho-KOPR was normalized against that of the total KOPR in the same lane. Staining intensity of each lane (p-KOPR/total KOPR) was then normalized against that of the U50,488H lane, which was designated as 100%. Each value represents the mean  $\pm$  S.E.M (n=4). Data were analyzed by two-way ANOVA followed by Bonferroni *post-hoc* test. (\*\*\*:  $p < 0.001$ , compared to untreated group; ###:  $p < 0.001$ , compared to U50,488H-treated group).

## **Time course and dose-response relationship of U50,488H-induced KOPR phosphorylation**

FmK6H-N2A cells were treated with 0.1  $\mu\text{M}$  U50,488H for 0.5, 1, 2, 5 and 10 min and KOPR phosphorylation was probed with pS356/pT357, pT363 and pS369 antibodies. KOPR phosphorylation by U50,488H at these phosphoresidues occurred very rapidly. Maximal pS356/pT357, pT363 and pS369 antibody staining reached a plateau in 30 sec, 1 min and 2 min, respectively (Figure 21). Based on the results, we chose 2-min incubation time with U50,488H for the following *in vitro* experiments.

Different concentrations of U50,488H were used to determine  $\text{EC}_{50}$  values for KOPR phosphorylation at each residue. Cells were treated with 0.01  $\mu\text{M}$ , 0.1  $\mu\text{M}$ , 0.3  $\mu\text{M}$ , 1  $\mu\text{M}$ , 3  $\mu\text{M}$  and 10  $\mu\text{M}$  U50,488H for 2 min. U50,488H promoted KOPR phosphorylation in a dose-dependent manner (Figure 22). The  $\text{EC}_{50}$  values of phosphorylation at S356/T357, T363 and S369 were determined to be 0.1  $\mu\text{M}$ , 0.48  $\mu\text{M}$  and 0.24  $\mu\text{M}$ , respectively. Based on these results, 3  $\mu\text{M}$  U50,488H was chosen for the following *in vitro* experiments.

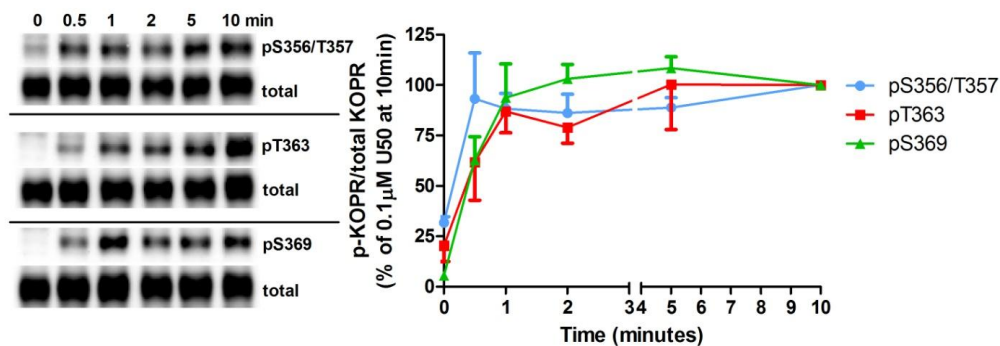


**Figure 21. Time course of U50,488H-induced KOPR phosphorylation** FmK6H-N2A cells were treated with 0.1  $\mu$ M U50,488H at 37°C for different durations (0, 0.5, 1, 2, 5 and 10 min). Cells were lysed with lysis buffer and then receptors were affinity-purified using Ni-NTA agarose beads. Eluted samples were subject to western blot using the three phospho-KOPR specific antibodies. Membranes were stripped and blotted again for total KOPR. Left panel represents one of three to four experiments performed. Quantitation of staining intensity was performed (see Fig. 1 legend) and each value is mean  $\pm$  SEM.

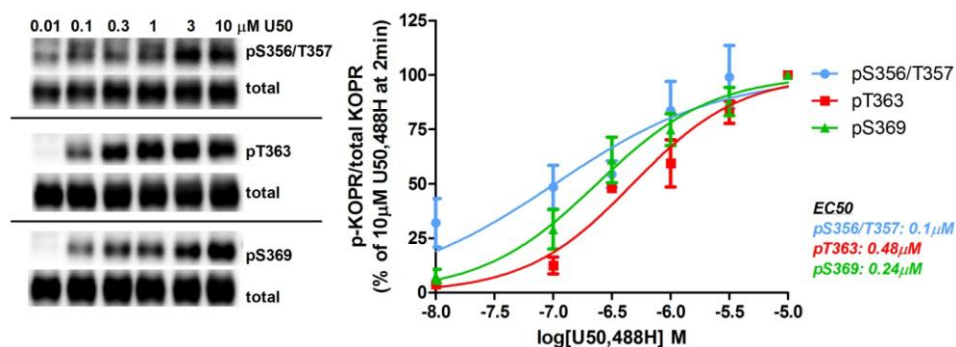


**Figure 22. Dose-response relationship of U50,488H-induced KOPR phosphorylation**

FmK6H-N2A cells were treated with different concentrations of U50,488H (0.01  $\mu\text{M}$ , 0.1  $\mu\text{M}$ , 0.3  $\mu\text{M}$ , 1  $\mu\text{M}$ , 3  $\mu\text{M}$  and 10  $\mu\text{M}$ ) for 2 min at 37°C. Cells were lysed with lysis buffer and then KOPR receptors were partially purified using Ni-NTA agarose beads. Receptor samples were resolved in 8% SDS-PAGE and then immunoblotted with pS356/pT357, pT363 and pS369 antibodies. Membranes were stripped and blotted again for total KOPR detection. Left panel represents one of three to seven experiments performed. Quantitation of staining intensity was performed (see Fig. 1 legend) and each value is mean  $\pm$  SEM (n=3-7).

### **Roles of GRKs in U50,488H-induced KOPR phosphorylation**

GRKs have been shown to be involved in agonist-induced GPCR phosphorylation. We first examined the endogenous GRKs present in N2A cells by western blot using GRK2, GRK3 and pan GRKs4/5/6 antibodies. When cell extracts (15 and 30  $\mu\text{g}$  protein) were subject to SDS-PAGE, immunoblotting with GRK2 or GRK3 antibodies revealed one band with the expected  $M_r$  80 kDa for GRK2 and 83 kDa for GRK3 and staining intensity of about 1 to 2 ratio between the two lanes (Fig. 23A and Fig. 23B), indicating the presence of GRK2 and GRK3. Because the antibody recognizes GRKs4/5/6 and GRK5 and GRK6 have similar molecular weights, overexpression of GRK5 and GRK6 was used as the positive controls for identification of the two enzymes. As shown in Fig. 23C, GRK6, but not GRK5, was present in N2A cells. The data indicate that N2A cells endogenously express GRK2, GRK3 and GRK6.

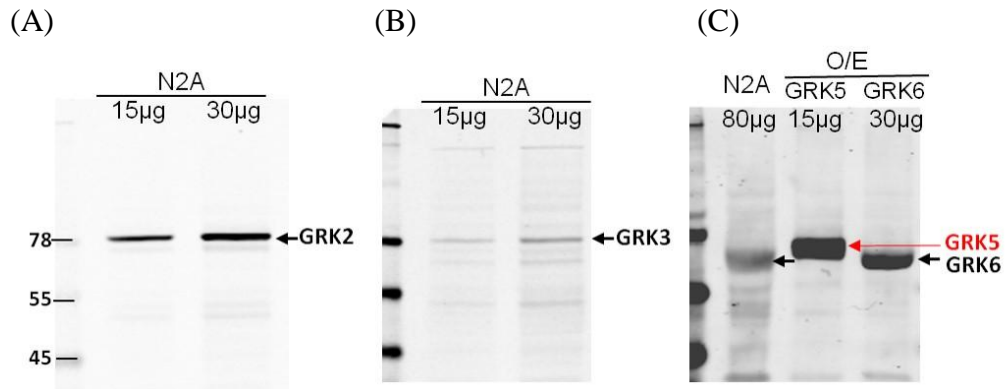


**Figure 23. Detection of endogenous GRKs 2, 3 and 6 in Neuro2a cells** N2A cells were lysed with lysis buffer and then 15 or 30 µg of proteins were subject to western blot with specific GRK2 (A) and GRK3 (B) antibodies. For GRK5 and GRK6 (C), because the antibody recognized GRKs4/5/6, cells transfected with GRK5 and GRK6 cDNAs were used as the positive controls. Forty-eight hours after transfection using Lipofectamine 2000, cells were lysed and then were subject to 8% SDS-PAGE and immunoblotting using pan GRK4-5-6 antibody. These results indicate that N2A cells endogenously express GRKs 2, 3 and 6.

Knockdown of endogenous GRK2, GRK3 and GRK6 with individual siRNAs was used to examine which GRK isoforms were involved in KOPR phosphorylation upon U50,488H stimulation. GRK2 and GRK3 belong to the same subfamily, which have  $G_{\beta\gamma}$ -binding domains in the C-terminal regions, whereas GRK5 and GRK6 do not. The specificity of each individual siRNA against GRKs 2, 3, 5 and 6 was checked by western blot. Fig. 24 shows that GRK2 siRNA knocked down GRK2, without affecting GRK3 or GRK6, demonstrating its specificity among the three GRKs. Similarly, GRK3 siRNA and GRK6 siRNA are specific for GRK3 and GRK6, respectively, among the three GRKs.

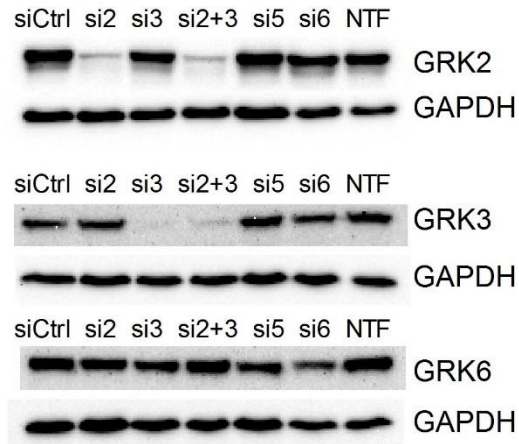


**Figure 24. Specificity of siRNAs against GRK2, GRK3, and GRK6 in N2A cells**

FmK6H N2A cells were left untransfected or transfected with control siRNA (siCtrl), siRNAs against GRK2, GRK3, GRK2+3, GRK5 and GRK6 using Lipofectamine 2000 for 48 hr. Cells were lysed with lysis buffer and then subjected to western blot with GRK2, GRK3 and GRK6 antibodies.

Cells were left untransfected or transfected with control siRNA or siRNA targeting GRK2, GRK3 or both. Compared to control siRNA, GRK2 siRNA or GRK2 siRNA + GRK3 siRNA reduced GRK2 by about 50%. Similarly, GRK3 siRNA or GRK2 siRNA + GRK3 siRNA reduced GRK3 by about 50% (Fig. 25). The control siRNA did not affect U50,488H-promoted phosphorylation at S356/T357, T363 and S369, compared to no-transfection (NTF). Therefore, NTF was omitted in following experiments. Knockdown of GRK2, GRK3 or both GRKs2/3 significantly attenuated U50,488H-promoted KOPR phosphorylation as detected by immunoblotting with pS356/pT357, pT363 and pS369 antibodies (Figure 25). For S356/T357, knockdown of GRK2 or GRK3 decreased U50,488H-promoted phosphorylation by about 55%, whereas knockdown of GRK2+3 totally blocked U50,488H-induced phosphorylation. For T363, knockdown of GRK2 reduced U50,488H-induced phosphorylation by about 60%, whereas knockdown of GRK3 and GRK2+3 reduced KOPR phosphorylation by about 80%. For S369, knockdown of GRK2 inhibited KOPR phosphorylation by ~35%, whereas knockdown of GRK3 and GRK2+3 reduced by about 60% and 65%, respectively. The attenuation was more profound for phosphorylation of T363 than S369. This indicates GRK2 and GRK3 are involved in U50,488H-induced KOPR phosphorylation.

GRK6 knockdown was similarly performed with siRNA targeting GRK6, which reduced GRK6 levels by about 40%. Knockdown of GRK6 significantly reduced U50,488H-caused KOPR phosphorylation at S356/T357, T363 and S369 by about 50%, 45% and 50%, as detected with phospho-specific antibodies (Figure 26). Thus, GRK6 is also involved in U50,488H-induced KOPR phosphorylation.

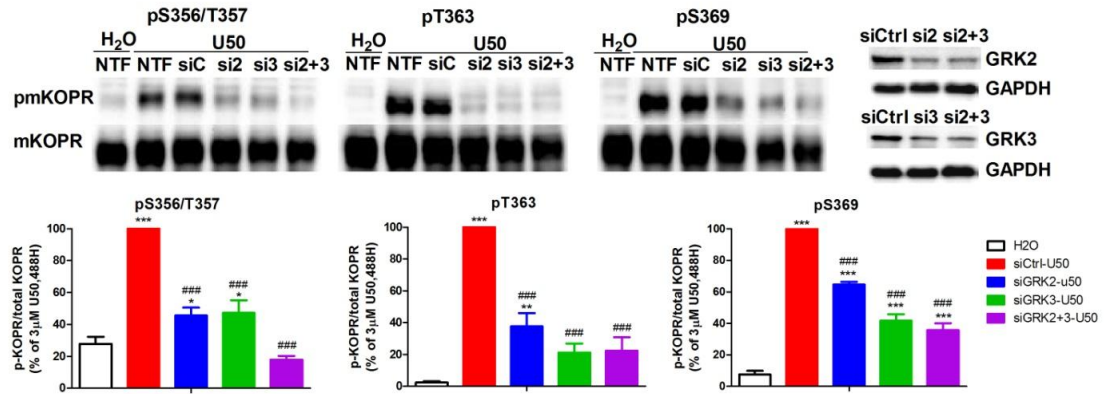


**Figure 25. Effects of knockdown of GRK2 and GRK3 on U50,488H-induced KOPR phosphorylation at S356/T357, T363 and S369** FmK6H-N2A cells were left untransfected (NTF) or transfected with control siRNA (siCtrl, siC) or siRNAs targeting GRK2, GRK3 or both. Forty-eighty hours later, cells were treated with vehicle or 3  $\mu$ M U50,488H for 2 min. Cells were solubilized and the KOPR was partially purified with Ni-NTA agarose. SDS-PAGE and immunoblotting were performed on the eluates. Top panel shows representative blots and the experiments were performed 3-5 times with similar results. Quantitation of staining intensity was performed (see Fig. 20 legend). Data represent the mean  $\pm$  S.E.M. The data were analyzed with one-way ANOVA followed by Newman-Keuls *post-hoc* test (\*:  $p < 0.05$ , \*\*:  $p < 0.01$ , \*\*\*:  $p < 0.001$ , compared to vehicle control group; ###:  $p < 0.001$ , compared to U50,488H-treated siRNA control group). GRK2 and GRK3 levels were reduced by 50% as determined with immunoblotting.

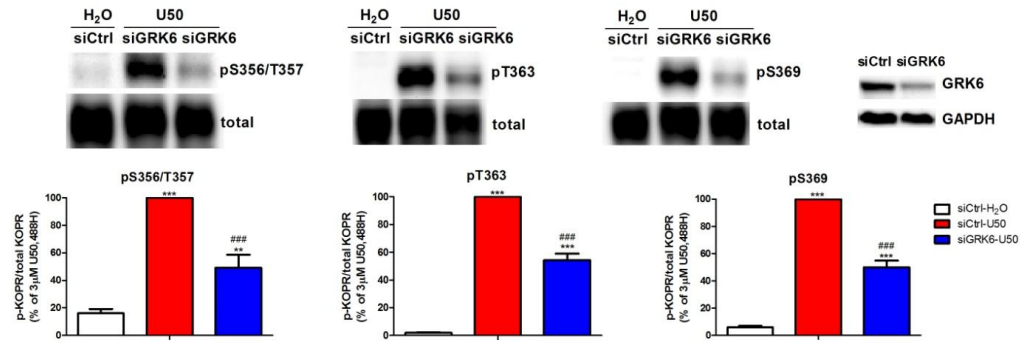


**Figure 26. Effect of GRK6 knockdown on U50,488H-induced KOPR phosphorylation at S356/T357, T363 and S369** Fmk6H-N2A cells were transfected with control siRNA (siCtrl) or GRK6 siRNA (siGRK6) with Lipofectamine 2000 for 48 hr. Cells were treated with vehicle or 3  $\mu$ M U50,488H for 2 min and then were lysed with lysis buffer. KOPR was partially purified using Ni-NTA agarose. Elutes were resolved with 8% SDS-PAGE and then immunoblotting was performed with phospho-KOPR antibodies (pS356/pT357, pS356 and pT363) and then total KOPR antibodies. GRK6 levels were reduced by 40% by siRNA as determined with western blot. A representative blot for each antibody is shown in the top panel. Staining intensity was quantified (see Fig. 20 legend). Data represent the mean  $\pm$  S.E.M (n=6) and were analyzed by one-way ANOVA followed by Newman-Keuls *post-hoc* test [\*\*:  $p < 0.01$ , \*\*\*:  $p < 0.01$ , compared to vehicle control group (siCtrl-H<sub>2</sub>O); ###:  $p < 0.001$ , compared to U50,488H-treated siRNA control group (siCtrl-U50)].

GRK5 was reported to participate in agonist-induced KOPR desensitization (Appleyard et al., 1999), suggesting that GRK5 is involved in KOPR phosphorylation. Since N2A cells do not express GRK5 endogenously, we examined the role of GRK5 by its overexpression. Overexpression of GRK5 promoted higher U50,488H-promoted phosphorylation level of KOPR at S356/T357, T363 and S369 by 2-, 1.6- and 1.6-fold, respectively, compared with the vector control. Furthermore, GRK5 siRNA was used to determine the specificity of the effects of GRK5 overexpression. Co-transfection of GRK5 siRNA with GRK5, which reduced GRK5 by about 80%, blocked GRK5 overexpression-caused KOPR phosphorylation at each residue (Figure 27).

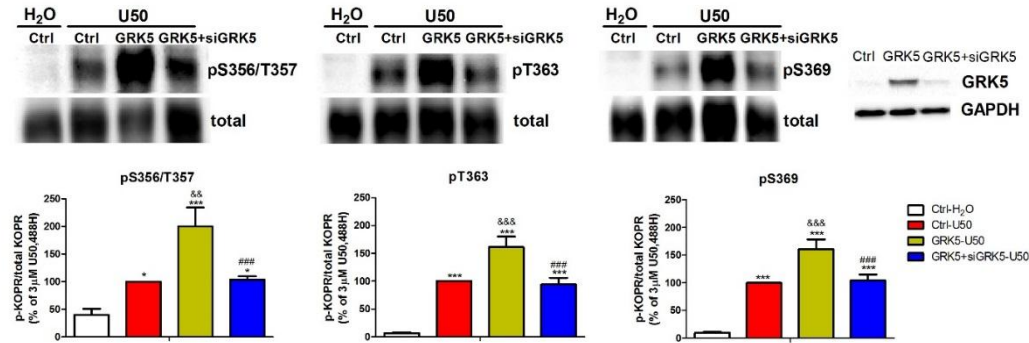


**Figure 27. Effects of GRK5 expression and expression + knockdown on U50,488H-induced KOPR phosphorylation at S356/T357, T363 and S369** FmK6H-N2A cells were co-transfected with the vector pcDNA3 and control siRNA (Ctrl), GRK5 cDNA and control siRNA (GRK5), and GRK5 cDNA and GRK5 siRNA (GRK5+siGRK5) with Lipofectamine 2000 for 48 hr. Cells were treated with vehicle or 3  $\mu$ M U50,488H for 2 min and then lysed for partial KOPR purification with Ni-NTA agarose. Elutes were loaded onto 8% SDS-PAGE for western blot for detection of pKOPR (pS356/pT357, pS356 and pT363) and total KOPR. The expression of GRK5 and knockdown of GRK5 were validated by western blot. Results represent the mean  $\pm$  S.E.M (n=6-8). Data were analyzed by one-way ANOVA followed by Newman-Keuls *post-hoc* test [\*:  $p < 0.05$ , \*\*\*:  $p < 0.01$ , compared to H<sub>2</sub>O-treated control group (Ctrl-H<sub>2</sub>O); ###:  $p < 0.001$ , compared to U50,488H-treated GRK5 overexpression group (GRK5-U50);  $\Delta\Delta$ :  $p < 0.01$ ,  $\Delta\Delta\Delta$ :  $p < 0.001$ , compared to U50,488H-treated control group (Ctrl-U50)].

Taken together, U50,488H-induced KOPR phosphorylation at S356/T357, T363 and S369 was regulated by GRK2, GRK3, GRK5 and GRK6. Thus, phosphorylation of the four sites in the C-terminal domain are regulated similarly by the four GRKs, indicating that there is no differential KOPR phosphorylation by GRKs2/3 versus GRKs5/6.

### **Roles of PKCs on KOPR phosphorylation *in vitro***

Other protein kinases are also reported to be involved in GPCR phosphorylation. Activation of the KOPR has been shown to stimulate PKC (Bian et al., 2000; Bohn et al., 2000). S356, T357, T363 and S369 are also PKC consensus phosphorylation sites. We first examined the endogenous PKC isoforms present in N2A cells using RT-PCR with isoform specific primers. Control reactions were performed with no PCR primers. PCR products were resolved with agarose electrophoresis along with the size markers. The primers were designed as such to yield PCR products of 400-560 bp. As shown in Fig. 28, DNA products of expected sizes were found in the RT-PCR reaction mixtures, but not in RT-control mixtures, for PKC $\alpha$ , PKC $\beta$ , PKC $\gamma$ , PKC $\zeta$ , PKC $\iota/\lambda$ , PKC $\delta$ , PKC $\epsilon$ , and PKC $\theta$ . These results indicate that N2A cells endogenously express PKC $\alpha$ , PKC $\beta$  and PKC $\gamma$  (conventional PKCs), PKC $\zeta$  and PKC $\iota/\lambda$  (atypical PKCs), as well as PKC $\delta$ , PKC $\epsilon$  and PKC $\theta$ , but not PKC $\eta$  (Novel PKCs). Among these isoforms, PKC $\theta$  PCR product was barely detectable.

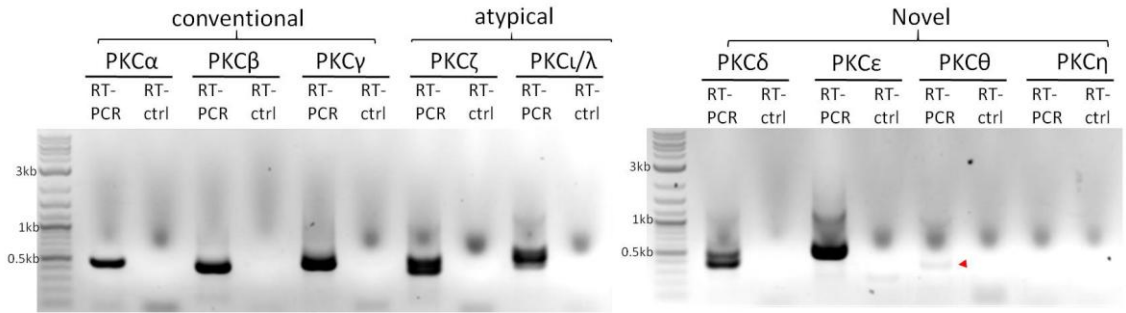


**Figure 28. Endogenous PKC isoforms in N2A cells, detected with RT-PCR**

N2A cells were solubilized with Trizol reagent and RNA was extracted. RNA was used for RT-PCR for detection of different isoforms of PKC (conventional PKCs: PKC $\alpha$ , PKC $\beta$  and PKC $\gamma$ ; atypical PKCs: PKC $\zeta$  and PKC $\iota/\lambda$ ; novel PKCs: PKC $\delta$ , PKC $\epsilon$ , PKC $\theta$  and PKC $\eta$ ). For the PCR control, no PCR primers were added (RT-ctrl). The PCR cycle was as follows: initial denature at 95°C for 30 sec followed by 35 cycles (95°C, 45 sec; 55°C, 45 sec; 72°C, 1 min) and then the final elongation at 72°C for 10 min. PCR products were resolved with 1% agarose gel electrophoresis and then the image was captured. This figure shows the presence of PKC isoforms (predicted PCR product sizes) as follows: PKC $\alpha$  (496bp), PKC $\beta$  (428bp), PKC $\gamma$  (552bp), PKC $\zeta$  (428bp), PKC $\iota/\lambda$  (456bp), PKC $\delta$  (428bp), PKC $\epsilon$  (547bp), and PKC $\theta$  (494bp). PKC $\theta$  PCR product is barely detectable (red arrowhead). No PKC $\eta$  PCR product was detected. The experiment was carried out twice with similar results.

PKC was shown to be involved in heterologous desensitization of many 7TMRs, including the KOPR (Finley et al., 2008). Thus, whether PKC stimulation independent of KOPR activation enhanced KOPR phosphorylation was examined by use of the PKC activator phorbol-12-myristate-13-acetate (PMA). Incubation of cells with different concentrations of PMA for 30 min enhanced KOPR phosphorylation at S356/T357, T363 and S369 in dose-dependent manner with EC<sub>50</sub> values of 6.6 nM, 7.5 nM and 19 nM, respectively (Figure 29A). Based on this result, 0.1 μM PMA was used in the following time course experiment. As shown in Fig. 29B, PMA enhanced KOPR phosphorylation at S356/T357, T363 and S369 in a time-dependent fashion, reaching a plateau at 5, 15 and 15 min, respectively.

For comparison of agonist-dependent and agonist-independent KOPR phosphorylation, cells were treated with U50,488H (3 μM) and PMA (0.1 μM) for different durations (0, 1, 5, 15 and 30 min). For S356/T357, PMA promoted a much higher peak phosphorylation level than U50,488H. For T363, U50,488H induced phosphorylation to greater extents than PMA. For S369, U50,488H and PMA caused similar maximal phosphorylation levels. However, their phosphorylation time courses were different. PMA showed much slower kinetics, reaching the maximal phosphorylation level at 5 min (S356/T357) or 15 min (T363 and S369), whereas U50,488H attained the plateau at 1 min (Figure 29B). This results indicate that U50,488H and PMA showed different KOPR phosphorylation patterns and kinetics, possibly leading to different signaling and regulatory outcomes.

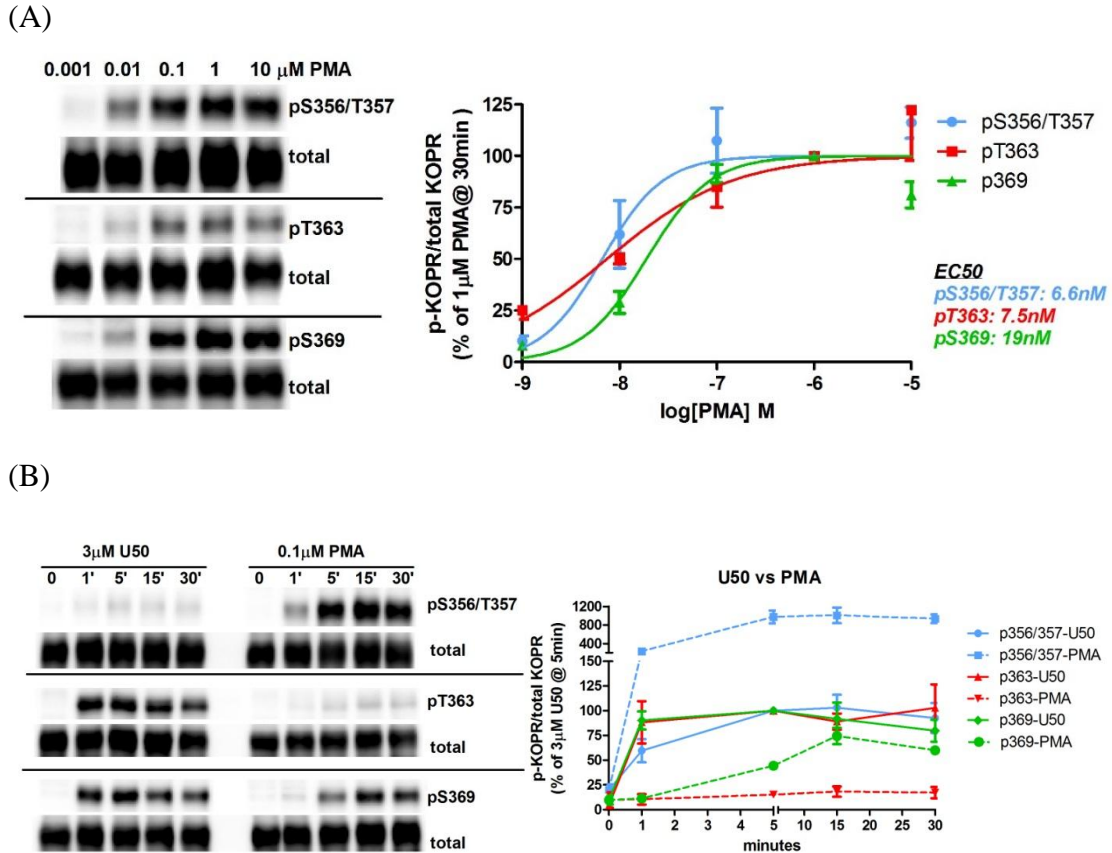


**Figure 29. Effect of PKC activation on KOPR phosphorylation**

(A) N2A-FmK6H cells were treated with different concentrations of the PKC activator phorbol-12-myristate-13-acetate (PMA) (0.001, 0.01, 0.1, 1 and 10  $\mu$ M) for 30 min. (B) Cells were incubated with 3  $\mu$ M U50,488H or 0.1  $\mu$ M PMA for 0, 1, 5, 15 and 30 min. (A,B) Cells were solubilized and the receptors were partially purified with a Ni-NTA agarose column. Eluates were used for western blot assay. One representative blot of each experiment is shown. The data are the mean  $\pm$  S.E.M (n=3-4).

PKC was also demonstrated to participate in homologous desensitization of 7TMRs, such as MOPR and CXCR4 (Busillo et al., 2010; Chen et al., 2013). Whether PKC is involved in U50,488H-induced KOPR phosphorylation was investigated using PKC inhibitors. The non-selective PKC inhibitor GF109203X (4  $\mu$ M) reduced U50,488H promoted KOPR phosphorylation at S356/T357, T363 and S369 by 80%, 60% and 30%, respectively (Fig. 30A) (two-way ANOVA, for S356/T357, U50,488H main effect,  $F_{1,8}=161.9$ ,  $p<0.0001$ ; GF109203X main effect,  $F_{1,8}= 161$ ,  $p<0.0001$ ; U50,488H  $\times$  GF109203X interaction,  $F_{1,8}= 65$ ,  $p<0.0001$ ; for T363, U50,488H main effect,  $F_{1,12}=239$ ,  $p<0.0001$ ; GF109203X main effect,  $F_{1,12}= 40.3$ ,  $p<0.0001$ ; U50,488H  $\times$  GF109203X interaction,  $F_{1,12}= 42.5$ ,  $p<0.0001$ ; for S369, U50,488H main effect,  $F_{1,12}=208$ ,  $p<0.0001$ ; GF109203X main effect,  $F_{1,12}= 4.29$ ,  $p=0.06$ ; U50,488H  $\times$  GF109203X interaction,  $F_{1,12}= 6$ ,  $p=0.03$ ). In addition, GF109203X alone affected the basal phosphorylation level of S356/T357, but not T363 and S369 (Figure 30A).

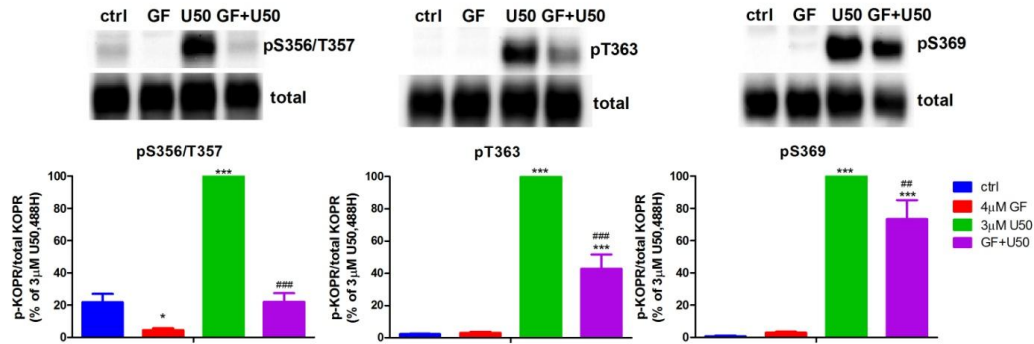
Another non-selective PKC inhibitor chelerythrine (CHL) (1  $\mu$ M) decreased U50,488H-promoted KOPR phosphorylation at T363 and S369 by 60%, but had no effect at S356/T357, without affecting basal phosphorylation (Figure 30B) (two-way ANOVA, for S356/T357, U50,488H main effect,  $F_{1,12}=53.8$ ,  $p<0.0001$ ; CHL main effect,  $F_{1,12}= 2.38$ ,  $p=0.15$ ; U50,488H  $\times$  CHL interaction,  $F_{1,12}= 1.03$ ,  $p=0.33$ ; for T363, U50,488H main effect,  $F_{1,19}=33.26$ ,  $p<0.0001$ ; CHL main effect,  $F_{1,19}= 199.7$ ,  $p<0.0001$ ; U50,488H  $\times$  CHL interaction,  $F_{1,19}= 36.6$ ,  $p<0.0001$ ; for S369, U50,488H main effect,  $F_{1,20}=595$ ,  $p<0.0001$ ; CHL main effect,  $F_{1,20}= 115$ ,  $p<0.0001$ ; U50,488H  $\times$  CHL interaction,  $F_{1,20}= 107$ ,  $p<0.0001$ ).

The selective PKC $\alpha$  and PKC $\beta$ 1 inhibitor Go6976 (100 nM) reduced U50,488H-

induced KOPR phosphorylation at S356/T357 and S369 by about 30% and 20%, but not at T363, with no effect on basal phosphorylation (Figure 31) (two-way ANOVA, for S356/T357, U50,488H main effect,  $F_{1,8}=72.73$ ,  $p<0.0001$ ; Go6976 main effect,  $F_{1,8}= 3.81$ ,  $p=0.087$ ; U50,488H  $\times$  Go6976 interaction,  $F_{1,8}= 2.36$ ,  $p=0.163$ ; for T363, U50,488H main effect,  $F_{1,8}=332$ ,  $p<0.0001$ ; Go6976 main effect,  $F_{1,8}= 0.4$ ,  $p=0.54$ ; U50,488H  $\times$  Go6976 interaction,  $F_{1,8}= 0.32$ ,  $p=0.59$ ; for S369, U50,488H main effect,  $F_{1,8}=236.9$ ,  $p<0.0001$ ; Go6976 main effect,  $F_{1,8}= 3.02$ ,  $p=0.12$ ; U50,488H  $\times$  Go6976 interaction,  $F_{1,8}= 4.02$ ,  $p=0.08$ ). These results suggested different PKC isoforms caused different phosphorylation patterns on KOPR.

siRNA knockdown of PKC $\alpha$  or PKC $\epsilon$  did not significantly affect U50,488H-induced KOPR phosphorylation at S356/T357, T363 and S369 (Figure 32). Knockdown efficiency of PKC $\alpha$  and PKC $\epsilon$  were 45% and 43%, respectively. As shown in Fig. 27, there are eight PKC isoforms in N2A cells. Knockdown of one isoform by siRNA may lead to substitution by other PKC isoforms, which makes it difficult to interpret the data. This is the reason why we decided to use PKC inhibitors in our studies. Thus, we did not examine the effects of the other six PKC isoforms on KOPR phosphorylation using PKC siRNAs.

(A)



(B)

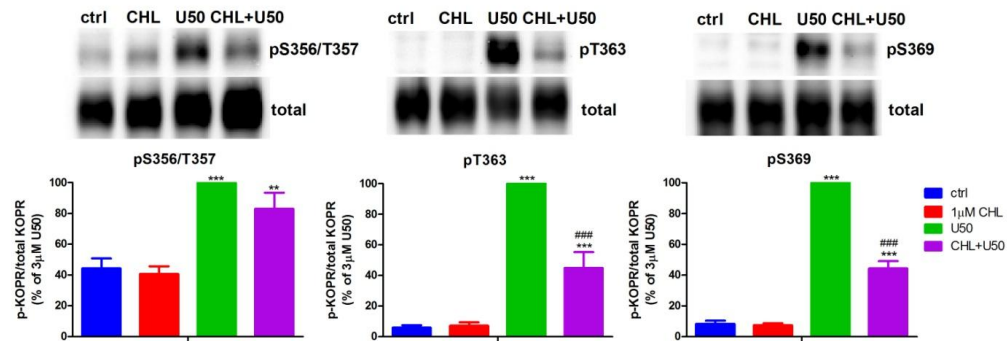


**Figure 30. Effects of two nonselective PKC inhibitors on U50,488H-induced KOPR phosphorylation at S356/T357, T363 and S369** N2A-FmK6H cells were pretreated with the nonselective PKC inhibitor GF109203X (GF) (4 μM) (A) or chelerythrine chloride (CHL) (1 μM) (B) for 30 min followed by 2-min incubation with 3 μM U50,488H or vehicle. Cells were solubilized and the receptors were partially purified with Ni-NTA agarose. Eluates were subject to western blot assay. One representative blot of each phospho-KOPR antibody is shown. Quantitation of staining intensity was performed (see Fig. 20 legend). The data shown are the mean ± S.E.M (n=3-6) and were analyzed by two-way ANOVA followed by Newman-Keuls *post-hoc* test (\*:  $p < 0.05$ , \*\*:  $p < 0.01$ , \*\*\*:  $p < 0.001$ , compared to untreated group; #:  $p < 0.01$ , ####:  $p < 0.001$ , compared

to U50,488H-treated group).

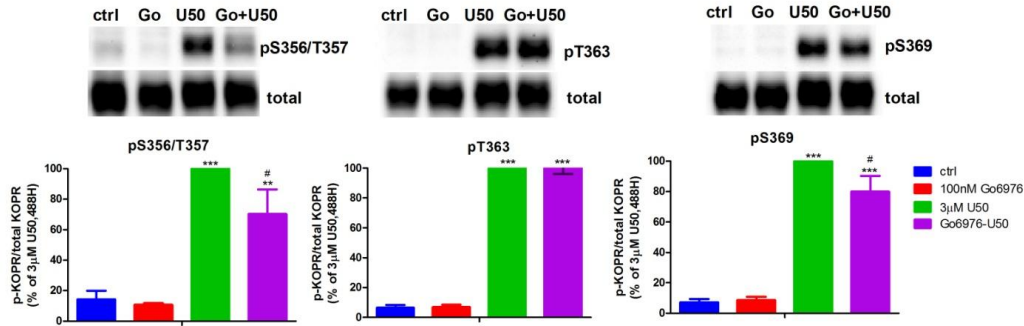


**Figure 31. Effect of the selective PKC $\alpha$  and  $\beta$ 1 inhibitor Go6976 on U50,488H-induced KOPR phosphorylation at S356/T357, T363 and S369** N2A-FmK6H cells were pretreated with the selective PKC  $\alpha$  and  $\beta$ 1 inhibitor Go6976 (100 nM) for 30 min followed by 2-min incubation with 3  $\mu$ M U50,488H or vehicle. Cells were solubilized and the receptors were partially purified with Ni-NTA agarose. Western blot assay was performed on the eluates. One representative blot of each phospho-KOPR antibody is shown. The data shown are the mean  $\pm$  S.E.M of 3 independent experiments and were analyzed by two-way ANOVA followed by Newman-Keuls *post-hoc* test (\*\*:  $p < 0.01$ , \*\*\*:  $p < 0.001$ , compared to control group; #:  $p < 0.05$  compared to U50,488H-treated group).

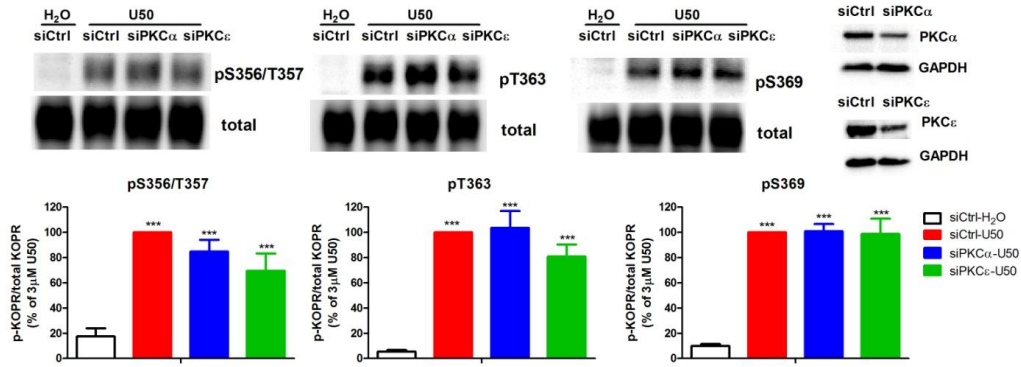


**Figure 32. Effects of knockdown of PKC $\alpha$  and PKC $\epsilon$  on U50,488H-induced KOPR phosphorylation at S356/T357, T363 and S369 phosphoresidues** FmK6H cells were transfected with siRNAs targeting PKC $\alpha$  or PKC $\epsilon$  (siPKC $\alpha$  and siPKC $\epsilon$ , respectively) or the control siRNA (siCtrl) with Lipofectamine 2000 for 48 hr. Cells were treated with vehicle or 3  $\mu$ M U50,488H for 2 min and then lysed. Receptors were partially purified using Ni-NTA agarose bead. Western blot was carried out with antibodies against pS356/pT357, pT363 and pS369. Top panel shows representative blots. Each value presents the mean  $\pm$  S.E.M of 5 independent experiments. The data were analyzed by one-way ANOVA followed by Newman-Keuls *post-hoc* test (\*\*\*:  $p < 0.001$ , compared to vehicle control group). Knockdown of PKC $\alpha$  and PKC $\epsilon$  were confirmed by immunoblotting.

### **PKC-mediated KOPR phosphorylation on KOPR internalization**

Whether PKC-mediated KOPR phosphorylation regulates U50,488H-induced KOPR internalization was examined with on-cell western assay. Cells were treated with a nonselective PKC inhibitor, GF109203X (4  $\mu$ M) or CHL (1  $\mu$ M), for 30 min followed by incubation with 10  $\mu$ M U50,488H for 30 min. Both GF109203X and CHL reduced slightly, but statistically significantly, U50,488H-induced internalization (Figure 33) (two-way ANOVA, for GF109203X experiment, U50,488H main effect  $F_{1,12}= 539.8$ ,  $p<0.0001$ ; GF109203X main effect  $F_{1,12}= 14.73$ ,  $p=0.0024$ ; U50,488H  $\times$  GF109203X interaction  $F_{1,12}=8$ ,  $p=0.015$ ; for CHL experiment, U50,488H main effect  $F_{1,12}= 813$ ,  $p<0.0001$ ; CHL main effect  $F_{1,12}= 3.85$ ,  $p=0.07$ ; U50,488H  $\times$  CHL interaction  $F_{1,12}=1.61$ ,  $p=0.23$ ). These results suggest that PKC may play a minor role in regulating U50,488H-induced KOPR internalization.

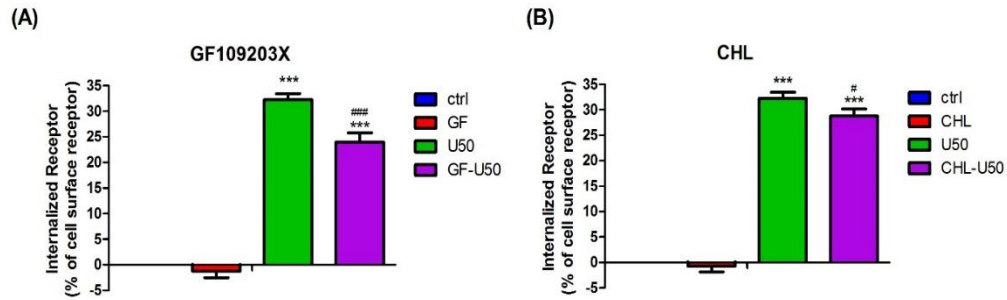


**Figure 33. Effects of PKC inhibitors on U50,488H-induced internalization** FmK6H cells were pretreated with the PKC inhibitors GF109203X (4  $\mu$ M) (A) or CHL (1  $\mu$ M) (B) for 30 min followed by 30-min incubation with 10  $\mu$ M U50,488H. Cells were fixed with 4% paraformaldehyde for on-cell western assay. FLAG-KOPR on cell surface were labeled with M1 mouse anti-FLAG antibody and then anti-mouse-IgG conjugated with 800CW, sapphire7000 and DRAQ5. Data presented are the mean  $\pm$  S.E.M of 4 independent experiments and were analyzed with two-way ANOVA followed by Newman-Keuls *post-hoc* test (\*\*\*:  $p < 0.001$ , compared to vehicle control group; #:  $p < 0.05$ , ###:  $p < 0.001$ , compared with U50,488H-treated group).

**Investigation on suitability of phospho-KOPR antibodies in immunocytochemistry:  
test on internalized KOPR following U50,488H treatment**

It is commonly accepted that antibodies useful for immunoblotting may not be useful for immunocytochemistry and *vice versa*. We tested the phospho-KOPR antibodies (anti-pS356/pT357, pT363 and pS369 antibodies) in immunocytochemistry. Internalized receptors following agonist treatment are phosphorylated and form intracellular clusters, which are more readily detected than receptors in plasma membranes. Cells were treated with vehicle or U50,488H for 30 min followed by immunocytochemical staining with each of the three phospho-KOPR antibodies. As a positive control, the KOPR, which was FLAG-tagged, was recognized with anti-FLAG M1 antibodies (green). Without U50,488H treatment, the KOPR was present mainly on plasma membranes (Figure 34 top panel green). U50,488H treatment for 30 min caused the KOPR (green color) to move from plasma membrane to intracellular compartments (Figure 34 bottom panel green). Following U50,488H treatment, pT363 antibody recognized internalized KOPR (red), which overlapped with the green staining by anti-FLAG M1 antibodies (Figure 34). It is noteworthy that when cells were treated with vehicle, KOPR remained in plasma membranes, which was recognized by anti-FLAG, but not by pT363 antibody, indicating that pT363 antibody does not recognize unphosphorylated KOPR.

pS356/pT357 and pS369 antibodies did not show similar patterns of staining as pT363 antibodies in control and U50,488H-treated cells. pS356/pT357 and pS369 antibodies yielded nonspecific staining in control cells (data not shown). Thus, only pT363 antibody was suitable for immunocytochemistry on cells *in vitro*.

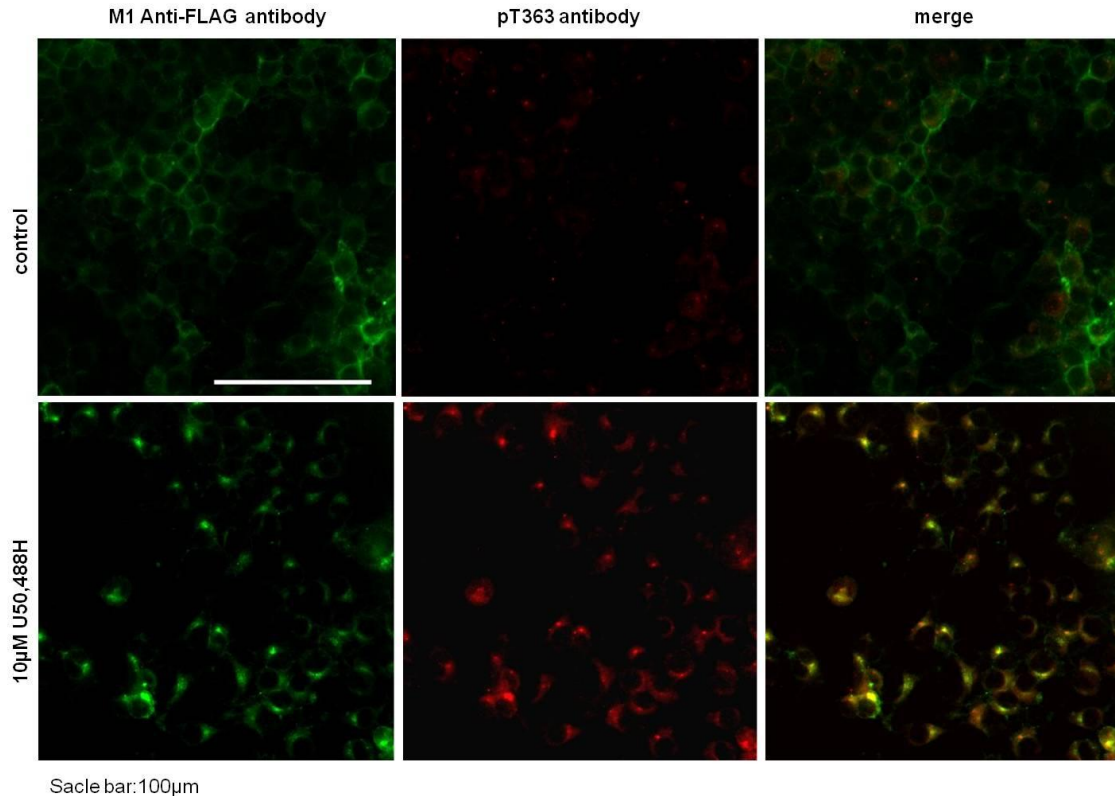


**Figure 34. Internalized KOPR following U50,488H treatment is phosphorylated at T363** FmK6H cells were incubated with M1 mouse anti-FLAG antibody to label cell surface KOPR for 30 min followed by 30-min incubation with 10  $\mu$ M U50,488H. Cells were fixed with 4% paraformaldehyde and then were incubated with pT363 phospho-KOPR antibody, followed by anti-mouse-IgG conjugated with Alexa-Fluor 488 and anti-rabbit-IgG conjugated with Alexa-Fluor 594 secondary antibodies, which reacted with M1 mouse anti-FLAG antibody (KOPR, green color) and rabbit pT363 phospho-antibody (Red color), respectively. Cells were examined under a fluorescence microscope and images were captured. The images represent one of the three experiments performed with similar results.

A chicken antibody generated against a KOPR peptide containing pS369 was obtained from Dr. Michael Bruchas' lab. It was also tested in western blot and immunocytochemistry. For western blot, after 3  $\mu$ M U50,488H treatment for 2 min, this chicken pS369 antibody recognized a 52-kDa band, not shown in the vehicle control group. There were several other nonspecific bands in both control and U50,488H-treated cells. For immunocytochemistry, chicken pS369 antibody stained nonspecific pattern in control cells (data not shown). Therefore, this chicken pS369 antibody is appropriate for Western blot assay but not immunocytochemistry.

We also tested our own phosphospecific KOPR antibodies in immunohistochemistry of the brain section (caudate putamen, nucleus accumbens and claustrum) and spinal cord lumbar section. However, it is difficult to identify the difference in staining patterns between saline and U50,488H (10 mg/kg, 30min, s.c.) treatment. Therefore, phosphospecific antibodies did not work for immunohistochemistry in tissues.

### **Studies on roles of PKC in KOPR-related pharmacological effects**

Activation of the KOPR produces many effects, including analgesia (von Voigtlander et al., 1983; Dykstra et al., 1987), antipruritic effects (Gmerek and Cowan, 1988), sedation and dysphoria (Dykstra et al., 1987). In the following experiments, we investigated the role of PKC in the pharmacological effects of KOPR activation. Activation of KOPR has been shown to inhibit calcium currents through PKC in rat dorsal root ganglion neurons and to activate ERK signaling via PKC in astrocytes (King et al., 1999; Belcheva et al., 2005). We have shown that PKC is involved in U50,488H-

promoted KOPR phosphorylation. Here we tested the hypothesis that PKC may trigger downstream signaling and be involved in some pharmacological effects of the KOPR *in vivo*. The nonselective PKC inhibitor CHL was used in the study because CHL is a cell permeable inhibitor that can cross blood brain barrier into the brain (Brennan et al., 2009).

### **Effect of PKC inhibitor CHL on KOPR phosphorylation in mouse brains**

The role of PKC in KOPR phosphorylation following U50,488H stimulation in brains was examined by using PKC inhibitor CHL. Male adult CD-1 mice were pretreated H<sub>2</sub>O or CHL (5 mg/kg, s.c.) for 1 hr followed by 15-min saline or U50,488H (10 mg/kg, s.c.) administration. Mouse brains (minus cerebellum) were removed, KOPR was purified and western blot was performed with antibodies against pT363 and pS369. U50,488H promoted KOPR phosphorylation at T363 and S369. CHL reduced U50,488H-induced phosphorylation at S369 by about 25% (two-way ANOVA, U50,488H main effect  $F_{1,8}=44.81$ ,  $p=0.0002$ ; CHL main effect,  $F_{1,8}=0.88$ ,  $p=0.37$ ; U50,488H× CHL interaction,  $F_{1,8}=6.86$ ,  $p=0.03$ ) (Figure 35), but not at T363 (two-way ANOVA, U50,488H main effect,  $F_{1,8}=20.23$ ,  $p=0.002$ ; CHL main effect,  $F_{1,8}=0.11$ ,  $p=0.75$ ; U50,488H× CHL interaction,  $F_{1,8}=0.46$ ,  $p=0.515$ ). CHL alone did not affect basal level of KOPR phosphorylation at T363 or S369. Thus, PKC appears to play a role in U50,488H-induced KOPR phosphorylation at S369, but not at T363, in brains. Phosphorylation at S356/T357 was not examined because the signal was low (data not shown).

Effect of CHL was dose-related. Pretreatment with CHL (1 mg/kg, s.c.) for 1 hr followed by 30-min or 1-hr U50,488H (5 mg/kg, s.c.) did not affect KOPR phosphorylation at T363 and S369. The treatment paradigm [CHL (5 mg/kg, s.c.) for 1 hr

followed by 15-min U50,488H (10 mg/kg)] is identical to that used in the rotarod behavior test (Figure 40). Whether pretreatment with CHL (1 mg/kg) followed by 5 mg/kg U50,488H for 15 min, which was used in the locomotor activity test (Figure 39), affects U50,488H-promoted KOPR phosphorylation needs to be further examined.

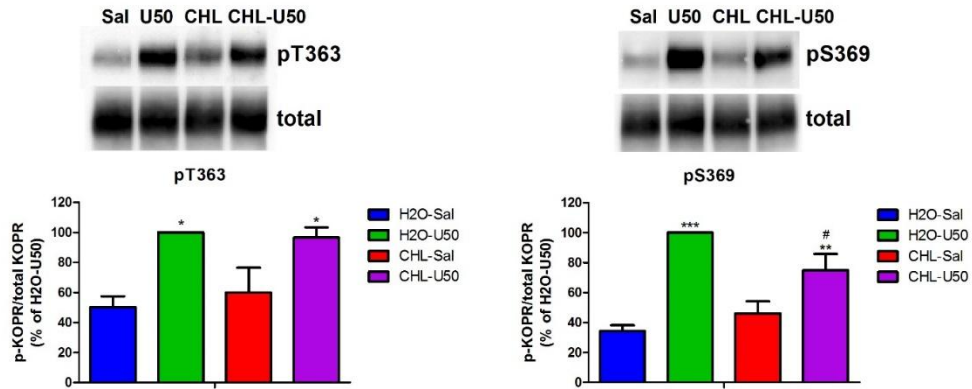


**Figure 35. Effect of the PKC inhibitor CHL on U50,488H-induced KOPR phosphorylation in mouse brains** Male adult CD1 mice were pretreated with H<sub>2</sub>O or CHL (5 mg/kg. s.c.) for 1 hr followed by saline or 10 mg/kg U50,488H (s.c.) for 15 min. Mice were euthanized, brains (minus cerebella) removed and KOPR purified. Western blot was performed with pT363 and pS369 antibodies. The data shown are the mean  $\pm$  S.E.M of 3 independent experiments and were analyzed by two-way ANOVA followed by Newman-Keuls *post-hoc* test (\*:  $p < 0.05$ , \*\*:  $p < 0.01$  \*\*\*:  $p < 0.001$ , compared to H<sub>2</sub>O-Sal group; #:  $p < 0.05$  compared to H<sub>2</sub>O-U50,488H group).

### **Effect of PKC inhibition on KOPR-mediated analgesia**

KOPR agonists have long been known to have analgesic effect (von Voigtlander et al., 1983; Dykstra et al., 1987). Whether PKC inhibition affected U50,488H-induced analgesia in the formalin test was examined. Male adult CD-1 mice were treated with the PKC inhibitor CHL (1 mg/kg, s.c.) for 1 hr in the home cage and then injected with U50,488 (1 mg/kg, s.c.). Five minutes later, 20  $\mu$ l of 5% formalin was injected into the bottom of the left hind paw. Fifteen to 20 min later, mice were recorded for the time spent on licking formalin-injected paws for 20 min, which is referred to as the phase II reaction of the formalin test. U50,488H treatment reduced the licking time, indicating antinociceptive effects (two-way ANOVA, U50,488H main effect,  $F_{1,36}=58.21$ ,  $p<0.0001$ ; CHL main effect,  $F_{1,36}=0.12$ ,  $p=0.73$ ; U50,488H  $\times$  CHL interaction  $F_{1,36}=0.28$ ,  $p=0.6$ ). Pretreatment with CHL did not affect U50,488H-induced reduction in licking time (Figure 36), indicating that PKC does not play a role in U50,488H-induced antinociception in the formalin test.

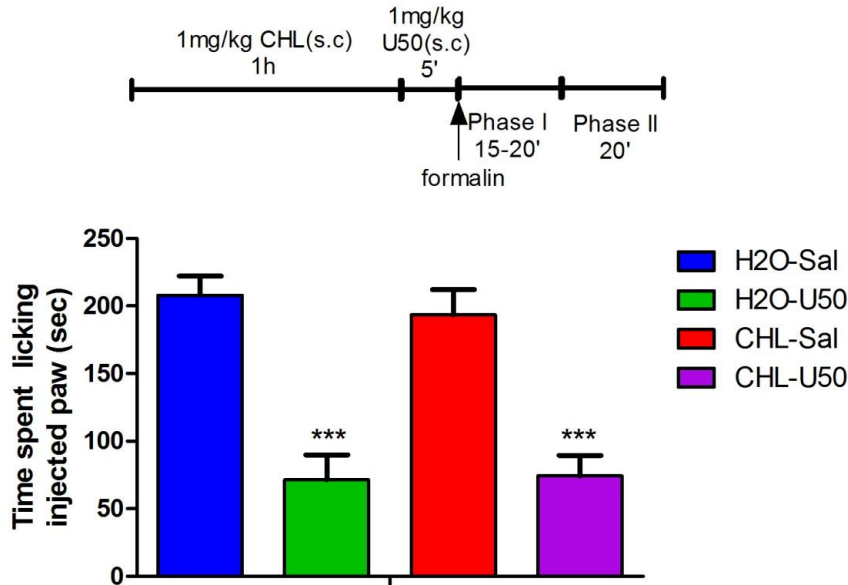


**Figure 36. Effect of the PKC inhibitor CHL on U50,488H-induced analgesia in the formalin test** Male adult CD1 mice were subcutaneously injected with the PKC inhibitor CHL (1 mg/kg) or H<sub>2</sub>O for 1 h in the home cage followed by U50,488H (1 mg/kg, s.c.) or saline treatment in the test chamber. Five minutes later, Mice were injected with 5% formalin into the bottom of their left hind paws under isoflurane anesthesia. Fifteen to 20 min later when the phase I reaction (flinching) was over, mice were recorded for 20 min for the time they spent on licking their injected hind paws (phase II reaction). Results shown are the mean  $\pm$  S.E.M (n=10). Data were analyzed with two-way ANOVA followed by Bonferroni *post-hoc* test (\*\*\*:  $p < 0.001$ , compared to vehicle control group, H<sub>2</sub>O-Sal group).

### **Effect of PKC inhibition on KOPR-mediated antipruritic effect**

Activation of KOPR produces antipruritic effects (Gmerek and Cowan, 1988). The role of PKC in KOPR-induced antipruritic effect was examined. Mice were treated with vehicle or CHL (5 mg/kg, s.c.) and placed in test cages for 1 hr and then injected with vehicle or U50,488H (5 mg/kg, s.c.). Twenty min later, the pruritogen compound 48/80 (20  $\mu$ l) was injected into the nape of the neck in mice and scratching bouts were then counted for 30 min. U50,488H treatment decreased the number of scratching bouts, indicating its antipruritic effect (two-way ANOVA, U50,488H main effect,  $F_{1,32}=69.83$ ,  $p<0.0001$ ; CHL main effect,  $F_{1,32}=0.63$ ,  $p=0.43$ ; U50,488H  $\times$  CHL interaction,  $F_{1,32}=0.32$ ,  $p=0.56$ ). CHL treatment alone did not affect the number of scratching bouts, neither did it affect U50,488H-caused anti-scratching effect (Figure 37). These results indicate that PKC do not participate in U50,488H-induced anti-scratching effect. Higher dose 10 mg/kg CHL alone reduced compound 48/80-induced scratching bouts, compared to saline-treated group ( $n=5$ ), indicating the dose of 10 mg/kg CHL may be too high, leading to off-target effects. Therefore, effect of 10 mg/kg CHL was not tested on U50,488H-induced anti-scratching effect.

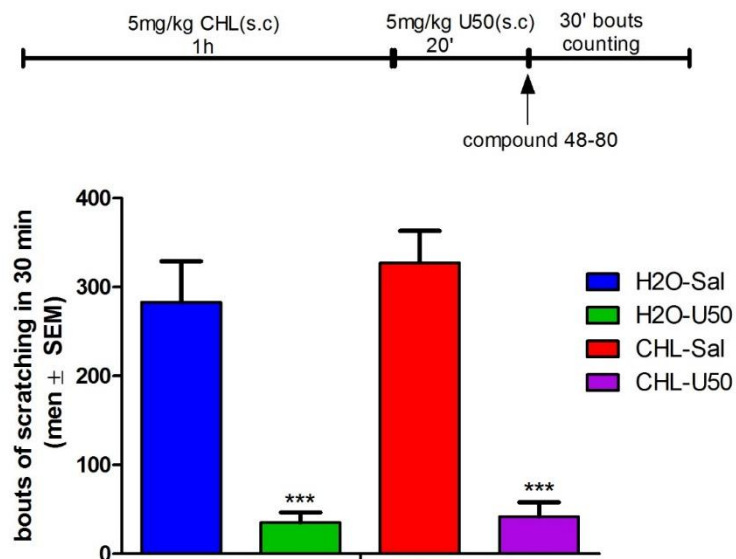


**Figure 37. Effect of the PKC inhibitor CHL on U50,488H-induced anti-scratching behavior** Male adult CD1 mice were acclimated in test cages for 1 hr and injected with the PKC inhibitor CHL (5 mg/kg, s.c.) or vehicle for 1 hr followed by subcutaneous 5 mg/kg U50,488H or saline administration. The pruritogen compound 48/80 was subcutaneously injected into the nape of the neck and then the number of scratching bouts was counted for 30 min. Data represent the mean  $\pm$  S.E.M (n=8-10). Data were analyzed with two-way ANOVA followed by Bonferroni *post-hoc* test (\*\*\*:  $p < 0.001$ , compared to vehicle control group, H<sub>2</sub>O-Sal group).

Tolerance to drug effect has been shown to be related to receptor phosphorylation. Whether U50,488H treatment develops tolerance to its anti-scratching effect was examined. Male adult CD-1 mice were subcutaneously injected with U50,488H (5 mg/kg) for 6 days. Mice were tested their anti-scratching effect on day 1 and day 6. On the test days, mice were acclimated in the test cages for 1 hr and then injected with U50,488H for 20 min followed by compound 48/80. Acute treatment of U50,488H caused anti-scratching effect, compared to acute vehicle-treated group. After 6 days of treatment, U50,488H-treated group still showed similar extents of anti-scratching effect, indicating no tolerance development (two-way ANOVA, drug main effect,  $F_{1,17}=32.2$ ,  $p<0.0001$ ; time main effect,  $F_{1,17}=0.14$ ,  $p=0.7$ ; drug  $\times$  time interaction,  $F_{1,17}=1.55$ ,  $p=0.23$ ) (Figure 38). Because the result showed no tolerance, we did not further investigate the effect of PKC inhibition on drug tolerance.

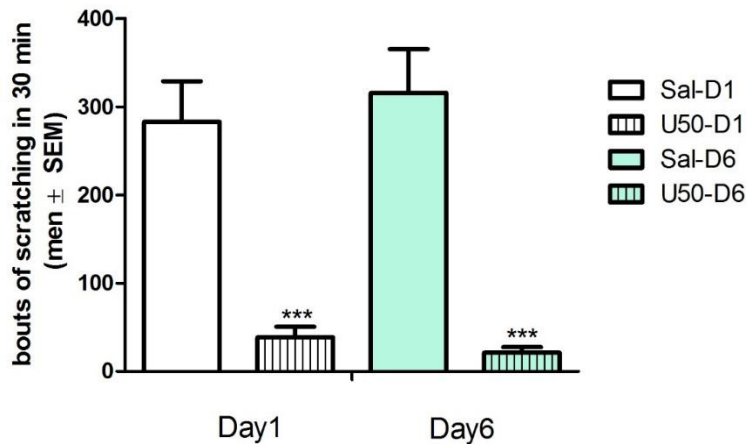


**Figure 38. Repeated U50,488H injection did not cause tolerance development in**

**anti-scratching test** Male CD1 mice were treated with saline or U50,488H (5 mg/kg, s.c.)

once a day for 6 days. Mice were test on day 1 and day 6. On the test days, mice were

acclimated for 1 hr in test cages and then injected with saline or U50,488H for 20 min,

followed by subcutaneous administration of compound 48/80 into the nap of neck.

Numbers of scratching bouts were counted for 30 min. Data represent the mean  $\pm$  S.E.M

(n=9-10). Data were analyzed with two-way ANOVA followed by Bonferroni *post-hoc*

test (\*\*\*:  $p < 0.001$ , compared saline-treated group).

### **Effect of PKC inhibition on KOPR-mediated sedation and motor incoordination**

KOPR agonists have been shown to induce sedation and motor incoordination (Kieffer, 1999). Novelty-induced locomotion and rotarod performance assays are well-established methods to assess these effects, respectively. Here we investigated whether PKC participated in U50,488H-induced sedation and motor incoordination.

For novelty-induced locomotion, mice were injected with the PKC inhibitor CHL (1 mg/kg) or H<sub>2</sub>O and then 1 hr later with 5 mg/kg U50,488H or saline. Mice were immediately placed in locomotor activity chambers. Total distance traveled (cm), total activity, ambulatory activity and stereotypy activity were recorded for 1hr in 5-min bins. The areas under the curves (AUC) of the first 30-min period of all the groups were calculated. U50,488H-treated mice displayed decreased total distance traveled, total activity, ambulatory activity and stereotypy activity, indicating sedative effects (two-way ANOVA for total distance, U50,488H main effect,  $F_{1,44}=32.33$ ,  $p<0.001$ ; CHL main effect,  $F_{1,44}=0.15$ ,  $p=0.7$ ; U50,488H× CHL interaction,  $F_{1,44}=7.2$ ,  $p=0.01$ ). CHL alone did not have effects on any of the four parameters. CHL treatment attenuated the reduction in total distance traveled caused by U50,488H (Fig. 39A) (Newman-Keuls post-test,  $p<0.05$  vs H<sub>2</sub>O-U50), but had no effects on U50,488H-induced reduction in total, ambulatory and stereotypy activities (Figure 39B, C and D). These results suggest that PKC may be involved in U50,488H-induced sedation.

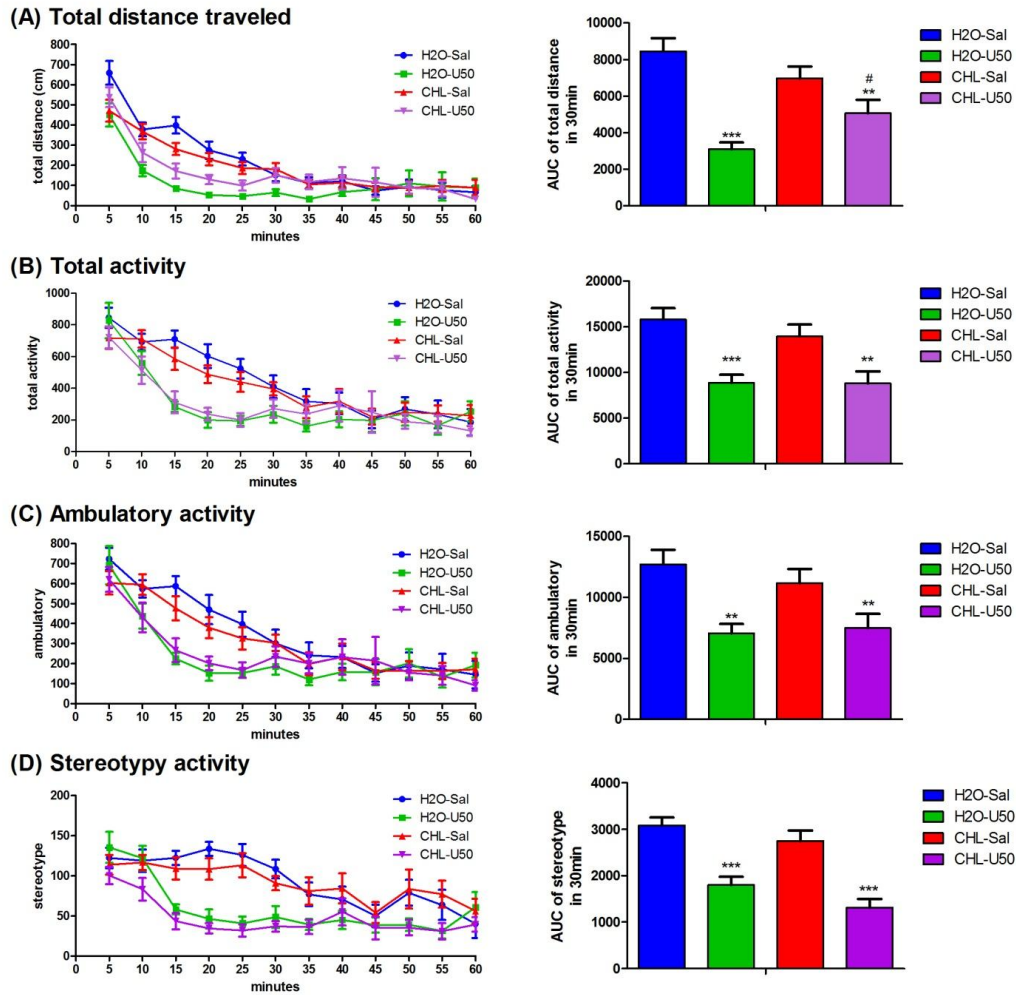


**Figure 39. Effect of the PKC inhibitor CHL on U50,488H-induced sedation in the novelty-induced locomotor activity model** Male adult CD1 mice were injected with the PKC inhibitor CHL (1 mg/kg, s.c.) in the home cage and 1 hr later with 5 mg/kg U50,488H (s.c.). Mice were immediately placed into locomotor activity chambers for activity recording which was done in 5-min bins for 1 hr. (A) total distance traveled (cm), (B) total activity, (C) ambulatory activity and (D) stereotypy activity (the number of beam breaking) were recorded by Fusion software. Data are the mean  $\pm$  S.E.M (n=12). Area under curve (AUC) during the first 30 min were presented as bar graphs in the right panel and analyzed with two way-ANOVA followed by Newman-Keuls *post-hoc* test (\*\*):

$p < 0.01$ ; \*\*\*:  $p < 0.001$ , compared to vehicle control group, H<sub>2</sub>O-Sal group; #:  $p < 0.05$ , compared to U50,488H-treated group, H<sub>2</sub>O-U50,488H group).

For the rotarod performance test, mice were trained 2 days before the test day. Each mouse was trained to run on the rod for 3 trials with a 5-min break between trials. The rod was set to accelerate from 3 to 30 rpm during the 5-min training period. On the test day, mice were tested for the baseline first. Mice were subsequently given CHL (1 mg/kg or 5 mg/kg) or H<sub>2</sub>O and then 1 hr later treated with 10 mg/kg U50,488H or saline. Mice were tested at 10, 20, 30 min after U50,488H injection. Mice treated with 10 mg/kg U50,488H stayed on the rod for shorter periods of time at 10, 20 and 30 min after U50,488H, indicating motor incoordination (two-way ANOVA for 10 min, U50,488H main effect,  $F_{1,74}=21.47$ ,  $p<0.0001$ ; CHL main effect,  $F_{2,74}=1.59$ ,  $p=0.21$ ; U50,488H×CHL interaction,  $F_{2,74}=2.23$ ,  $p=0.11$ ; for 20 min, U50,488H main effect,  $F_{1,74}=29.23$ ,  $p<0.0001$ ; CHL main effect,  $F_{2,74}=1.88$ ,  $p=0.16$ ; U50,488H×CHL interaction,  $F_{2,74}=2.79$ ,  $p=0.07$ ; for 30 min, U50,488H main effect,  $F_{1,74}=38.73$ ,  $p<0.0001$ ; CHL main effect,  $F_{2,74}=1.23$ ,  $p=0.3$ ; U50,488H×CHL interaction,  $F_{2,74}=0.91$ ,  $p=0.41$ ). Pretreatment with 5 mg/kg CHL attenuated U50,488H-induced impaired rotarod performance at 10 min and 20 min (Bonferroni post-hoc test,  $p<0.05$  vs H<sub>2</sub>O-U50), but not at 30 min. In contrast, pretreatment with 1 mg/kg CHL did not affect U50,488H-induced deficiency in rotarod performance (Figure 40). These results suggested PKC may regulate U50,488H-mediated sedation and motor impairment effects.

For the rotarod performance test, 5 mg/kg U50,488 did not cause significant motor incoordination (data not shown), but 10 mg/kg did. Thus, 10 mg/kg U50,488H was used to examine the effect of PKC inhibition on KOPR-induced motor incoordination.

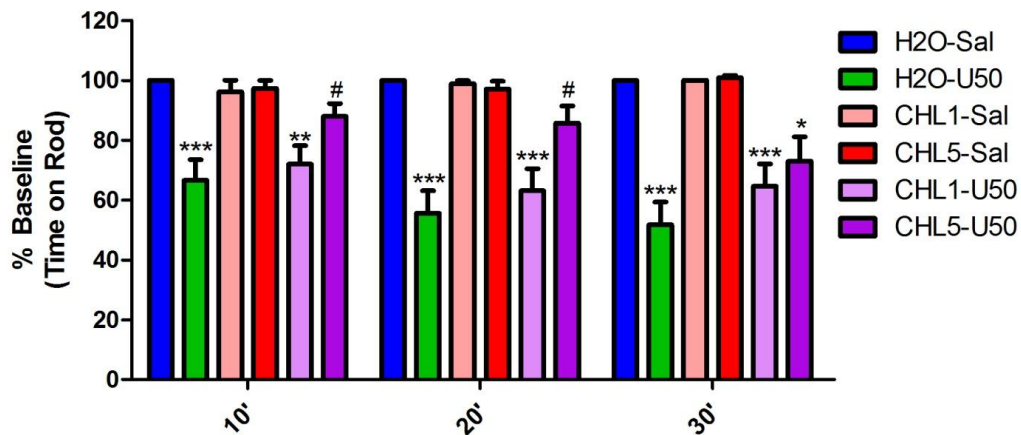


**Figure 40. Effect of the PKC inhibitor CHL on U50,488H-induced motor incoordination in the rotarod performance assay** Male adult CD1 mice were trained to run on a rotarod machine 2 days before the test day. On the training day, mice were placed on the rotarod for 5 min with the rotation revolution changing from 3 to 30 rpm. Each mouse was trained for 3 trails with a break of 5 min between trials. On the test day, mice were tested on the rod first to establish the baseline. All the mice were able to stay on the rotarod for the entire 5 min, so the baselines were 300 sec for all the groups. Mice were subcutaneously injected with the PKC inhibitor CHL (1 mg/kg, CHL1 or 5 mg/kg, CHL5) or H<sub>2</sub>O 1 hr prior to subcutaneous administration of U50,488H (10 mg/kg) or saline. Ten, 20 and 30 min after U50,488H injection, mice were tested on the rotarod for the time staying on the rod. Results are shown as the percentage of time staying on the rod following drug administration compared with the baseline. Data are shown as the mean  $\pm$  S.E.M (n=10-19) and were analyzed with two-way ANOVA followed by Bonferroni *post-hoc* tests (\*\*:  $p < 0.01$ , \*\*\*:  $p < 0.001$ , compared with control H<sub>2</sub>O-Sal group; #:  $p < 0.05$ , compared to H<sub>2</sub>O-U50,488H group).

## **Effect of PKC inhibition on KOPR-mediated aversion in the conditioned place aversion (CPA) test**

KOPR agonists cause psychotomimetic effects in humans (Pfeiffer et al., 1986) and aversion in animals (Dykstra et al., 1987). The CPA test was used to examine effects of PKC inhibition on KOPR-mediated aversion. Mice were tested for their preference to either chamber of the apparatus on day 0 without any drug treatment. Most animals stayed in both sides for similar amounts of time. Some mice had high preference for either chamber (>65% of 15 min), which were excluded from the study. Mice were conditioned for 6 days. In the morning sessions, mice were injected with sterile distilled water for 1 hr followed by 15-min saline treatment in the home cages. Mice were then placed in the non-drug paired side for 30-min conditioning. In the afternoon sessions, mice were injected with H<sub>2</sub>O or the PKC inhibitor CHL (0.1, 1 or 5 mg/kg, s.c.) followed by saline or U50,488H (5 mg/kg, s.c.) administration and allowed to stay in the home cage for 15 min for U50,488H effect to emerge. Mice then were placed in the drug-paired side for 30-min conditioning. Mice were tested on day 7 (Figure 41A). Two-way ANOVA of preference scores revealed a significant main effect of time on day 7 versus day 0 on U50,488H-treated group ( $F_{1,178}=4.61$ ,  $p=0.03$ ). CHL at 1 mg/kg and 5 mg/kg, but not at 0.5 mg/kg, reduced U50,488H-induced aversion on day 7 ( $p<0.05$  for 1 mg/kg CHL-U50,  $p<0.01$  for 5 mg/kg CHL-U50 vs H<sub>2</sub>O-U50) (Figure 41B). CHL alone at 1 mg/kg and 5 mg/kg did not induce any preference or aversion. Because higher doses of CHL (1 and 5 mg/kg) alone did not affect preference, 0.5 mg/kg CHL alone was not tested. Collectively, these results suggest that PKC plays a role in U50,488H-induced CPA.

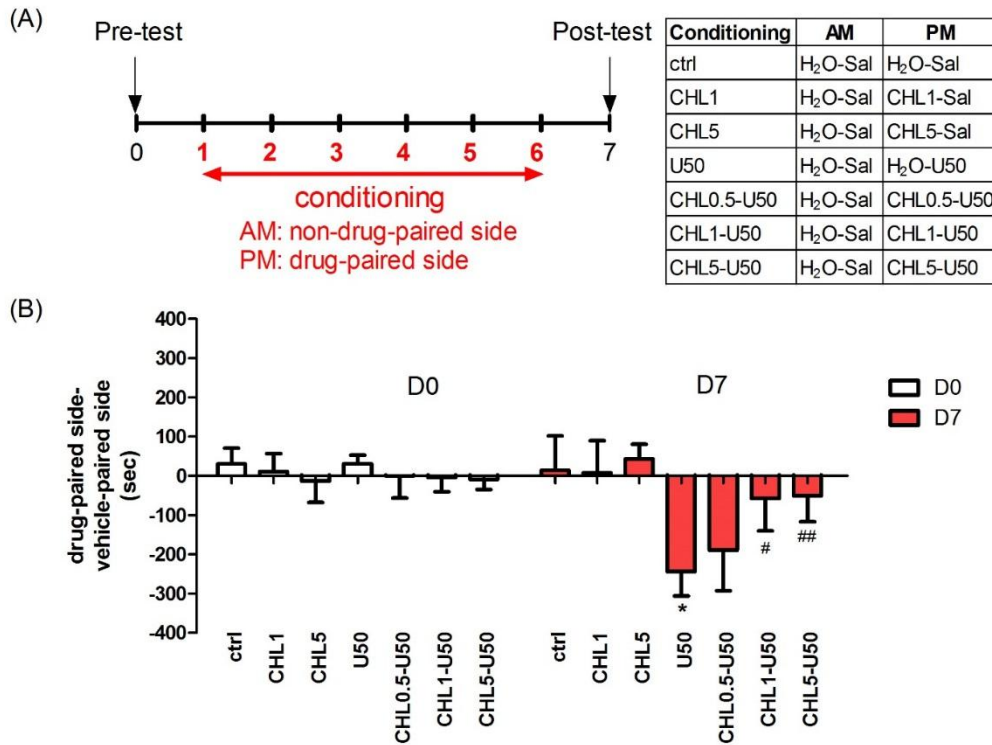


**Figure 41. Effect of the PKC inhibitor CHL on U50-induced CPA** Male adult CD1 mice were pre-tested on day 0 (D0) to determine the time spent on each side. Mice were conditioned twice a day for 6 days according to the design in the top panel. During the conditioning period from day 1 to day 6, mice were injected with H<sub>2</sub>O (s.c.) followed one hour later by saline (15 min, s.c.) in the morning and then placed in the non-drug paired chambers for 30 min. In the afternoon, mice were pre-treated with the PKC inhibitor CHL 0.5 mg/kg (CHL0.5), 1 mg/kg (CHL1) or 5 mg/kg CHL (CHL5) or H<sub>2</sub>O for 1 hr followed by U50,488H (5 mg/kg) or saline in the home cage for 15 min and then placed in the drug-paired chambers for 30 min. The post-test was performed on day 7 (D7), in which mice were allowed free access to either side for 15 min and the time spent on either side was recorded. Data represent the mean  $\pm$  S.E.M (n=9-19) and were analyzed with two-way ANOVA followed by Bonferroni *post-hoc* tests (\*:  $p < 0.05$ , \*\*:  $p < 0.01$ , \*\*\*:  $p < 0.001$ , compared with ctrl group on D7; #:  $p < 0.05$ , ##:  $p < 0.01$ , compared to U50-

treated group on D7).

## Discussion

### **Study on KOPR phosphorylation following U50,488H stimulation *in vitro***

Our previous study showed that U50,488H caused phosphorylation of the mKOPR at S356, T357, T363 and S369 in the C-terminal domain using the LC-MS/MS approach and immunoblotting with phospho-KOPR specific antibodies (Chen et al., 2016). In this study, we characterized time course, dose-response relationship and antagonist blockade of U50,488H-promoted mKOPR phosphorylation and determined the protein kinases (GRKs and PKC) involved in KOPR phosphorylation in FmK6H-N2A cells using phospho-specific antibodies.

### **Time course of KOPR phosphorylation**

At 37°C, U50,488H very rapidly promoted KOPR phosphorylation at S356/T357, T363 and S369, reaching the peaks in 30 sec, 1 min and 2 min, respectively, and remaining at the peak levels for at least 10 min, the longest interval examined (Figure 21). These results on the KOPR have similarities and differences from those on the MOPR. The MOPR full agonist DAMGO induced MOPR phosphorylation at S375 very rapidly reaching the peaks at 20 seconds; however, phosphorylation occurred much more slowly at T379 and T376, reaching the plateau at 30 minutes (Doll et al., 2011; Just et al., 2013). Thus, different subtypes of opioid receptors showed different time courses of agonist-promoted phosphorylation.

### *Hierarchical relationship of KOPR phosphorylation sites*

It is difficult to determine the order of phosphorylation among these residues because KOPR phosphorylation occurs so rapidly. However, in our previous studies using

phospho-site KOPR mutants and LC-MS/MS have revealed the hierarchy. Mutation of either T363 or S369 to Ala affected phosphorylation of the other and also S356/T357 phosphorylation, whereas S356A, T357A and S356A/T357A substitution did not affect phosphorylation of T363 or S369. Our stable isotope labeling by amino acids in cell culture (SILAC) and LC-MS/MS data showed that although U50,488H did not increase single phosphorylation at T357, it enhanced double phosphorylation at T363/S369 and T357/S369 and triple phosphorylation at S356/T357/S369. Taken together, these results indicate that T363 and S369 are two initial sites of U50,488H-induced KOPR phosphorylation followed by S356 and T357 (Chen et al., 2016).

### **GRK-induced KOPR phosphorylation**

GRKs are major protein kinases involved in phosphorylating GPCRs upon agonist treatment. In our current cell model (N2A cells), there are endogenous GRKs2, 3 and 6, with low or no GRK5, as revealed by immunoblotting (Figure 23). After siRNAs knockdown of endogenous GRKs2, 3 and 6, KOPR phosphorylation at S356/T357, T363 and S369 following U50,488H stimulation was decreased (Figure 25 and 26). Because N2A cells express low or no GRK5 endogenously, its effect was examined by overexpression and a combination of overexpression and knockdown. Overexpression of GRK5 promoted higher levels of U50,488H-induced phosphorylation at all the residues and siRNA knockdown eliminated the effects of GRK5 overexpression, demonstrating the specificity of GRK5 effect (Figure 27). These results thus indicate that GRKs 2, 3, 5 and 6 are all involved in U50,488H-promoted KOPR phosphorylation at S356/T357, T363 and S369.

## Bar code hypothesis

The concept of "bar code" has emerged recently. At the receptor level, agonists cause different active receptor conformations, leading to recruitment of specific subsets of GRKs to act on GPCR and result in different phosphorylation patterns. Distinct phosphorylation patterns may recruit  $\beta$ -arrestins in different conformations, resulting in distinct functional changes (Reiter et al., 2012; Wisler et al., 2014). Different GRKs have been reported to phosphorylate distinct residues (bar codes), which lead to receptor regulation and/or  $\beta$ -arrestin-mediated downstream signaling (Nobles et al., 2011).

For example, in the case of the  $\beta$ 2-adrenergic receptor ( $\beta$ 2AR), while isoproterenol (a balanced ligand) increases GRK2- and GRK6-mediated receptor phosphorylation, carvedilol (a  $\beta$ -arrestin biased ligand) enhances only GRK6-mediated receptor phosphorylation. GRK6-phosphorylated at pS355 and pS356 contributed to  $\beta$ -arrestin-mediated ERK activation, while GRK2-mediated phosphorylation of pT360, pS364, pS396, pS401, pS407 and pS411 was required for receptor internalization. Both GRK2 and GRK6 contribute to isoproterenol-induced receptor desensitization (Nobles et al., 2011).

DAMGO promoted MOPR internalization, but morphine did not. Morphine caused MOPR phosphorylation at only S375 by the action of GRK5. In contrast, DAMGO-promoted MOPR phosphorylation was mediated by GRKs 2/3, which was initiated at S375, followed by phosphorylation at T370, T376 and T379 (Lau et al., 2011; Just et al., 2013), demonstrating that higher order phosphorylation of the MOPR is required for agonist-induced internalization. These studies show that different GRKs cause different phosphorylation patterns on GPCRs, resulting in differential receptor

regulation and signaling.

In contrast to these studies, our results that GRKs2, 3, 5 and 6 cause phosphorylation of the same residues in the KOPR following U50,488H indicate that there are no differential phosphorylation patterns in U50,488H-promoted GRK-mediated KOPR phosphorylation. Whether other structurally distinct KOPR agonists, such as MOM-salvinorin B, dynorphins and ethylketocyclazocine, show different phosphorylation patterns regulated by different GRKs needs to be further examined. Whether different GRKs promote different high-order KOPR phosphorylation in these KOPR agonists remains to be investigated.

#### **Other studies related to GRK-mediated KOPR phosphorylation**

Our findings that U50,488H induced mouse KOPR phosphorylation at S356/T357, T363 and S369, which is mediated at least in part by GRKs, showed some similarities and differences when compared with the observations of Chavkin and colleagues (Appleyard et al., 1999; McLaughlin et al., 2003). These researchers reported that U50,488H (10  $\mu$ M, 30min) induced KOPR phosphorylation at S369 by immunoblotting using phospho-specific antibody against rat KOPR 359-372 containing pS369. U50,488H-mediated rKOPR desensitization and internalization were eliminated by S369A mutation or expression of GRK2 dominant mutant GRK2(K220R) in HEK293 cells (McLaughlin et al., 2003). In *Xenopus* oocytes, U69,593-induced rKOPR desensitization was enhanced by co-expression of GRK3 or GRK5 and  $\beta$ -arrestin 2 and mutation of S369 to Ala in the C-terminal domain attenuated the desensitization. In contrast, substitution with Ala of S356, T357 or T363 in the C-terminal domain or S255,

S260 and S262 in the third intracellular loop did not have any effect on desensitization (Appleyard et al., 1999). Thus, GRKs2, 3 and 5-mediated rKOPR phosphorylation at S369 was involved in KOPR desensitization and internalization. As the rat and mouse KOPRs share the same C-terminal domain sequence, it is likely that they are regulated by the agonists similarly at the S369 residue.

These researchers used site-directed mutagenesis approach and did not find phosphorylation at S356, T357 or T363. Our previous results showed hierarchical relationship of KOPR phosphorylation sites that S369A mutation not only abolished S369 phosphorylation, but also reduced S356/T357 and T363 phosphorylation (Chen et al., 2016). In N2A cells, while U50,488H caused internalization of the mKOPR, etorphine did not. Compared to etorphine, U50,488H promoted higher levels of single phosphorylation at T363 and S369, double phosphorylation at T363+S369 and T357+S369. In addition, U50,488H promoted triple phosphorylation at S356+T357+S369, but etorphine did not. Thus phosphorylation at S356, T357 or T363 in the form of higher-order phosphorylation contributes to receptor internalization and perhaps yet unknown functions.

### **Phosphorylation sites in GPCRs**

Agonist-promoted GPCR phosphorylation commonly occurs in the C-terminal domain and, to lower extents, in the 3<sup>rd</sup> intracellular loop. In this study, we followed up our previous report that U50,488H caused KOPR phosphorylation at S356, T357, T363 and S369 in the C-terminal domain. The C-terminal domain of KOPR has 2 serine and 2 threonine residues, all of which are phosphorylated by U50,488H treatment. Most other

GPCRs studied to date have more complex phosphorylation patterns. For example, the  $\beta$ 2AR has 10 serine and threonine residues in the C-terminal domain; T360, S364, S396, S401, S407 and S411 are phosphorylated by GRKs2/3 and S355 and S356 are phosphorylated by GRKs5/6 (Nobles et al., 2011). The MOPR has 12 serine and threonine residues in the C-terminal domain. Among them, T370, S375, T376 and T379 are phosphorylated by GRKs2/3; S375 is also phosphorylated by GRK5; S363 and T370 are phosphorylated by PKC (Mann et al., 2014). However, at the present time, we cannot rule out the possibility that agonist-promoted KOPR phosphorylation may occur at Ser and Thr residues in the 3<sup>rd</sup> intracellular loop.

GRK2 and GRK3 have been reported to show preference for Ser or Thr residues downstream of acidic residues (Eason et al., 1995; Onorato et al., 1991), while GRK5 and GRK6 prefer residues downstream of basic residues (Kunapuli et al., 1994; Pitcher et al., 1998). The sequence of the KOPR C-terminal domain is DENFKRCFRDFCFPIKMRM ERQS<sup>356</sup>T<sup>357</sup>NRVRNT<sup>363</sup>VQDPAS<sup>369</sup>MRDVGF MNV. The N-terminal residues of the four phosphorylation sites within C terminal domain of KOPR are neither acidic nor basic amino acid. Thus, KOPR phosphorylation by GRKs did not follow this preference.

### **PKC-mediated KOPR phosphorylation**

PKC has been reported to be involved in stimulation of p44/42 MAPK and phosphodiesterase following KOPR activation (Bian et al., 2000; Bohn et al., 2000). We examined the role of PKC in agonist-independent and agonist-dependent KOPR phosphorylation.

#### ***PKC-mediated agonist-independent KOPR phosphorylation***

PMA was used to activate PKC. PMA, a diester of phorbol and a DAG analog, interacts with DAG/phorbol ester binding domain of PKC to activate PKC. Conventional and novel PKCs, but not atypical PKCs, are regulated by DAG. The result that PMA promoted KOPR phosphorylation at S356/T357, T363 and S369 (Figure 10) indicates that conventional and novel PKCs play roles in agonist-independent KOPR phosphorylation.

Compared with U50,488H-induced KOPR phosphorylation (agonist-dependent), PMA showed different phosphorylation levels and slower rates at S356, T357, T363 and S369 (Figure 29B). At S356/T357, PMA caused much higher maximal phosphorylation levels than U50,488H (~10 fold). At T363, U50,488H promoted much faster phosphorylation and attained higher levels of maximal phosphorylation than PMA (~7 fold). At S369, U50,488H induced faster phosphorylation than PMA, reaching similar maximal levels at 1 min and 15 min, respectively. Because PMA and U50,488H had different levels and time courses of KOPR phosphorylation, they may lead to different downstream cellular functions. PKC-mediated KOPR phosphorylation may, at least in part, contribute to heterologous desensitization of KOPR by CXCR4 activation. Activation of CXCR4 decreased KOPR-mediated chemotaxis, antinociception and calcium mobilization (Finley et al., 2008). One possible mechanism is that CXCR4 stimulation activates PKC, which in turn phosphorylates KOPR, leading to KOPR desensitization.

### ***Involvement of PKC in agonist-dependent KOPR phosphorylation***

#### ***Endogenous PKC isoforms in N2A cells***

We determined the isoforms of PKC present in N2A cells using RT-PCR with

isoform-specific primers. There are 8 endogenous PKC isoforms: the conventional isoforms PKC $\alpha$ , PKC $\beta$  and PKC $\gamma$ , the atypical isoforms PKC $\zeta$  and PKC $\iota/\lambda$  and the novel forms PKC $\delta$ , PKC $\epsilon$  and PKC $\theta$  (Figure 28). Our result is consistent with the previous findings that N2A cells endogenously express PKC $\alpha$ , PKC $\gamma$ , PKC $\delta$  and PKC $\epsilon$  using isoform specific antibodies for western blot (Tanimukai et al., 2002).

#### Effect of PKC knockdown on KOPR phosphorylation

We examined whether PKC $\alpha$  and PKC $\epsilon$  were involved in KOPR phosphorylation with siRNAs specific for each isoform. Knockdown of PKC $\alpha$  did not affect KOPR phosphorylation at any site (Figure 32). However, PKC $\epsilon$  knockdown resulted in a trend of decrease in U50,488H-induced S356/T357 and T363 phosphorylation, but the decrease did not reach statistical significance.

PKC $\epsilon$  has been reported to be involved in attenuation of U50,488H effects following chronic U50,488H treatment in ventricular myocytes (Zhou et al., 2002). Acute U50,488H (30  $\mu$ M) treatment inhibits electrically-stimulated  $[Ca^{2+}]_i$  transient; chronic U50,488H (1  $\mu$ M) treatment abolishes this inhibitory effect and PKC $\epsilon$  is involved in this process.

Because of the presence of many PKC isoforms in N2A cells, knockdown of one isoform may lead to substitution by other PKC isoforms, which makes it difficult to interpret the data. Thus we decided to use PKC inhibitors to examine the roles of PKC in KOPR phosphorylation.

#### Effect of PKC inhibitors on KOPR phosphorylation

Two nonselective PKC inhibitors (GF109203X and CHL) and one selective PKC inhibitor (Go6976) were used in this study. GF109203X inhibited U50,488H-induced

phosphorylation at all the residues (S356/T357, T363 and S369) (Figure 30A), indicating the involvement of PKC. Our previous study showed that S356/T357 had high basal phosphorylation level (Chen et al., 2016). GF109203X reduced basal S356/T357 phosphorylation, demonstrating that PKC contributes to this basal phosphorylation. This is similar to the finding on the MOPR. S363 in MOPR showed basal phosphorylation (El Kouhen et al., 2001). GF109203X inhibited MOPR phosphorylation under basal conditions and in response to morphine stimulation (Johnson et al., 2006). The other nonselective PKC inhibitor, CHL, reduced U50,488H-caused KOPR phosphorylation at T363 and S369 (Figure 30B), but did not affect basal and U50,488H-promoted S356/T357 phosphorylation. Selective PKC $\alpha$  and PKC $\beta$ 1 inhibitor Go6976 slightly, but significantly, inhibited U50,488H-promoted S356/T357 and S369 phosphorylation (Figure 31). To the best of my knowledge, this is the first report showing the involvement of PKC in agonist-promoted KOPR phosphorylation.

The three PKC inhibitors had different effects on basal and U50,488H-induced KOPR phosphorylation. The reason may be that different PKC inhibitors affect different PKC isoform populations and also that they affect the same isoforms to different extents. GF109203X inhibits all PKC isoforms (conventional, novel and atypical PKCs), while CHL affects two PKC subfamilies (conventional and novel PKCs). The findings that GF109203X reduced basal and U50,488H-induced S356/T357 KOPR phosphorylation, but CHL did not, indicate that atypical PKC isoforms play roles in S356/T357 phosphorylation. However, we cannot determine the PKC isoforms that are specifically involved in phosphorylating at S356, T357, T363 and S369 using these PKC inhibitors.

*Dose chosen for each PKC inhibitor*

GF109203X and CHL inhibit PKC by different mechanisms. GF109203X, an aminoalkyl bisindolylmaleimide, acts on the ATP binding site of the catalytic domain of PKC (Toullec et al., 1991), while CHL, a benzophenanthridine alkaloid, acts on the protein substrate binding site of the catalytic domain, but does not compete with ATP (Herbert et al., 1990). GF109203X inhibits all PKC isoforms (conventional PKC $\alpha$ , PKC $\beta$  and PKC $\gamma$ , atypical PKC $\zeta$  and novel PKC $\delta$ , PKC $\epsilon$ ) (Martiny-Baron et al., 1993; Hofmann, 1997). CHL inhibits conventional and novel PKCs (Herbert et al., 1990). Martiny-Baron et al. (1993) reported the IC<sub>50</sub> values of GF109203X in inhibiting PKC isoforms as follows: conventional PKC $\alpha$  (8.4 nM), PKC $\beta$  (18 nM) and PKC $\gamma$  (210 nM); atypical PKC $\zeta$  (132 nM); novel PKC $\delta$  and PKC $\epsilon$  (5.8  $\mu$ M). GF109203X has been reported to inhibit PKA (IC<sub>50</sub> value 33  $\mu$ M) (Jacobson et al., 1995). In this study, 4  $\mu$ M GF109203X was used, which would completely inhibit conventional and atypical PKCs and partially blocked novel PKC, but had no effect on PKA. The IC<sub>50</sub> value of CHL was reported to be 660 nM for conventional and novel PKCs (Herbert et al., 1990). CHL at 1  $\mu$ M used in this study was sufficient to inhibit conventional and novel PKCs. The IC<sub>50</sub> values of Go6976 against PKC $\alpha$  and PKC $\beta$ 1 are 2.3 nM and 6.2 nM, respectively (Martiny-Baron et al., 1993). Go6976 at 100nM in this study was sufficient to completely block PKC $\alpha$  and PKC $\beta$ 1.

### **U50,488H-induced KOPR internalization**

GPCR phosphorylation causes recruitment of  $\beta$ -arrestin leading to receptor internalization. Our finding that PKC inhibitors partially inhibited U50,488H-promoted mKOPR internalization (Figure 33) suggests that PKC-mediated mKOPR

phosphorylation is partially involved in U50,488H-induced KOPR internalization. The result is consistent with the finding that CHL inhibited DOPR-induced internalization in primary prefrontal cortex neuron (but is not consistent in HEK293 cells) (Charfi et al., 2014). To the best of my knowledge, this is the first report showing the involvement of PKC in agonist-promoted KOPR internalization.

Previous studies have shown that GRKs play a major role in KOPR internalization. GRK2 and GRK3 mediate U50,488H-induced human KOPR internalization in CHO and NG108-15 cells (Li et al., 1999; Schulz et al., 2002). GRK2 and phosphorylation of S369 residue in the rat KOPR was reported to be involved in U50,488H-induced rKOPR internalization in HEK293 cells. In contrast, PKA/PKC inhibitor (staurosporine), MEK inhibitor (PD98059) and phospholipase C inhibitor (U73,122) did not inhibit U50,488H-induced rKOPR internalization (McLaughlin et al., 2003). Our findings together with these reports demonstrate that both GRK and PKC regulate KOPR phosphorylation, but it appears that GRKs play more important roles than PKC in phosphorylating KOPR, leading to receptor internalization.

### **Multiple protein kinases are involved in GPCR phosphorylation**

In this study, KOPR phosphorylation is found to be regulated by GRKs and several PKC isoforms. It has been shown multiple phosphorylation sites in GPCRs are regulated by different protein kinases. For example,  $\beta$ 2-adrenergic receptor was phosphorylated by GRKs at S355, S356, T360, S364, S396, S401, S407 and S411 and PKA at S261, S262, S345 and S346. (Tran et al., 2004). M3-muscarinic receptor phosphorylation is regulated by GRKs, casein kinase 1 $\alpha$  (CK1 $\alpha$ ) and CK2 (Torrecilla et

al., 2007). CXCR4 phosphorylation were shown to be mediated by GRKs at S324, S325, S330 and S339 and PKC at at S324 and S325 (Busillo et al., 2010). MOPR was phosphorylated by GRKs at S356, T357 and S375, PKC at S363 and CaMKII at S363 and T370 (Chen et al., 2013).

Complex regulation by multiple protein kinases of GPCR phosphorylation resulting in distinct phosphorylation patterns may provide flexible mechanisms for cells to regulate distinct signaling outcomes. For example, in the case of the M3 muscarinic receptor, GRK-mediated receptor phosphorylation contributes to GRK6-mediated receptor desensitization and GRK2-mediated receptor internalization. In addition, CK1 $\alpha$  phosphorylates M3 muscarinic receptor leading to activation of the ERK pathway, whereas CK2 phosphorylates M3-muscarinic receptor resulting in enhancement in JUN-kinase signaling (Torrecilla et al., 2007). Thus, whether there is any differentiation of downstream signaling via GRK- and PKC-mediated KOPR phosphorylation needs further examination.

The rate and extent of phosphorylation occurring at different GPCR residues may also contribute to different cellular responses. For example, our previous study has demonstrated with immunoblotting that etorphine causes lower levels of KOPR phosphorylation at all the four residues, compared to U50,488H. In addition, SILAC followed by LC-MS/MS studies showed that U50,488H promoted higher levels of single phosphorylation, primarily at T363 and S369, and double phosphorylation at T363+S369 and T357+S369. Only U50,488H induced triple phosphorylation at S356+T357+S369 (Chen et al., 2016). U50,488H induced robust KOPR internalization, while etorphine caused no internalization, indicating that an above-threshold phosphorylation is required

for KOPR internalization, consistent with results on the MOPR (Lau et al., 2011). In this study, PMA-induced KOPR phosphorylation was much slower in reaching maximal phosphorylation level than U50,488H, which may lead to different cellular responses. Thus, GPCR phosphorylation by multiple protein kinases can be regulated in spatial and temporal manners (phosphorylation patterns and rates) to cause different cellular functions.

Different cells or tissues are likely to express different populations and levels of GRKs, PKC isoforms and other protein kinases, leading to distinct phosphorylation rates and patterns, recruitment of different  $\beta$ -arrestins and then activation downstream signal pathways. For example, U50,488H did not cause internalization of rKOPR in CHO cells (Li et al., 1999), but did so in HEK293 cells (McLaughlin et al., 2003). CHO cells and HEK293 cells may have different composition of GRKs and  $\beta$ -arrestins, leading to different cell-specific internalization outcomes.

GRKs have been reported to be regulated by PKC. PKC phosphorylates GRK2 and GRK5, leading to GRK2 activation but GRK5 inhibition (Chuang et al., 1995; Winstel et al., 1996; Pronin and Benovic, 1997). In N2A cells, there is endogenous GRK2 but not GRK5. The possibility that effects of PKC inhibition are partially due to GRK2 inhibition, resulting in reduced KOPR phosphorylation, cannot be excluded.

### **Generation and specificity of phospho-KOPR antibodies**

Our previous LC-MS/MS study identified the phosphorylation sites of mKOPR to be S356, T357, T363 and S369 in the C-terminal domain following treatment with 10  $\mu$ M U50,488H for 30 minutes (Chen et al., 2016). Based on these results, we designed and

custom-synthesized three phosphopeptides of 9 amino acids in length with the pS or pT in the middle, named pS356, pT363 and pS369 (Table1). Phosphopeptides were conjugated to keyhole limpet hemocyanin (KLH) as an antigen. Two rabbits were injected with each phosphopeptide-KLH antigen to generate antiserum, which was contracted to Covance Co. (Princeton, NJ). Antiserum was first tested in ELISA for immunoreactivity with the phosphopeptide antigen and then tested for specificity for phosphopeptides by dot blot assay against phosphopeptide and unphosphorylated peptide. Antiserum with high phosphopeptide specificity was then purified by affinity chromatography using phosphopeptide conjugated to SulfoLink Resin. The eluted fractions were collected to examine their specificity by Western blot against phosphorylated mKOPR activated by U50,488H (Chen et al., 2016). Anti-pS356 antibody did not show its specificity for phosphorylated KOPR. Instead, we obtained another anti-pS356/pT357 antibody from Dr. Stefan Schulz of Jena University Hospital, Germany. The phospho-peptide sequences are shown in Table1.

**Table1. Sequences of phosphopeptides used as the antigens for antiserum generation**

Peptide	Sequence		Antibody
KOPR-C-tail	<b>Human</b>	<sup>334</sup> DENFKRCFRDFCFPLKMRMERQ <sup>356</sup> STSRVRN <sup>363</sup> TVQDPAYLRDIDGMNKPV <sup>380</sup>	
	<b>mouse</b>	-----I----- <b>STN</b> ----- <b>T</b> ----- <b>SM</b> --VG-----	
hK352-360		MERQ <sub>p</sub> STSRV	pS356
m/hK359-367		RVRN <sub>p</sub> TVQDP	pT363
mK365-373		QDPA <sub>p</sub> SMRDV	pS369
hK352-360		MERQ <sub>p</sub> S <sub>p</sub> TSRV	pS356/pT357

In Western blot, pS356/T357, pT363 and pS369 antibodies recognized a broad and diffuse band of 52KDa, of which the intensity was enhanced by U50,488H. Phosphatase treatment eliminated or greatly reduced immunoreactivity with pS356/T357, pT363 and pS369 antibodies in control and U50,488H-treated groups, indicating the immunoreactivity of 52KD is due to phosphorylation of KOPRs. In addition, phosphatase treatment reduced pS356/pT357 staining in control and U50,488H-treated samples, indicating phospho-specificity of the antibody and a level of constitutive phosphorylation of the sites. Mutation of each phosphoresidue (S356A, T357A, S356/T357A, T363A and S369A) decreased the staining of individual pS356/T357, pT363 and pS369 antibodies (Chen et al., 2016). Taken together, these results show that antibodies showed high specificity for phosphorylated KOPR.

Anti-FLAG-M1 antibody was used to detected total KOPR, showing two bands of 52KDa (glycosylated form in trans-Golgi and plasma membrane) and 45KDa (glycosylated intermediates in the ER and cis-Golgi) (Li et al., 2007). U50,488H induced phosphorylation of 52KDa band, but not 45KDa. This is consistent with the notion that agonist enhances phosphorylation of fully glycosylated KOPR in cell membrane.

### **Pros and cons of combined SILAC and LC-MS/MS and immunoblotting with phosphospecific antibodies**

SILAC and LC-MS/MS assay can provide information on higher order of phosphorylation (double and triple phosphorylation), not just single phosphorylation, and relative amounts of phosphorylated forms among different treatments. However, LC-MS/MS instruments are expensive and need specialists to operate. Using phosphospecific

antibodies for immunoblotting detects a specific phosphosite from a mixture of single, double and triple phosphorylation. For example, anti-pS369 antibody can recognize KOPR phosphorylation at S369, T363/S369, T357/S369 and S356/T357/S369. Immunoblotting is easy for laboratories to set up when phospho-specific antibody is available.

### **Effects of KOPR expression level and 6XHis tag on agonist-promoted KOPR phosphorylation**

FmK6H N2A cells was used in this study. The expression level of KOPR in this stable clone cell line is about 5 pmole/mg. The high expression level facilitated partial purification and detection of phosphorylated KOPR. On the other hand, the high expression level may permit all the GRKs to participate in phosphorylating the KOPR, making it difficult to differentiate the roles of each GRK. There is six-histidine tag added in-frame to the C-terminus of the KOPR to facilitate KOPR purification. Although the KOPR does not have a typical PDZ-binding motif, the C-terminal 4 amino acids (377-380) of the KOPR have been shown to bind to a PDZ domain-containing protein, NHERF1/EBP50, which facilitates recycling of internalized KOPR and activates Na<sup>+</sup>, H<sup>+</sup>- exchanger (Li et al., 2002b; Huang et al., 2004). We believe that the 6xHis tag probably does not affect KOPR phosphorylation because the phosphorylation sites S356, T357, T363 and S369 appear to be readily accessible to all the kinases.

### **The role of PKC on U50,488H-induced pharmacological effects *in vivo***

By use of PKC inhibitors in cultured cells, we have found that PKC is involved in

U50,488H-induced phosphorylation of KOPR at S356/T357, T363 and S369. This is the first report that PKC is involved in U50,488H-promoted KOPR phosphorylation. We then proceeded to examine whether PKC is involved in U50,488H-induced phosphorylation of the KOPR in mouse brains. We found that PKC was indeed involved in U50,488H-induced KOPR phosphorylation at S369. U50,488H promoted PKC-mediated KOPR phosphorylation at pS369 may lead to  $\beta$ -arrestin recruitment and  $\beta$ -arrestin-dependent signaling to cause downstream functions.

PKC has been shown to be involved in KOPR signal transduction. Activation of KOPR inhibits calcium currents through PKC in rat dorsal root ganglion neurons and stimulates ERK signaling via PKC in astrocytes (King et al., 1999; Belcheva et al., 2005). Here we showed that PKC was involved in U50,488H-promoted KOPR phosphorylation. We then tested the hypothesis that PKC is involved in KOPR-mediated pharmacological effects *in vivo*. Effects of PKC inhibition on KOPR-induced analgesia (von Voigtlander et al., 1983; Dykstra et al., 1987), antipruritic effects (Gmerek and Cowan, 1988), sedation, motor incoordination (Kieffer, 1999) and dysphoria (Dykstra et al., 1987) were examined using the PKC inhibitor CHL.

### **Limitation of using a PKC inhibitor in behavior studies**

CHL partially inhibited KOPR phosphorylation at pS369. The effect of PKC inhibition also include its impact on signaling downstream of KOPR activation. By use of PKC inhibitors, Bohn et al. and Bian et al. showed that PKC was involved in KOPR-mediated activation of p44/42 MAPK activation in C6 glioma cells and modulation of calcium current in ventricular myocytes, respectively (Bian et al., 2000; Bohn et al.,

2000). In addition, CHL has been reported to have PKC-independent effects such as antiplatelet, antibacterial and apoptosis effects. CHL activates MEK kinase via oxidative stress mechanisms to induce apoptosis without any inhibitory effect of PKC in HeLa cells (Yu, et al., 2000). In this study, we cannot exclude these PKC-independent effects. For each *in vivo* pharmacological end point, we included an experimental group which was treated with CHL alone to control for any nonspecific effects. In all the behavioral end points examined, CHL alone had no effects. When CHL had no effect on U50,488H-induced behaviors, one can conclude that PKC has no role in KOPR-mediated behavior. When CHL affects U50,488H-promoted behaviors, its effects can be attributed to reduction in KOPR phosphorylation and/or downstream signaling.

#### **PKC-mediated KOPR phosphorylation following U50,488H treatment *in vivo***

U50,488H promoted KOPR phosphorylation at T363 and S369 in mouse brains. CHL inhibited U50,488H-induced KOPR phosphorylation at S369, but not at T363, indicating that PKC regulates KOPR phosphorylation at S369 in brains (Figure 35). KOPR phosphorylation at S369 in brains following U50,488H treatment was inhibited in GRK3 knockout mice (McLaughlin et al., 2004). Thus, both GRK3 and PKC participate in U50,488H-promoted KOPR phosphorylation at S369. Because of the low U50,488H-stimulated vs. basal differences in S356 and T357 phosphorylation, we opted not to examine KOPR S356/T357 phosphorylation in brains. Control mice showed high basal levels of T363 and S369 phosphorylation, which may be caused by endogenous dynorphin peptides.

The specificity of anti-pT363 and anti-pS369 antibodies in the brains were

examined in WT and KOPR knockout (KO) mice. In the WT mouse brains, U50,488H enhanced the staining intensity of broad and diffuse bands of ~55 kDa detected by pT363 and pS369 antibodies, compared to saline-treated WT mice. In contrast, pT363 and pS369 antibodies did not yield any staining in vehicle-treated or U50,488H-treated KOPR KO mice (data not shown).

CHL had different effects on U50,488H-induced KOPR phosphorylation between *in vitro* (N2A cells) and *in vivo* (CD1 mice). In FmK6H-N2A cells, CHL inhibited U50,488H-induced phosphorylation at pT363 and pS369, whereas in brains of CD1 mice, CHL inhibited KOPR phosphorylation only at pS369 following U50,488H injection. The discrepancy may be due to differences in cells (N2A cells vs. a heterogeneous population of cells in the whole brain), KOPR expression level and composition of PKC isoforms. In addition, although we used a CHL dose reported in the literature (Lavaur et al., 2009), the actual concentration in the brain was not known.

### **Effect of PKC inhibition on KOPR-induced analgesic effect and anti-pruritic effect**

Whether PKC is involved in KOPR-induced analgesia was examined. CHL did not affect U50,488H-induced analgesia, indicating PKC-mediated KOPR phosphorylation is not involved (Figure 36). Our results are consistent with previous reports showing that KOPR agonist-induced analgesia is mediated by G-protein signaling (Bruchas and Chavkin, 2010; White et al., 2015). Roth et al. recently reported that U69593 and salvinorin A (unbiased KOPR agonists) and RB64 (G-biased KOPR agonist) showed similar levels of KOPR-induced analgesia in WT and  $\beta$ -arrestin-2 KO mice (White et al., 2015), indicating that KOPR agonist-induced analgesia is G protein-

mediated.

Whether PKC plays a role in KOPR-induced anti-scratching effect was investigated. CHL did not inhibit U50,488H-induced antipruritic effect, indicating that PKC does not participate in KOPR anti-scratching effect (Figure 37). These results are in line with those of Bohn et al. These researchers reported that U50,488H showed similar anti-scratching effects in WT and  $\beta$ -arrestin-2 KO mice (Morgenweck et al., 2015), demonstrating that the anti-scratching effects resulting from KOPR activation are G protein-mediated.

Drug tolerance has been shown to relate to receptor phosphorylation. In this study, mice repeatedly treated with U50,488H (5 mg/kg) for 7 days did not develop tolerance to KOPR-mediated antipruritic effect (Figure 38). In contrast, Chavkin et al showed that chronic treatment with U50,488H resulted in tolerance to analgesic effect of U50,488H (McLaughlin et al., 2004). The escalating doses they used (10, 25, 50 and 75 mg/kg once a day) are much higher than doses normally used in rodents (10 mg/kg or lower). U50,488H at 10 mg/kg causes sedation and motor incoordination in mice. U50, 488H at 50 and 75 mg/kg would cause very severe sedation effect and perhaps even off-KOPR effects. Thus, we did not follow their dosing regimen for the tolerance experiments.

### **Effect of PKC inhibition on KOPR-mediated sedation and motor incoordination**

Inhibition of novelty-induced locomotor activity is well-established method for evaluating sedation. U50,488H decreased novelty-induced locomotor activity and CHL partially reversed hypolocomotion (Figure 39), indicating that PKC participates in KOPR-mediated sedation.

Rotarod assay is widely used for measurement of balance and motor coordination. U50,488H caused deficit in rotarod performance and CHL partially inhibited U50,488H-induced motor incoordination (Figure 40), demonstrating that PKC plays a role in KOPR-mediated motor incoordination.

These observations are in accord with those of Roth et al. These researchers reported that U69593 and salvinorin A (unbiased KOPR agonists) showed more motor deficiency in WT mice than in  $\beta$ -arrestin2 KO mice. RB64 (a G-biased KOPR agonist) did not cause motor incoordination and hypolocomotion in WT and  $\beta$ -arrestin2 KO mice (White et al., 2015). These results indicate that KOPR agonist-induced sedation and motor incoordination are  $\beta$ -arrestin-dependent. Our results suggest that U50,488H-induced PKC-mediated KOPR phosphorylation may in part contribute to recruitment of  $\beta$ -arrestin-dependent pathway, which leads to behavioral responses.

### **Effect of PKC inhibition on KOPR-induced CPA**

KOPR agonists cause dysphoria and psychotomimetic effects in humans (Pfeiffer et al., 1986) and aversion in animals (Dykstra et al., 1987). In this study, we examined if PKC is involved in U50,488H-induced CPA. We found that U50,488H induced CPA in mice and the PKC inhibitor CHL (1 and 5 mg/kg) inhibited U50,488H-induced CPA (Figure 41), indicating PKC plays a role in U50,488H-induced CPA, which may include U50,488H-induced PKC-mediated KOPR phosphorylation. Our results are in line with those of Chavkin et al., but different from those of Roth's group. Chavkin's group showed that in AtT20 cells and astrocytes, KOPR agonists activated p38 MAPK in a  $\beta$ -arrestin- and GRK-dependent manner. In addition, they demonstrated that swim stress caused

KOPR-dependent activation of p38 MAPK and that p38 inhibition blocked KOPR agonist-induced CPA without affecting analgesia and associative learning. They thus postulated that KOPR-induced aversion was  $\beta$ -arrestin-mediated (Bruchas et al., 2007; Bruchas and Chavkin, 2010). In contrast, Roth et al. reported that U69593 and salvinorin A (unbiased KOPR agonists) and RB64 (a G-biased KOPR ligand) produced similar levels of CPA in WT and  $\beta$ -arrestin2 KO mice (White et al., 2015), suggesting that G protein-, not  $\beta$ -arrestin2-mediated signaling, plays a role in KOPR-caused aversion. However, the possibility that  $\beta$ -arrestin1 may have compensatory effect for  $\beta$ -arrestin2 deficiency cannot be ruled out. We recently found that KOPR activation by U50,488H produced robust recruitment of  $\beta$ -arrestin1 and  $\beta$ -arrestin2 in HEK cells (Chen and Liu-Chen, unpublished observations). Thus, one possible interpretation of our results is that U50,488H-induced PKC-mediated KOPR phosphorylation may result in recruitment of  $\beta$ -arrestin1, leading to CPA. Another possibility is that the effect of PKC inhibition on CPA may be due to its alteration of the downstream signaling as discussed above.

#### **Doses of U50,488H chosen for behavior tests**

In this study, for various behavior tests different doses of U50,488H were used, which were chosen according to the results of DiMattio and Liu-Chen (manuscript in preparation). The  $A_{50}$  values of U50,488H for the formalin test and anti-scratching test were 0.6 mg/kg and 2 mg/kg, respectively. Thus, 1 mg/kg and 5 mg/kg U50,488H were used for the formalin test and anti-scratching test, respectively. U50,488H-induced CPA did not show dose-response relationship from 0.25 mg/kg to 10 mg/kg. Five mg/kg was used for CPA test in this study, which is the same dose used in the study of Dr. Chavkin's

group (Ehrich et al., 2015). For the rotarod experiment, 5 mg/kg and 10 mg/kg were examined for U50,488H-induced motor incoordination; only 10 mg/kg U50,488H caused significant impairment, which was used in this study.

## **Future studies**

### **$\beta$ -arrestin recruitment following GRK- or PKC-mediated KOPR phosphorylation in cells**

Receptor phosphorylation results in recruitment of  $\beta$ -arrestin, leading to receptor trafficking and  $\beta$ -arrestin-mediated signaling. Thus, in the future, we need to consider whether GRK- or PKC-mediated KOPR phosphorylation induce recruitment of different isoforms/ levels of  $\beta$ -arrestins, leading to different end points. Recently, our preliminary result showed U50,488H increased the recruitment of  $\beta$ -arrestin1 and  $\beta$ -arrestin2 in HEK cells (Chen and Liu-Chen, unpublished observations). Effects of GRKs or PKCs on U50,488H-induced  $\beta$ -arrestin recruitment can be determined by using siRNAs against GRKs or PKC inhibitors.

### **Effects of PKC inhibition, GRK knockdown and $\beta$ -arrestin knockdown on U50,488H-induced KOPR internalization in mouse brains**

We have generated KOPR-tdTomato (KOPR-tdT) knockin mice. Preliminary results have revealed that KOPR-tdT is present in brain regions enriched in the KOPR, including the claustrum, nucleus accumbens, striatum, deep layers of the cortex (Huang and Liu-Chen, unpublished observations). These mice may be valuable for agonist-promoted receptor trafficking studies after PKC inhibition with an inhibitor or knockdown of GRK isoforms or  $\beta$ -arrestin isoforms using virus infection in the specific brain regions.

### **Phosphorylation-deficient mice**

We are in the process of generating a knockin mouse line harboring a KOPR mutant with all the four phosphorylation sites mutated to Ala (S356A/T357A/

T363A/S369A). This mouse line will be very useful for determination of the functional roles of agonist-induced KOPR phosphorylation in animals.

## CONCLUSIONS

In the chapter 1, the underlying mechanism of KOPR-mediated neurite outgrowth was examined. U50,488H caused neurite outgrowth to a greater extent than etorphine. The effects of both drugs were mediated by the KOPR,  $G_i/o_\alpha$  protein and ERK1/2 pathway. The difference between two drugs is that etorphine shows lower efficacy than U50,488H.

The chapter 2 studied KOPR phosphorylation *in vitro* in N2A cells stably transfected with the mouse KOPR and *in vivo* in mouse brains.

In N2A cells, U50,488H promoted KOPR phosphorylation at S356, T357, T363 and S369 in the C-terminal domain. The protein kinases (GRKs and PKCs) were involved in U50,488H-induced KOPR phosphorylation. GRK2, GRK3, GRK5 and GRK6 all participated in KOPR phosphorylation following U50,488H treatment. PKC activation promoted agonist-independent KOPR phosphorylation and PKC played a role in agonist (U50,488H)-dependent KOPR phosphorylation. This is the first report that PKC is involved in agonist-induced KOPR phosphorylation.

In brains of CD-1 mice, U50,488H promoted KOPR phosphorylation at T363 and S369 and the PKC inhibitor CHL reduced S369 phosphorylation without affecting T363 phosphorylation. Effects of PKC inhibition on KOPR-mediated behaviors in CD1 mice were examined. PKC is involved in KOPR-mediated sedation, motor incoordination and CPA but not analgesia and anti-scratching effect.

In summary, we provide evidence for the regulatory role of KOPR in neuronal development and mechanistic insights for the process. Understanding of kinetics of KOPR phosphorylation, biochemical mechanisms involved in each phosphorylation site

and functional roles of KOPR phosphorylation *in vivo* may provide a new way for the development of KOPR agonists for therapeutic use.

## REFERENCES

- Aguila B, Coulbault L, Davis A, Marie N, Hasbi A, Le bras F, Toth G, Borsodi A, Gurevich VV, Jauzac P and Allouche S (2012)  $\beta$ arrestin1-biased agonism at human delta-opioid receptor by peptidic and alkaloid ligands. *Cell Signal* **24**:699-707.
- Al Hasani R and Bruchas MR (2011) Molecular mechanisms of opioid receptor-dependent signaling and behavior. *Anesthesiology* **115**:1363-1381.
- Appleyard SM, Celver J, Pineda V, Kovoor A, Wayman GA and Chavkin C (1999) Agonist-dependent desensitization of the kappa opioid receptor by G protein receptor kinase and beta-arrestin. *J Biol Chem* **274**:23802-23807.
- Belcheva MM, Clark AL, Haas PD, Serna JS, Hahn JW, Kiss A and Coscia CJ (2005) {micro} and {kappa} Opioid Receptors Activate ERK/MAPK via Different Protein Kinase C Isoforms and Secondary Messengers in Astrocytes. *J Biol Chem* **280**:27662-27669.
- Belcheva MM, Vogel Z, Ignatova E, Avidor-Reiss T, Zippel R, Levy R, Young EC, Barg J and Coscia CJ (1998) Opioid modulation of extracellular signal-regulated protein kinase activity is ras-dependent and involves Gbetagamma subunits. *J Neurochem* **70**:635-645.
- Bi J, Tsai NP, Lin YP, Loh HH and Wei LN (2006) Axonal mRNA transport and localized translational regulation of kappa-opioid receptor in primary neurons of dorsal root ganglia. *Proc Natl Acad Sci U S A* **103**:19919-19924.
- Bian JS, Zhang WM, Pei JM and Wong TM (2000) The role of phosphodiesterase in mediating the effect of protein kinase C on cyclic AMP accumulation upon kappa-opioid receptor stimulation in the rat heart. *J Pharmacol Exp Ther* **292**:1065-1070.
- Blukat A, Pizard A, Breit A, Wernstedt C, Alhenc-Gelas F, Muller-Esterl W and Dikic I (2001) Determination of bradykinin B2 receptor *in vivo* phosphorylation sites and their role in receptor function. *J Biol Chem* **276**:40431-40440.
- Bohn LM, Belcheva MM and Coscia CJ (2000) Mitogenic signaling via endogenous kappa-opioid receptors in C6 glioma cells: Evidence for the involvement of protein kinase C and the mitogen-activated protein kinase signaling cascade. *J Neurochem* **74**:564-573.
- Bohn LM, Lefkowitz RJ, Gainetdinov RR, Peppel K, Caron MG and Lin FT (1999) Enhanced morphine analgesia in mice lacking beta-arrestin 2. *Science* **286**:2495-2498.
- Brennan AR, Yuan P, Dickstein DL, Rocher AB, Hof PR, Manji H and Arnsten AF (2009) Protein kinase C activity is associated with prefrontal cortical decline in aging. *Neurobiol Aging* **30**:782-792.
- Bruchas MR and Chavkin C (2010) Kinase cascades and ligand-directed signaling at the kappa opioid receptor. *Psychopharmacology (Berl)* **210**:137-147.

- Bruchas MR, Land BB, Aita M, Xu M, Barot SK, Li S and Chavkin C (2007) Stress-induced p38 mitogen-activated protein kinase activation mediates kappa-opioid-dependent dysphoria. *J Neurosci* **27**:11614-11623.
- Bruchas MR, Macey TA, Lowe JD and Chavkin C (2006) Kappa opioid receptor activation of p38 MAPK is GRK3- and arrestin-dependent in neurons and astrocytes. *J Biol Chem* **281**:18081-18089.
- Busillo JM, Armando S, Sengupta R, Meucci O, Bouvier M and Benovic JL (2010) Site-specific phosphorylation of CXCR4 is dynamically regulated by multiple kinases and results in differential modulation of CXCR4 signaling. *J Biol Chem* **285**:7805-7817.
- Butcher AJ, Prihandoko R, Kong KC, McWilliams P, Edwards JM, Bottrill A, Mistry S and Tobin AB (2011) Differential G-protein-coupled receptor phosphorylation provides evidence for a signaling bar code. *J Biol Chem* **286**:11506-11518.
- Charfi I, Nagi K, Mnie-Filali O, Thibault D, Balboni G, Schiller PW, Trudeau LE and Pineyro G (2014) Ligand- and cell-dependent determinants of internalization and cAMP modulation by delta opioid receptor (DOR) agonists. *Cell Mol Life Sci* **71**:1529-1546.
- Chen C, Chiu YT, Wu W, Huang P, Mann A, Schulz S and Liu-Chen LY (2016) Determination of sites of U50,488H-promoted phosphorylation of the mouse kappa opioid receptor (KOPR): Disconnect between KOPR phosphorylation and internalization. *Biochem J* **473** 497-508.
- Chen C, Li JG, Chen Y, Huang P, Wang Y and Liu-Chen LY (2006) GEC1 interacts with the kappa opioid receptor and enhances expression of the receptor. *J Biol Chem* **281**:7983-7993.
- Chen LT, Gilman AG and Kozasa T (1999) A candidate target for G protein action in brain. *J Biol Chem* **274**:26931-26938.
- Chen Y, Mestek A, Liu J and Yu L (1993) Molecular cloning of a rat kappa opioid receptor reveals sequence similarities to the mu and delta opioid receptors. *Biochem J* **295 ( Pt 3)**:625-628.
- Chen YJ, Oldfield S, Butcher AJ, Tobin AB, Saxena K, Gurevich VV, Benovic JL, Henderson G and Kelly E (2013) Identification of phosphorylation sites in the COOH-terminal tail of the mu-opioid receptor. *J Neurochem* **124**:189-199.
- Chuang TT, LeVine H, 3rd and De Blasi A (1995) Phosphorylation and activation of beta-adrenergic receptor kinase by protein kinase C. *J Biol Chem* **270**:18660-18665.
- DeWire SM, Yamashita DS, Rominger DH, Liu G, Cowan CL, Graczyk TM, Chen XT, Pitis PM, Gotchev D, Yuan C, Koblish M, Lark MW and Violin JD (2013) A G protein-biased ligand at the mu-opioid receptor is potently analgesic with reduced gastrointestinal and respiratory dysfunction compared with morphine. *J Pharmacol Exp Ther* **344**:708-717.

DiMattio KM, Ehlert FJ and Liu-Chen LY (2015) Intrinsic relative activities of kappa opioid agonists in activating G $\alpha$  proteins and internalizing receptor: Differences between human and mouse receptors. *Eur J Pharmacol* **761**:235-244.

Doll C, Konietzko J, Poll F, Koch T, Hollt V and Schulz S (2011) Agonist-selective patterns of micro-opioid receptor phosphorylation revealed by phosphosite-specific antibodies. *Br J Pharmacol* **164**:298-307.

Dosaka-Akita K, Tortella FC, Holaday JW and Long JB (1993) The kappa opioid agonist U-50,488H antagonizes respiratory effects of mu opioid receptor agonists in conscious rats. *J Pharmacol Exp Ther* **264**:631-637.

Dykstra LA, Gmerek DE, Winger G and Woods JH (1987) Kappa opioids in Rhesus monkeys. I. diuresis, sedation, analgesia and discriminative stimulus effects. *J Pharmacol Exp Ther* **242**:413-420.

Eason MG, Moreira SP and Liggett SB (1995) Four consecutive serines in the third intracellular loop are the sites for  $\beta$ -adrenergic receptor kinase-mediated phosphorylation and desensitization of the  $\alpha_{2a}$ -adrenergic receptor. *J Biol Chem* **270**:4681-4688.

Ehrich JM, Messinger DI, Knakal CR, Kuhar JR, Schattauer SS, Bruchas MR, Zweifel LS, Kieffer BL, Phillips PE and Chavkin C (2015) Kappa Opioid Receptor-Induced Aversion Requires p38 MAPK Activation in VTA Dopamine Neurons. *J Neurosci* **35**:12917-12931.

El Kouhen R, Burd AL, Erickson-Herbrandson LJ, Chang CY, Law PY and Loh HH (2001) Phosphorylation of Ser363, Thr370, and Ser375 residues within the carboxyl tail differentially regulates mu-opioid receptor internalization. *J Biol Chem* **276**:12774-12780.

Finley MJ, Chen X, Bardi G, Davey P, Geller EB, Zhang L, Adler MW and Rogers TJ (2008) Bi-directional heterologous desensitization between the major HIV-1 co-receptor CXCR4 and the kappa-opioid receptor. *J Neuroimmunol* **197**:114-123.

Flavell SW and Greenberg ME (2008) Signaling mechanisms linking neuronal activity to gene expression and plasticity of the nervous system. *Annu Rev Neurosci* **31**:563-590.

Fricker AD, Rios C, Devi LA and Gomes I (2005) Serotonin receptor activation leads to neurite outgrowth and neuronal survival. *Brain Res Mol Brain Res* **138**:228-235.

Gaffuri AL, Ladarre D and Lenkei Z (2012) Type-1 cannabinoid receptor signaling in neuronal development. *Pharmacology* **90**:19-39.

Ge X, Qiu Y, Loh HH and Law PY (2009) GRIN1 regulates micro-opioid receptor activities by tethering the receptor and G protein in the lipid raft. *J Biol Chem* **284**:36521-36534.

Georganta EM, Tsoutsi L, Gaitanou M and Georgoussi Z (2013) delta-opioid receptor activation leads to neurite outgrowth and neuronal differentiation via a STAT5B-

Galphai/o pathway. *J Neurochem* **127**:329-341.

Ghosh M and Schonbrunn A (2011) Differential temporal and spatial regulation of somatostatin receptor phosphorylation and dephosphorylation. *J Biol Chem* **286**:13561-13573.

Gmerek DE and Cowan A (1988) Role of opioid receptors in bombesin-induced grooming. *Ann N Y Acad Sci* **525**:291-300.

Granier S, Manglik A, Kruse AC, Kobilka TS, Thian FS, Weis WI and Kobilka BK (2012) Structure of the delta-opioid receptor bound to naltrindole. *Nature* **485**:400-404.

Hahn JW, Jagwani S, Kim E, Rendell VR, He J, Ezerskiy LA, Wesselschmidt R, Coscia CJ and Belcheva MM (2010) Mu and kappa opioids modulate mouse embryonic stem cell-derived neural progenitor differentiation via MAP kinases. *J Neurochem* **112**:1431-1441.

He JC, Gomes I, Nguyen T, Jayaram G, Ram PT, Devi LA and Iyengar R (2005) The G alpha(o/i)-coupled cannabinoid receptor-mediated neurite outgrowth involves Rap regulation of Src and Stat3. *J Biol Chem* **280**:33426-33434.

He JC, Neves SR, Jordan JD and Iyengar R (2006) Role of the Go/i signaling network in the regulation of neurite outgrowth. *Can J Physiol Pharmacol* **84**:687-694.

Herbert JM, Augereau JM, Gleye J and Maffrand JP (1990) Chelerythrine is a potent and specific inhibitor of protein kinase C. *Biochem Biophys Res Commun* **172**:993-999.

Hermeking H (2006) 14-3-3 proteins and cancer biology. *Semin Cancer Biol* **16**:161.

Hofmann J (1997) The potential for isoenzyme-selective modulation of protein kinase C. *FASEB J* **11**:649-669.

Huang P, Steplock D, Weinman EJ, Hall RA, Ding Z, Li J, Wang Y and Liu-Chen L-Y (2004) kappa Opioid receptor interacts with Na(+)/H(+)-exchanger regulatory factor-1/Ezrin-radixin-moesin-binding phosphoprotein-50 (NHERF-1/EBP50) to stimulate Na(+)/H(+) exchange independent of G(i)/G(o) proteins. *J Biol Chem* **279**:25002-25009.

Hwangpo TA, Jordan JD, Premsrirut PK, Jayamaran G, Licht JD, Iyengar R and Neves SR (2012) G Protein-regulated inducer of neurite outgrowth (GRIN) modulates Sprouty protein repression of mitogen-activated protein kinase (MAPK) activation by growth factor stimulation. *J Biol Chem* **287**:13674-13685.

Iida N and Kozasa T (2004) Identification and biochemical analysis of GRIN1 and GRIN2. *Methods Enzymol* **390**:475-483.

Jacobson PB, Kuchera SL, Metz A, Schachtele C, Imre K and Schrier DJ (1995) Anti-inflammatory properties of Go 6850: a selective inhibitor of protein kinase C. *J Pharmacol Exp Ther* **275**:995-1002.

Johnson EA, Oldfield S, Braksator E, Gonzalez-Cuello A, Couch D, Hall KJ, Mundell SJ, Bailey CP, Kelly E and Henderson G (2006) Agonist-selective mechanisms of mu-opioid receptor desensitization in human embryonic kidney 293 cells. *Mol Pharmacol* **70**:676-685.

Just S, Illing S, Trester-Zedlitz M, Lau EK, Kotowski SJ, Miess E, Mann A, Doll C, Trinidad JC, Burlingame AL, von Zastrow M and Schulz S (2013) Differentiation of opioid drug effects by hierarchical multi-site phosphorylation. *Mol Pharmacol* **83**:633-639.

Kang JH, Toita R, Kim CW and Katayama Y (2012) Protein kinase C (PKC) isozyme-specific substrates and their design. *Biotechnol Adv* **30**:1662-1672.

Kieffer BL (1999) Opioids: first lessons from knockout mice [Review]. *Trends in Pharmacological Sciences* **20**:19-26.

Kim E, Clark AL, Kiss A, Hahn JW, Wesselschmidt R, Coscia CJ and Belcheva MM (2006) Mu- and kappa-opioids induce the differentiation of embryonic stem cells to neural progenitors. *J Biol Chem* **281**:33749-33760.

King AP, Hall KE and Macdonald RL (1999) kappa- and mu-Opioid inhibition of N-type calcium currents is attenuated by 4beta-phorbol 12-myristate 13-acetate and protein kinase C in rat dorsal root ganglion neurons. *J Pharmacol Exp Ther* **289**:312-320.

Knapp RJ, Malatynska E, Collins N, Fang L, Wang JY, Hruby VJ, Roeske WR and Yamamura HI (1995) Molecular biology and pharmacology of cloned opioid receptors [review]. *FASEB J* **9**:516-525.

Kong H, Raynor K, Yano H, Takeda J, Bell GI and Reisine T (1994) Agonists and antagonists bind to different domains of the cloned  $\kappa$  opioid receptor. *Proc Natl Acad Sci U S A* **91**:8042-8046.

Koob GF and Bloom FE (1988) Cellular and molecular mechanisms of drug dependence. [review]. *Science* **242**:715-723.

Kunapuli P, Gurevich VV and Benovic JL (1994) Phospholipid-stimulated autophosphorylation activates the G protein-coupled receptor kinase GRK5. *J Biol Chem* **269**:10209-10212.

Lau EK, Trester-Zedlitz M, Trinidad JC, Kotowski SJ, Krutchinsky AN, Burlingame AL and von Zastrow M (2011) Quantitative encoding of the effect of a partial agonist on individual opioid receptors by multisite phosphorylation and threshold detection. *Sci Signal* **4**:ra52.

Lavaur J, Mineur YS and Picciotto MR (2009) The membrane cytoskeletal protein adducin is phosphorylated by protein kinase C in D1 neurons of the nucleus accumbens and dorsal striatum following cocaine administration. *J Neurochem* **111**:1129-1137.

Law P-Y, Wong YH and Loh HH (2000) Molecular mechanisms and regulation of opioid receptor signaling. *Ann Rev Pharmacol Toxicol* **40**:389-430.

Le Grand JN, Chakrama FZ, Seguin-Py S, Fraichard A, Delage-Mourroux R, Jouvenot M and Boyer-Guittaut M (2011) GABARAPL1 (GEC1): original or copycat? *Autophagy* **7**:1098-1107.

Lefkowitz RJ (1998) G protein-coupled receptors. III. New roles for receptor kinases and beta-arrestins in receptor signaling and desensitization. [Review] [47 refs]. *J Biol Chem* **273**:18677-18680.

Lefkowitz RJ (2004) Historical review: a brief history and personal retrospective of seven-transmembrane receptors. *Trends Pharmacol Sci* **25**:413-422.

Lefkowitz RJ and Shenoy SK (2005) Transduction of receptor signals by beta-arrestins. *Science* **308**:512-517.

Li J-G, Luo LY, Krupnick JG, Benovic JL and Liu-Chen L-Y (1999) U50,488H-induced internalization of the human kappa opioid receptor involves a beta-arrestin- and dynamin-dependent mechanism. Kappa receptor internalization is not required for mitogen-activated protein kinase activation. *J Biol Chem* **274**:12087-12094.

Li J, Li JG, Chen C, Zhang F and Liu-Chen LY (2002a) Molecular basis of differences in (-)(trans)-3,4-dichloro-N-methyl-N-[2-(1-pyrrolidiny)-cyclohexyl]benzeneacetamide - induced desensitization and phosphorylation between human and rat kappa-opioid receptors expressed in Chinese hamster ovary cells. *Mol Pharmacol* **61**:73-84.

Li J-G, Chen C and Liu-Chen L-Y (2002b) Ezrin-radixin-moesin-binding phosphoprotein-50/Na<sup>+</sup>/H<sup>+</sup> exchanger regulatory factor (EBP50/NHERF) blocks U50,488H-induced down-regulation of the human kappa opioid receptor by enhancing its recycling rate. *J Biol Chem* **277**:27545-27552.

Li JG, Chen C, Huang P, Wang Y and Liu-Chen LY (2012) 14-3-3zeta Protein regulates anterograde transport of the human kappa-opioid receptor (hKOPR). *J Biol Chem* **287**:37778-37792.

Li JG, Chen C and Liu-Chen LY (2007) N-Glycosylation of the human kappa opioid receptor enhances its stability but slows its trafficking along the biosynthesis pathway. *Biochemistry* **46**:10960-10970.

Li JG, Zhang F, Jin XL and Liu-Chen L-Y (2003) Differential regulation of the human kappa opioid receptor by agonists: etorphine and levorphanol reduced dynorphin A- and U50,488H-induced internalization and phosphorylation. *J Pharmacol Exp Ther* **305**:531-540.

Liu-Chen L-Y (2004) Agonist-induced regulation and trafficking of kappa opioid receptors. *Life Sci* **75**:511-536.

- Lord JAH, Waterfield AA, Hughes J and Kosterlitz H (1977) Endogenous opioid peptides: multiple agonists and receptors. *Nature (London)* **267**:495-499.
- Manglik A, Kruse AC, Kobilka TS, Thian FS, Mathiesen JM, Sunahara RK, Pardo L, Weis WI, Kobilka BK and Granier S (2012) Crystal structure of the micro-opioid receptor bound to a morphinan antagonist. *Nature* **485**:321-326.
- Mann A, Illing S, Miess E and Schulz S (2014) Different Mechanisms of Homologous and Heterologous mu-Opioid Receptor Phosphorylation. *Br J Pharmacol*.
- Mansour A, Fox CA, Akil H and Watson SJ (1995) Opioid-receptor mRNA expression in the rat CNS: anatomical and functional implications. *Trends Neurosci* **18**:22-29.
- Mansuy V, Boireau W, Fraichard A, Schlick JL, Jouvenot M and Delage-Mourroux R (2004) GEC1, a protein related to GABARAP, interacts with tubulin and GABA(A) receptor. *Biochem Biophys Res Commun* **325**:639-648.
- Marti-Solano M, Guixa-Gonzalez R, Sanz F, Pastor M and Selent J (2013) Novel Insights into Biased Agonism at G Protein-Coupled Receptors and their Potential for Drug Design. *Curr Pharm Des* **19**:5156-5166.
- Martiny-Baron G, Kazanietz MG, Mischak H, Blumberg PM, Kochs G, Hug H, Marme D and Schachtele C (1993) Selective inhibition of protein kinase C isozymes by the indolocarbazole Go 6976. *J Biol Chem* **268**:9194-9197.
- Masuh I, Mototani Y, Sahara Y, Asami J, Nakamura S, Kozasa T and Inoue T (2008) Dynamic expression patterns of G protein-regulated inducer of neurite outgrowth 1 (GRIN1) and its colocalization with Galphao implicate significant roles of Galphao-GRIN1 signaling in nervous system. *Dev Dyn* **237**:2415-2429.
- Mattson MP (2008) Glutamate and neurotrophic factors in neuronal plasticity and disease. *Ann N Y Acad Sci* **1144**:97-112.
- McLaughlin JP, Myers LC, Zarek PE, Caron MG, Lefkowitz RJ, Czyzyk TA, Pintar JE and Chavkin C (2004) Prolonged kappa opioid receptor phosphorylation mediated by G-protein receptor kinase underlies sustained analgesic tolerance. *J Biol Chem* **279**:1810-1818.
- McLaughlin JP, Xu M, Mackie K and Chavkin C (2003) Phosphorylation of a carboxy-terminal serine within the kappa opioid receptor produces desensitization and internalization. *J Biol Chem* **278**:34631-34640.
- McLennan GP, Kiss A, Miyatake M, Belcheva MM, Chambers KT, Pozek JJ, Mohabbat Y, Moyer RA, Bohn LM and Coscia CJ (2008) Kappa opioids promote the proliferation of astrocytes via Gbetagamma and beta-arrestin 2-dependent MAPK-mediated pathways. *J Neurochem* **107**:1753-1765.
- Morgenweck J, Frankowski KJ, Prisinzano TE, Aube J and Bohn LM (2015)

- Investigation of the role of betaarrestin2 in kappa opioid receptor modulation in a mouse model of pruritus. *Neuropharmacology* **99**:600-609.
- Mortimer D, Fothergill T, Pujic Z, Richards LJ and Goodhill GJ (2008) Growth cone chemotaxis. *Trends Neurosci* **31**:90-98.
- Nakata H and Kozasa T (2005) Functional characterization of Galphao signaling through G protein-regulated inducer of neurite outgrowth 1. *Mol Pharmacol* **67**:695-702.
- Nobles KN, Xiao K, Ahn S, Shukla AK, Lam CM, Rajagopal S, Strachan RT, Huang TY, Bressler EA, Hara MR, Shenoy SK, Gygi SP and Lefkowitz RJ (2011) Distinct phosphorylation sites on the beta(2)-adrenergic receptor establish a barcode that encodes differential functions of beta-arrestin. *Sci Signal* **4**:ra51.
- Olson GA, Olson RD and Kastin AJ (1991) Endogenous opiates: 1990. *Peptides* **12**:1407-1432.
- Onorato JJ, Palczewski K, Regan JW, Caron MG, Lefkowitz RJ and Benovic JL (1991) Role of acidic amino acids in peptide substrates of the  $\beta$ -adrenergic receptor kinase and rhodopsin kinase. *Biochem* **30**:5118-5125.
- Pfeiffer A, Brantl V, Herz A and Emrich HM (1986) Psychotomimesis mediated by kappa opiate receptors. *Science* **233**:774-776.
- Pitcher JA, Freedman NJ and Lefkowitz RJ (1998) G protein-coupled receptor kinases. *Annu Rev Biochem* **67**:653-692.
- Pitcher JA, Inglese J, Higgins JB, Arriza JL, Casey PJ, Kim C, Benovic JL, Kwatra MM, Caron MG and Lefkowitz RJ (1992) Role of beta gamma subunits of G proteins in targeting the beta-adrenergic receptor kinase to membrane-bound receptors. *Science* **257**:1264-1267.
- Pradhan AA, Becker JA, Scherrer G, Tryoen-Toth P, Filliol D, Matifas A, Massotte D, Gaveriaux-Ruff C and Kieffer BL (2009) *In vivo* delta opioid receptor internalization controls behavioral effects of agonists. *PLoS One* **4**:e5425.
- Pradhan AA, Smith ML, Kieffer BL and Evans CJ (2012) Ligand-directed signalling within the opioid receptor family. *Br J Pharmacol* **167**:960-969.
- Pradhan AA, Walwyn W, Nozaki C, Filliol D, Erbs E, Matifas A, Evans C and Kieffer BL (2010) Ligand-directed trafficking of the delta-opioid receptor *in vivo*: two paths toward analgesic tolerance. *J Neurosci* **30**:16459-16468.
- Premont RT, Inglese J and Lefkowitz RJ (1995) Protein kinases that phosphorylate activated G protein-coupled receptors. [review]. *FASEB J* **9**:175-182.
- Pronin AN and Benovic JL (1997) Regulation of the G protein-coupled receptor kinase GRK5 by protein kinase C. *J Biol Chem* **272**:3806-3812.

Raman M, Chen W and Cobb MH (2007) Differential regulation and properties of MAPKs. *Oncogene* **26**:3100-3112.

Ramser EM, Wolters G, Dityateva G, Dityatev A, Schachner M and Tilling T (2010) The 14-3-3zeta Protein Binds to the Cell Adhesion Molecule L1, Promotes L1 Phosphorylation by CKII and Influences L1-Dependent Neurite Outgrowth. *PLoS One* **5**:e13462.

Reinoso BS, Undie AS and Levitt P (1996) Dopamine receptors mediate differential morphological effects on cerebral cortical neurons *in vitro*. *J Neurosci Res* **43**:439-453.

Reiter E, Ahn S, Shukla AK and Lefkowitz RJ (2012) Molecular mechanism of beta-arrestin-biased agonism at seven-transmembrane receptors. *Annu Rev Pharmacol Toxicol* **52**:179-197.

Rios C, Gomes I and Devi LA (2006) mu opioid and CB1 cannabinoid receptor interactions: reciprocal inhibition of receptor signaling and neuritogenesis. *Br J Pharmacol* **148**:387-395.

Rives ML, Rossillo M, Liu-Chen LY and Javitch JA (2012) 6'-Guanidinonaltrindole (6'-GNTI) is a G protein-biased kappa-opioid receptor agonist that inhibits arrestin recruitment. *J Biol Chem* **287**:27050-27054.

Sato PY, Chuprun JK, Schwartz M and Koch WJ (2015) The evolving impact of g protein-coupled receptor kinases in cardiac health and disease. *Physiol Rev* **95**:377-404.

Schmid CL, Streicher JM, Groer CE, Munro TA, Zhou L and Bohn LM (2013) Functional Selectivity of 6'-Guanidinonaltrindole (6'-GNTI) at kappa-Opioid Receptors in Striatal Neurons. *J Biol Chem* **288**:22387-22398.

Schulz R, Wehmeyer A and Schulz K (2002) Visualizing preference of G protein-coupled receptor kinase 3 for the process of kappa-opioid receptor sequestration. *Mol Pharmacol* **61**:1444-1452.

Schwartz TW (1994) Locating ligand-binding sites in 7tm receptors by protein engineering. [review]. *Current Opinion in Biotechnology* **5**:434-444.

Shikano S, Coblitz B, Wu M and Li M (2006) 14-3-3 proteins: regulation of endoplasmic reticulum localization and surface expression of membrane proteins. *Trends Cell Biol* **16**:370-375.

Simonin F, Valverde O, Smadja C, Slowe S, Kitchen I, Dierich A, Le M, Roques BP, Maldonado R and Kieffer BL (1998) Disruption of the kappa-opioid receptor gene in mice enhances sensitivity to chemical visceral pain, impairs pharmacological actions of the selective kappa-agonist U-50,488H and attenuates morphine withdrawal. *EMBO Journal* **17**:886-897.

- Spitaler M and Cantrell DA (2004) Protein kinase C and beyond. *Nat Immunol* **5**:785-790.
- Tanimukai S, Hasegawa H, Nakai M, Yagi K, Hirai M, Saito N, Taniguchi T, Terashima A, Yasuda M, Kawamata T and Tanaka C (2002) Nanomolar amyloid beta protein activates a specific PKC isoform mediating phosphorylation of MARCKS in Neuro2A cells. *Neuroreport* **13**:549-553.
- Tong G, Sun Z, Wei X, Gu C, Kaye AD, Wang Y, Li J, Zhang Q, Guo H, Yu S, Yi D and Pei J (2011) U50,488H postconditioning reduces apoptosis after myocardial ischemia and reperfusion. *Life Sci* **88**:31-38.
- Torreccilla I, Spragg EJ, Poulin B, McWilliams PJ, Mistry SC, Blaukat A and Tobin AB (2007) Phosphorylation and regulation of a G protein-coupled receptor by protein kinase CK2. *J Cell Biol* **177**:127-137.
- Toullec D, Pianetti P, Coste H, Bellevergue P, Grand-Perret T, Ajakane M, Baudet V, Boissin P, Boursier E and Loriolle F (1991) The bisindolylmaleimide GF 109203X is a potent and selective inhibitor of protein kinase C. *J Biol Chem* **266**:15771-15781.
- Tran TM, Friedman J, Qunaibi E, Baameur F, Moore RH and Clark RB (2004) Characterization of agonist stimulation of cAMP-dependent protein kinase and G protein-coupled receptor kinase phosphorylation of the beta2-adrenergic receptor using phosphoserine-specific antibodies. *Mol Pharmacol* **65**:196-206.
- Trester-Zedlitz M, Burlingame A, Kobilka B and von Zastrow M (2005) Mass spectrometric analysis of agonist effects on posttranslational modifications of the beta-2 adrenoceptor in mammalian cells. *Biochemistry* **44**:6133-6143.
- Tsai NP, Tsui YC, Pintar JE, Loh HH and Wei LN (2010) Kappa opioid receptor contributes to EGF-stimulated neurite extension in development. *Proc Natl Acad Sci U S A* **107**:3216-3221.
- Valero T, Moschopoulou G, Mayor-Lopez L and Kintzios S (2012) Moderate superoxide production is an early promoter of mitochondrial biogenesis in differentiating N2a neuroblastoma cells. *Neurochem Int* **61**:1333-1343.
- van Kesteren RE and Spencer GE (2003) The role of neurotransmitters in neurite outgrowth and synapse formation. *Rev Neurosci* **14**:217-231.
- von Voigtlander PF, Lahti RA and Ludens JH (1983) U-50,488: a selective and structurally novel non-Mu (kappa) opioid agonist. *J Pharmacol Exp Ther* **224**:7-12.
- Wei LN (2011) The RNA superhighway: axonal RNA trafficking of kappa opioid receptor mRNA for neurite growth. *Integr Biol (Camb)* **3**:10-16.
- Wheeler-Aceto H and Cowan A (1991) Standardization of the rat paw formalin test for the evaluation of analgesics. *Psychopharmacology (Berlin)* **104**:35-44.
- White KL, Robinson JE, Zhu H, DiBerto JF, Polepally PR, Zjawiony JK, Nichols DE,

- Malanga CJ and Roth BL (2015) The G Protein-Biased kappa-Opioid Receptor Agonist RB-64 Is Analgesic with a Unique Spectrum of Activities *In Vivo*. *J Pharmacol Exp Ther* **352**:98-109.
- Winstel R, Freund S, Krasel C, Hoppe E and Lohse MJ (1996) Protein kinase cross-talk: membrane targeting of the beta-adrenergic receptor kinase by protein kinase C. *Proc Natl Acad Sci U S A* **93**:2105-2109.
- Wisler JW, Xiao K, Thomsen AR and Lefkowitz RJ (2014) Recent developments in biased agonism. *Curr Opin Cell Biol* **27**:18-24.
- Wu H, Wacker D, Mileni M, Katritch V, Han GW, Vardy E, Liu W, Thompson AA, Huang XP, Carroll FI, Mascarella SW, Westkaemper RB, Mosier PD, Roth BL, Cherezov V and Stevens RC (2012) Structure of the human kappa-opioid receptor in complex with JDTic. *Nature* **485**:327-332.
- Xu W, Wang Y, Ma Z, Chiu YT, Huang P, Rasakham K, Unterwald E, Lee DY and Liu-Chen LY (2013) l-Isocorypalmine reduces behavioral sensitization and rewarding effects of cocaine in mice by acting on dopamine receptors. *Drug Alcohol Depend* **133**:693-703.
- Zhang F, Li J, Li J-G and Liu-Chen L-Y (2002) (-)U50,488H [(trans)-3,4-dichloro-N-methyl-N-[2-(1-pyrrolidinyl)-cyclohexyl]benzeneacetamide] induces internalization and down-regulation of the human, but not the rat, kappa-opioid receptor: Structural basis for the differential regulation. *J Pharmacol Exp Ther* **302**:1184-1192.
- Zheng H, Zeng Y, Chu J, Kam AY, Loh HH and Law PY (2010a) Modulations of NeuroD activity contribute to the differential effects of morphine and fentanyl on dendritic spine stability. *J Neurosci* **30**:8102-8110.
- Zheng H, Zeng Y, Zhang X, Chu J, Loh HH and Law PY (2010b) mu-Opioid receptor agonists differentially regulate the expression of miR-190 and NeuroD. *Mol Pharmacol* **77**:102-109.
- Zheng H, Zhang Y, Li W, Loh HH and Law PY (2013) NeuroD modulates opioid agonist-selective regulation of adult neurogenesis and contextual memory extinction. *Neuropsychopharmacology* **38**:770-777.
- Zhou JJ, Bian JS, Pei JM, Wu S, Li HY and Wong TM (2002) Role of protein kinase C-epsilon in the development of kappa-opioid receptor tolerance to U50,488H in rat ventricular myocytes. *Br J Pharmacol* **135**:1675-1684.